WIDEBAND REFLECTANCE ACOUSTIC REFLEX THRESHOLDS IN NORMAL EARS OF YOUNGER AND OLDER ADULTS

by

Helen Salus-Braun

A dissertation submitted to the Graduate Faculty in Speech and Hearing Sciences
In partial fulfillment of the requirements for the degree of Doctor of Philosophy,
City University of New York

2010

The manuscript has been read and accepted for the

Graduate Faculty in Speech-Language-Hearing Sciences in satisfaction of the

dissertation requirement for the degree of Doctor of Philosophy.

Carol A. Silverman, Ph.D., MPH

_____	_____
Date	Chair of Examining Committee

Klara Marton, Ph.D.

_____	_____
Date	Executive Officer

THE CITY UNIVERSITY OF NEW YORK

Abstract

Wideband Reflectance Acoustic Reflex Thresholds in Normal Ears of Younger and Older Adults

by

Helen Salus-Braun

Adviser: Carol A. Silverman, Ph.D.

Introduction: The purpose of the study was to evaluate wideband reflectance (WBR), in comparison with the traditional acoustic-immittance (AI) method for the measurement of contralateral acoustic reflex thresholds (CARTs) for the broadband noise (BBN) and 1000-Hz tonal activators in younger versus adults, and to examine the any aging effects on the WBR CARTs.

Methods: The WBR (Mimosa instrumentation with a 24-chirp probe stimulus and signal averaging of 16 responses) and AI BBN and 1000-Hz CARTs of 10 younger (20-30 years of age) and 10 older adult females (60-70 years of age) with essentially normal-hearing sensitivity were investigated.

Results: The WBR frequency-response graphs revealed a positive peak in the low-frequency region and a negative peak at a higher frequency region. Good test-retest reliability was obtained for the WBR CARTs in both groups. The mean 1000-Hz CART was slightly, but significantly higher for the WBR than AI approach in the younger adults, and was essentially the same for both approaches in the older adults. No

significant age effect occurred for the WBR CARTs for either activator. The NTD was significantly larger with the WBR than AI approach in both age groups.

Discussion: In the frequency-response WBR graphs, the positive peak reflects increased energy reflectance by the middle ear; the negative peak reflects increased energy absorption into the middle ear. The significantly WBR than AI NTD suggests that the WBR rather than AI method should be used for NTD measurement for prediction of hearing sensitivity based on the CARTs, especially in older adults, in whom the traditional AI approach yields reduced NTDs. The significant improvement in the WBR BBN CARTs in comparison with the AI BBN CARTs may result from summation of the energy of the BBN activator and the chirp probe stimulus. Because the WBR approach yielded an expanded NTD that primarily is attributable to the improved WBR BBN CART as compared with the AI BBN CART and to the summation effect, future research needs to re-examine all other parameters of the acoustic reflex related to the BBN stimulus, such as latency, magnitude, and temporal integration and aging effects upon these parameters.

Acknowledgments

Dissertation preparation was an extraordinary journey on which I was a recipient of generous gifts of knowledge and love from many great people.

Interest in physics and physiology brought me first into the field of audiology and later into the PhD program. When I started the study that eventually led to the product presented on the following pages - my dissertation, I envisioned a process of academic instruction and inquiry that would cultivate critical thinking and help me to attain basic skills essential for auditory research. Although the accomplishment of this goal has its undeniable value, reflecting now back on the whole experience, additional, equal, if not greater benefits of mentorship, friendship and love were bestowed upon me. Although, words cannot truly capture my feelings of appreciation, the following lines are to acknowledge the people without whom nor there would be positive qualities in me, neither I would reach this milestone.

I am immensely grateful to Carol Ann Silverman, Ph.D., MPH accomplished researcher, respected pedagogue and uncommonly generous person for her mentorship. Her wise, kind, humorous and steady nurturing was essential for my success. Her calm constructive analytical approach to problems and unassuming ability to bring people together for collaboration are truly unique and admired by peers and students alike. I also had the privilege and enjoyment to learn from Dr. Silverman through our conversations outside the field of audiology. Dr. Silverman's perspectives ranged from serious and instructive, through entertaining, to very funny, and were always valuable. Many thanks also belong to Shlomo Silman, Ph.D., prolific researcher, altruistic and kind person. His creative mind, energetic demeanor and passion for research were sources of practical support as well as inspiration. Also, great thanks to Dr. Silman for lending me Mimosa Powerflow equipment. I am also thankful for the support, help and advice of Alan Richards, Ph.D., successful auditory scientist and clinician; Chris Linstrom, M.D., prominent neuro-otology surgeon and researcher; and Klara Marton, Ph.D., accomplished language scientist and effective leader of the Department of Speech and Hearing at the Graduate School University Center.

My gratitude goes to my dear parents. They always gave me love and support. I am sad that I could no longer share with them the joy of this accomplishment. My father George Jiri Salus, electrical engineer and respected researcher himself in former Czechoslovakia was my inspiration from as far back as I can remember. My mother Miluška, an early childhood teacher instilled in me faith that with dedication and patience almost any goal could be reached.

My dear family displayed deep love and endless tolerance during this endeavor. David, Rosalie and Anna balanced my life and supported me greatly, each in their own special way. My final acknowledgment goes to George, my best friend, partner and husband, kind, and intelligent person, skillful physician, for his patience and loyalty. For being everything I am not, he has my everlasting love!

Table of Contents

Chapter III.

Chapter IV.

Chapter V.

Appendices

List of Tables.

Page

Page

List of Figures

Page

CHAPTER I: INTRODUCTION

Purpose

General Purpose

The general purpose of the proposed study was to evaluate a new method (wideband reflectance) for the measurement of CARTs, as well as to gain a better understanding of the effects of the aging process on the auditory mechanism, specifically, the contralateral acoustic reflex arc. The findings of this experiment should aid in the ongoing efforts to build a precise functional model of the ear. The results of the investigation also have implications for clinical acoustic-reflex assessment of individuals with hearing impairment and CART-based prediction of hearing status in older adult subjects.

Specific Purpose

The purpose of the study on a group of younger adults and a group of older adults with normal-hearing sensitivity was threefold: (a) to refine the working set of criteria for defining the wideband CART; (b) to compare the tonal (1000-Hz) and BBN CART obtained with the two measurement approaches; (c) to examine the effect of age on the wideband reflectance and traditional tonal and BBN CARTs. The set of the criteria for defining the wideband reflectance CART that had been developed and refined by this investigator aided in obtaining of sensitive and specific wideband CARTs that were then compared with the traditional acoustic-immittance CARTs. The noise-tone difference (NTD), the difference between the tonal and BBN CARTs, were compared applying the two approaches, as this measure has implications for prediction of hearing loss from the acoustic reflex (e.g., the bivariate plot procedure) in younger and older adults.

The wideband reflectance CARTs and NTDs obtained in this study also may be combined with similar data from future investigations and thereby contribute to establishing normative CART and NTD data with 90th percentile values and bivariate plot normative data.

Definition and Explanation of Terms

Absent Acoustic Reflex

An absent acoustic reflex describes the condition whereby the acoustic-reflex threshold (ART) is elevated above the highest activator intensity level. The other term used to describe this condition is *no response* (Gelfand, Schwander, & Silman, 1990)

Acoustic

"The word "acoustic," an adjective, means intimately associated with sound waves or with the individual media, phenomena, apparatus, quantities, or units discussed in the science of sound waves" (Beranek, 1954, p.9).

Acoustic Reflex

The acoustic reflex is a term referring to contraction of the middle-ear muscles, particularly the stapedius, in response to sufficiently intense acoustic stimulation. The acoustic reflex occurs bilaterally, so a response can be monitored in either ear when one ear is stimulated. The term, ***ipsilateral acoustic reflex*** refers to stimulation and response in the same ear, whereas the term ***contralateral acoustic reflex*** refers to stimulation to one ear and monitoring of the response in the opposite ear. In the context of the proposed study, the right contralateral reflex describes the situation in which the stimulus is presented into the right ***activator ear*** and the response is measured in the left ***probe ear*** (see APPENDIX A, Figure A1).

The human acoustic reflex is believed to occur primarily due to the stapedius muscle contraction (rather than tensor tympani contraction), resulting in an outward deflection of the tympanic membrane. The acoustic reflex may be observed via an increase in the acoustic impedance of the middle ear when a 226-Hz probe tone is applied during traditional acoustic-immittance-based acoustic reflex testing. (It is the acoustic compliance component of middle ear impedance which is primarily affected due to the increased stiffness of the middle ear in normal adult ears, Gelfand, 1998).

Acoustic Reflex Latency

The acoustic reflex is not observed immediately upon the presentation of activating signal. Acoustic-reflex latency is the time interval between the presentation of the activating signal and the measurable acoustic-immittance or wideband reflectance change. The length of latency depends on both the stimulus intensity and frequency. The acoustic-reflex latency may vary between 20 ms and 150 ms (Gelfand, 1998).

Acoustic Reflex Magnitude

Acoustic-reflex magnitude is traditionally assessed through quantification of the middle-ear acoustic immittance (acoustic immittance after correcting or the ear-canal volume) change resulting from stapedial muscle contraction. The magnitude of the stapedius reflex related middle-ear impedance change (change at the level of the tympanic membrane), $\Delta Z_{ME\ REFLEX}$, equals the difference between middle-ear impedance during the stapedius muscle contraction ($Z_{ME\ REFLEX}$) and the middle-ear static impedance ($Z_{ME\ STATIC}$). The physical unit is acoustic ohm Ω.

$$\Delta Z_{ME\ REFLEX} = Z_{ME\ REFLEX} - Z_{ME\ STATIC} \quad [\Omega]$$

Similarly, the magnitude of the stapedius-reflex-related middle-ear acoustic-admittance change ($\Delta Y_{ME\ REFLEX}$) expressed in acoustic mmho, is computed as follows:

$$\Delta Y_{ME\ REFLEX} = Y_{ME\ REFLEX} - Y_{ME\ STATIC} \quad [mmho]$$

The middle-ear acoustic admittance change at the level of tympanic membrane is deduced directly from the admittance change at the probe. The impedance change as measured at the probe must be transformed in order to account for nonlinear changes between the probe and tympanic membrane. (Popelka, 1981).

Acoustic-Reflex Parameters

Acoustic-reflex parameters and their characteristics are presented in Table 1. The data are based on the findings of several investigators (Emmer, 2000; Gelfand, 1998; Gelfand & Piper, 1981; Jakimetz, Silman, Miller, & Silverman, 1989; Popelka, 1981; Silman,1979; Silverman et al., 1983; Thompson et al., 1980; Wilson, 1981; Gelfand & Piper, 1981)

Table 1

Acoustic-Reflex Parameters and Characteristics

Parameter	**Characteristics**
ART	***Pure tone 250 –4000 Hz activators***
	85 – 100 dB SPL
	Effects of hearing loss observed
	BBN activators
	65-80 dB SPL
	20 dB better than pure-tone elicited AR threshold
	AR related to the bandwidth – critical bandwidth
	The width of the critical band increases with increasing center frequency. The acoustic reflex critical band is substantially wider than the psychoacoustic critical band
	Effects of age and hearing loss observed

Table 1 Continued

Parameter	Characteristics
Latency of AR = time period between stimulation and the onset of the acoustic-immittance change	Depends on intensity and frequency Latency shortens with increasing intensity and frequency Latency is a measure of mechanical response of middle ear, rather than a neural response (neural transport time for the reflex arc). Electromyographic response of stapedius muscle is as short as 12 msec and 6 dB lower than impedanace obtained ART Latency relaxation at the onset of AR response was reported by some researchers (partial relaxation before contraction onset) ***Pure tone activators*** 150 msec at 80 dB SL at 1000 Hz 40 msec at 100 dB SL at 1000 Hz Other research: 25-130 msec for 500, 1500 Hz, shorter for higher frequencies ***Noise activators*** ***As short as 20 msec***
Magnitude of AR Amount of acoustic-immittance change associated with the acoustic reflex	Increasing stimulus level causes an increase in acoustic-reflex magnitude The relation between stimulus level and the resulting acoustic-reflex magnitude may be described by the acoustic-reflex growth function ***Pure tone activators*** 85 to 120 dB SPL Essentially linear growth ***Steeper AR growth function with increasing f reported by some researchers*** ***BBN activators*** 70 –110 dB SPL Essentially linear growth
Stimulus Duration	***Less than about 1 sec*** Temporal summation: the time-intensity trade applies. Differing results among researchers have been obtained. Interaction of age and duration observed for BBN stimuli with NTD greater in younger subjects for durations 300 to 1000 ms (Emmer, 2000).

Table 1 Continued

Parameter	Characteristics
	Several seconds and more
	Decrease in magnitude with prolonged stimulation:
	Greater adaptation of acoustic reflex (decrease in magnitude) as the activator frequency increases
	Faster adaptation with greater intensity
Loudness	Equal-loudness contours and equal-reflex contours comparison reveals controversial results in terms of relationship between loudness and AR (Differing results among different researchers have been obtained. The issue remains unresolved.

Acoustic Reflex Threshold (ART)

ART obtained via the acoustic-immittance technique

The ART "can be defined as the level of the activating stimulus that results in a change in an acoustic-immittance quantity (impedance or admittance) that is just detectable" (Popelka, 1981). Knowledge about the acoustic reflex has mostly been derived from the experiments assessing the changes in acoustic immittance during contraction of the middle-ear muscles at the level of tympanic membrane. Electromyographic recordings and cochlear microphonic measurements that show ARTs at levels substantially lower than those obtained via the traditional acoustic-immitance technique (Galambos & Rupert, 1959; Simmons, 1959).

Signal-averaging techniques are used to improve the signal-to-noise ratio of acoustic-immittance measurement. Such techniques are not yet available in commercially available devices. The results of ART studies employing signal averaging with the traditional acoustic-immittance technique have shown improved ARTs

(Terkildsen et al., 1973; Jerger et al., 1977; Zito & Roberto, 1980; Hayes & Jerger, 1983; Stach & Jerger, 1984).

ART obtained via wideband reflectance technique

With the traditional acoustic-immittance tehnique, the ART represents the activator level that results in just detectable baseline acoustic immittance change or related quantity shift. Similarly, the wideband reflectance ART is defined as the activator level that leads to just detectable baseline wideband reflectance shift, mathematically described as ∂ R = $R_{Baseline} - R_{Activator}$ (Feeney & Keefe, 2001). Reflectance measurements at the baseline, as well as at each activator level, are obtained as a function of frequency, and the magnitude of the shift will vary with the frequency (Feeney & Keefe, 1999, 2001). Feeney and Keefe (2001) noted that as the level of subsequently presented activators decreases, the response shifts maintains the same basic shape while decreasing in magnitude. Repeated baseline measurements exhibit certain normal variability. Therefore, determination of the ART based on the wideband reflectance technique is not straightforward and requires a rather complex approach.

Feeney and Keefe (2001) suggested following approaches for measurement of the ART based on the wideband reflectance technique. For the acoustic-reflex magnitude test, the ART equals the lowest activating signal level for which shifts in wideband reflectance (or the related quantity of admittance magnitude) meet the following criteria:

1. The pattern of wideband reflectance change across frequency is similar to that observed for higher activator–level conditions.
2. The wideband reflectance change exceeds two standard deviations beyond the mean of the absolute difference between baseline conditions for at least a half-octave range.

3. The wideband reflectance changes at all activator conditions higher than the threshold level meet the aforementioned criteria.

According to Feeney and Keefe (2001), using the correlation method, a high positive cross-correlation between the wideband reflectance response shift at the highest activator level and the lower activator level is consistent with a present reflex. They noted that the acoustic-reflex shifts in wideband reflectance are well defined up to 2000 Hz (in case of reflectance and admittance magnitude). Therefore the appropriate frequency range for the use of cross-correlation method is 250-2000 Hz.

Acoustic Reflex Threshold Noise-Tone Difference (ART NTD)

The tonal ART minus the BBN ART represents the NTD. For calculation of the NTD, the tonal ART can be for a single tonal activator (500-, 1000-, 2000-, or 4000-Hz) or can represent the average of tonal activators (Emmer, 2000).

Activator Ear

See ***Acoustic Reflex.***

Activator-Baseline Difference (ABD)

The term activator-baseline difference (ABD) refers to the shift in reflectance $\Delta \mathcal{R}$ (f) calculated as a difference between the baseline reflectance and activator reflectance in a given frequency:

$$\text{ABD (f)} = \Delta \mathcal{R} \text{ (f)} = \mathcal{R}_{\text{ACTIVATOR}} \text{ (f)} - \mathcal{R}_{\text{BASELINE}} \text{ (f)}$$

For example, if, at a particular frequency, the baseline reflectance was 52% and the activator reflectance was 61%, then the ABD in that frequency would have been 9% (Feeney & Keefe, 1999).

Adiabatic Variation

Adiabatic variation in volume of a gas results in temperature rise when the gas is compressed and temperature fall when the gas expands. The time during a cycle of compression and expansion is not sufficiently long to permit heat outflow (Beranek, 1954).

Admittance

See ***Immittance.***

Ambient Pressure

See ***Pressure.***

Capacitance (C) of an Electrical Line

Distributed capacitance.

Between the conductors of the line exists a uniformly distributed capacitance, *C*. It is expressed in Farads per unit length [Farad / m]. (Johnson, 1950)

Shunt capacitance.

On an infinitesimally small section of the line Δx, the shunt capacitance will be $C\Delta x$ expressed in Farads (Johnson, 1950).

Conductance (G) of an Electrical Line

Distributed conductance.

Distributed conductance of an electrical line represents the imperfection of the insulator of the line which allows leakage from one conductor to another. It should be noted that *G* is not the reciprocal of resistance, *R*. The physical units for distributed conductance are mmho per unit length (mmho/m) (Johnson, 1950).

Shunt conductance.

On an infinitesimally small section of the line Δx, the shunt conductance is GΔx expressed in mmho (Johnson, 1950).

Energy Reflectance ℜ(ω)

See ***Reflectance, Energy Reflectance***

Energy Reflection Coefficient K (ω)

Other terms used for **energy reflection coefficient** are *reflection coefficient* and ***pressure reflectance***. See ***Reflectance, Pressure Reflectance.***

Evanescent Mode

Evanescent mode of propagation of the sound refers to the non-planar mode of propagation. At the level of tympanic membrane, all the non-planar evanescent waves are in phase. They die off at a short distance, laterally from the tympanic membrane (Voss & Allen, 1994).

Functions of External Ear and Middle Ear and Methods for Assessing These Functions

The primary functions of the external and middle ears are to gather the energy of sound and conduct it into the inner ear through ossicular coupling, coupled motion of tympanic membrane, ossicles, and stapes footplate. They represent a cascade of interdependent acoustical and mechanical processes targeted at overcoming the air-to-fluid impedance mismatch and ensuring efficient energy transmission from the air to the cochlea. The response of the system to the stimulus is dependent upon the frequency of the driving sound pressure and is very well illustrated by measurements of acoustic impedance or reflection of energy as a function of frequency. The middle-ear input impedance reflects the acoustical and mechanical characteristics of the middle-ear

system. The contributing components are usually modeled either as a simple stiffness, mass, and resistance in series, or using Zwislocki's model or a modification the model. The acoustical and mechanical characteristics of the human middle ear affect many areas of physiological, psychological acoustics and medical engineering. These include the interpretation of the hearing threshold data, diagnosis of middle ear pathologies, design and calibration of headphones, and design of amplification

In summary, acoustic impedance/admittance at the tympanic membrane is an indicator of the behavior of the middle-ear system. The acoustic impedance is measured in the ear canal at some distance from the tympanic membrane. At low frequencies, the lumped impedance model is appropriate. At higher frequencies, because of the complicated configuration of the ear canal and tympanic membrane, a transmission-line-based approach is appropriate.

Immittance

Acoustic immittance.

The term immittance refers to the ability of the system to transfer energy. ***Admittance*** (***Y)*** describes system's acceptance of energy and ***impedance (Z)*** refers to the system's rejection of energy. The acoustic impedance at a given surface is the complex ratio of effective acoustic pressure averaged over the surface to effective volume velocity through it. Admittance is the reciprocal of impedance (Beranek, 1954). Impedance and admittance physical quantities and units (based on Beranek, 1954; Silman & Silverman, 1991) are presented in Table 2.

Table 2

Acoustic Impedance and Admittance Physical Quantities and Physical Units

	Acoustic impedance (Z)	**Acoustic admittance (Y)**
Quantities	Z Impedance	Y Admittance
	p Acoustic Pressure	p Acoustic Pressure
	μ Volume Velocity	μ Volume Velocity
Relationship	$Z = \frac{P}{\mu}$ [Ω]	$Y = \frac{1}{Z} = \frac{\mu}{p}$ [mmho]
Physical Units	$1\,\Omega = d\ s\ cm^{-5}$	$1\text{mmho} = \Omega^{-1}$
	$1\,\Omega = 10^5\ Pa\ s\ m^{-3} = N\ s\ m^{-5}$	

Within the scope of hearing science and audiology, the middle ear is the system that is most frequently assessed using acoustic-immittance instrumentation (See ***Instrumentation***). The measurements are typically made for a given probe-tone frequency ranging between 220 Hz and 1000 Hz, with 226 Hz being the frequency that is used most often.

Impedance and admittance are complex physical quantities, containing real and imaginary components and may be expressed using rectangular or polar notations. Magnitude values of impedance and admittance are frequently used for clinical purposes. Measurement of the magnitude impedance/admittance involves the vector addition of real and imaginary components.

The real component of impedance is resistance (*R*) and the imaginary component is reactance (X_T). The components of reactance are stiffness reactance, X_S, and mass

reactance, X_M. Similarly, admittance (*Y)* has a real component called conductance (*G),* and an imaginary component labeled susceptance (B_T). The susceptance contains two oppositely directed vector components, mass susceptance (B_M) and stiffness susceptance (B_S). The angle between the real and imaginary component is the phase angle, θ.

Margolis et al. (1999), in their comprehensive review of impedance, credit Heaviside (1886) with the concept of complex impedance for long electrical transmission lines. The concept of electrical transmission lines also serves as a foundation for wideband reflectance design. According to Margolis et al. (1999) the first acoustical application of impedance by Webster dates back to 1919. West, in 1928, was the first to obtain human ear acoustic impedance measurements for telephone receivers. Margolis et al. (1999) points out that Georg von Bekesy in the 1930s was the first to make tympanometric measurements by recording impedance as a function of ear-canal air pressure (although the term tympanometry would not be used for another three decades). The mechano-acoustic bridge was invented in Denmark by Metz, who assessed with his instrument a variety of ear pathologies in human subjects as well as in temporal bones. The first electro-acoustical instrument to record acoustic impedance as a function of ear-canal air pressure was developed by a Danish team—Terkildsen and Thomsen (1959) and Terkildsen and Nielsen (1960). Their prototype led to the later development of the clinical acoustic-immittance instrumentation.

Characteristic impedance, Z_0, of a freely traveling acoustic plane wave (specific acoustic impedance).

If a plane wave travels through a tube with rigid side walls and with a perfectly absorbing termination, a reflected wave will not occur and the particle velocity, *u,* and the

sound pressure, *p*, are in phase. The characteristic impedance of a gas, sometimes called specific acoustic impedance, is purely resistive. The Z_0 is the complex ratio of sound pressure at a point in an acoustic medium to the effective particle velocity. The Z_0 may be computed from the average density of the gas and the speed of sound as follows:

$$Z_0 = p/u = \rho_0 c \quad (N.s.m^{-3})$$

The physical units are Newton.second.meter^{-3} (Beranek, 1954; Tipler, 1976).

Characteristic impedance (Z_0) of an electrical line.

Characteristic impedance Z_0 is determined only by the characteristics of the line per unit length. It does not involve the length of the line or the character of the terminating load. A load impedance equal to characteristic impedance causes no reflection of the received wave, and for this termination only, the steady-state a-c sending end impedance of the line would be equal to characteristic impedance regardless of the length of the line. The characteristic impedance (Z_0) of an electrical line is computed as follows:

$Z_0 = \sqrt{Z/Y}$ (ohms) (Johnson, 1950)

Impedance

See ***Immittance***

Inductance (L) of an Electrical Line

Distributed inductance.

When a current flows in the conductors of the transmission line, a magnetic flux is set around the conductors. Any change in the flux induces a voltage. The inductances of the transmission line conductors are smoothly distributed throughout their length. Inductance is expressed in Henrys per unit length (Henry/m) (Johnson, 1950).

Series inductance.

On a infinitesimal section of the uniform line Δx, the inductance of the section, termed series inductance, is $L\Delta x$ expressed in Henrys (Johnson, 1950).

Instrumentation

Immittance instrumentation principles.

For decades, middle-ear function has been evaluated utilizing the acoustic impedance or admittance method. The instrumentation employed is an ***acoustic impedance meter*** or ***acoustic admittance meter***. The general term is ***acoustic-immittance device***.

The probe assembly of the acoustic-immittance measurement system is placed in the external auditory canal, lateral to the tympanic membrane. The probe assembly contains two transducers and a pressure pump. The first transducer, the so-called driver, functions as a loudspeaker through which the probe tone is presented in to the ear canal. The other transducer is a microphone used to monitor the sound-pressure in the ear canal. The pressure pump allows the air pressure in the ear canal to be varied.

With an **acoustic impedance meter**, the driver presents sound at a constant volume velocity. The resulting ear-canal sound pressure is transduced via the microphone of the probe assembly into electrical voltage. This ear canal pressure/voltage is directly proportional to the impedance.

With an **acoustic admittance meter**, the driver voltage is continuously adjusted so that the microphone voltage/ear-canal sound pressure is kept constant. The volume velocity is directly proportional to the admittance.

Values of the static-acoustic immittance of the ear canal (Z_{EC} or Y_{EC}) and of the whole ear acoustic immittance (total immittance, Z_T or Y_T) are obtained. The ear-canal acoustic immittance (Z_{EC} or Y_{EC}), also called the equivalent ear-canal volume, is measured at an extreme ear-canal air pressure (+200 or – 400 daPa) so the middle ear is excluded from the acoustic-immittance measurement. The total ear acoustic immittance (combined middle-ear and ear-canal admittance) usually is usually obtained at the air pressure associated with maximal transmission of sound energy (the tympanometric peak pressure).

The arrangement of the middle-ear and ear-canal components of acoustic immittance of the total ear (Z_{EC} or Y_{EC}) is analogous to parallel electric components of an electrical circuit (see APPENDIX A, Figure A2). This lumped element model is applicable for low-frequency probe tones up to approximately 2000 Hz. Based on parallel acoustic-immittance components of the ear, the values of the middle-ear immittance are then obtained as follows,

For impedance (Z):

$$1/Z_T = (1/ Z_{EC} + 1/Z_{ME})$$

$$Z_{ME} = [(Z_{EC})(Z_T)]/(Z_{EC} - Z_T)$$

For admittance at low probe-tone frequencies:

$$Y_T = Y_{EC} + Y_{ME}$$

$$Y_{ME} = Y_T - Y_{EC}$$

At high probe-tone frequencies, or for more precise calculation at low probe-tone frequencies, admittance is computed as follows (in admittance devices, the vectors of admittance and its components are obtained directly):

$$Y_{ME}^2 = G_{ME}^2 + B_{/ME}^2$$ (Popelka, 1981; Silman & Silverman, 1991)

Isothermal Variation

Isothermal variation in volume of a gas is a change in volume that takes place in a constant temperature. The heat that is generated during the compression has time to flow to other parts of the gas or, if the gas is confined, to flow to the walls of the container (Beranek, 1954; Tipler, 1976). (The opposite term is adiabatic variation.)

Lossless Line

The hypothetical case of a line without a loss is a case of a line for which R = G = 0 (i.e., resistance and conductance are equal to zero). This assumption is good for a line where the losses are much smaller than the energy that travels along the line (Johnson, 1950).

NTD (Noise-Tone difference)

See ***Acoustic Reflex Threshold Noise-Tone Difference (ART NTD)***

Planar Mode

Planar mode refers to the plane wave propagation of the sound in which the wave fronts are approximately parallel planes perpendicular to the direction of the propagation and do not expand laterally. If a plane wave is incident on a spherical obstacle, the plane symmetry is lost. Since a sound wave is a longitudinal wave, the motion of the molecules of the air occurs parallel with the direction of the propagation. On the other hand, in the propagation of transverse waves (e.g., light, radar, radio, television), the disturbance is perpendicular to the direction of the wave (Beranek, 1954; Tipler, 1976).

Power

Power (π) is a physical quantity, whose real component is computed from the pressure response and conductance of the system in the following manner:

$$\pi = \tfrac{1}{2} G |P|^2$$

The physical units in SI system are Watts. AttoWatts (aW) are typically used to describe the power absorbed by the middle ear.

$1\ aW = 10^{-18}\ W$ (Feeney & Keefe, 1999)

Pressure

Ambient air pressure (static pressure).

In the absence of a disturbance in the medium, gas particles (molecules) are, on the average, at rest. They have random motion, but no net movement of the particles in any direction occurs, so the particle displacement is zero. The value for ambient pressure may be determined from the readings of a barometer. In other words, ambient pressure (static pressure) at a point in a medium refers to the pressure that would exist at that point with no sound waves present (Beranek, 1954).

Sound pressure.

When a sound wave is propagated in a medium, the particles are accelerated and displaced from their rest positions. The particle velocity at any given moment differs from zero except during the moments that the particle's direction of motion changes. The pressure at any point varies above and below the ambient pressure. This incremental variation of pressure is called sound pressure (Beranek, 1954).

Instantaneous sound pressure [(p(t)].

The instantaneous sound pressure [p(t)] at a given point refers to the incremental change from the static pressure at a given instant caused by the presence of sound wave (Beranek, 1954).

Effective sound pressure (*p*).

The effective sound pressure (*p)* at a given point is the root mean square (rms) value of the instantaneous sound pressure over a time interval at that point. In the case of periodic sound pressures, the interval is an integral number of periods (Beranek, 1954).

The effective sound pressure value or effective amplitude is usually simply provided by measuring devices. Conceptually, it usually involves the following computation: first the values of all positive and negative instantaneous sound pressures or displacements are squared. The resulting values are all positive numbers or zeroes (for the resting position instances). The mean of all these numbers is obtained. The root square of the mean is the rms value. The rms pressure and amplitude of a sinusoidal signal is mathematically equal to 0.707 (0.707 = $1/\sqrt{2}$) times the peak sound pressure or peak amplitude, respectively (Gelfand, 1998).

Static pressure.

See ***Ambient Pressure.***

Reflectance

Energy reflectance [ℛ(ω)].

The energy reflectance $\mathcal{R}(\omega)$ is a physical quantity, representing the ratio of the reflected to incident energy. It is defined as squared pressure reflectance (squared reflectance coefficient):

$$\mathcal{R}(\omega) = |R(\omega)|^2$$

In the human ear canal, energy reflectance is a measure of the inefficiency of the middle ear and cochlea (Voss, Allen, 1994). The concept of energy reflectance served as a basis for the development of wideband reflectance instrumentation that is used for

middle-ear function assessment. The technique allows measurements over a wide band of frequencies. For detailed information, see APPENDIX B. and APPENDIX C.

Pressure Reflectance (Reflection Coefficient) [K(ω)]

"The pressure reflectance $R(\omega)$[1] is the transfer function which may be defined for a linear one-port network by the ratio of reflected complex pressure $p_r(\omega)$ divided by the incident complex pressure $p_i(\omega)$":

$K(\omega) = p_r(\omega)/p_i(\omega)$ (Voss & Allen, 1994)

For detailed information see APPENDIX B and APPENDIX C.

Reflectometry

Reflectometry is a diagnostic method developed primarily for the detection of middle-ear effusion. Reflectometry should not be confused with wideband reflectance, sometimes also called energy reflectance or power flow. Reflectometry operates on the basis of the quarter-wavelength theory. It utilizes the principle that an incident acoustic wave traveling in a tube that is closed at one end is almost completely reflected upon reaching the closed end. This reflected wave cancels the incident wave at a distance of one quarter of the wavelength from the closed end of the tube.

---

[1] In order to prevent confusion between the physical quantities of ***energy reflectance***, ***pressure reflectance*** and ***resistance***, the symbol $\mathcal{R}$ is used for energy reflectance, the symbol *K* is used to denote ***pressure reflectance***, and the symbol *R* is used to denote ***resistance***. This use of symbols is in agreement with Johnson (1950), whereas Voss & Allen (1994) use *R* to describe pressure reflectance and $\mathcal{R}$ to describe energy reflectance. Stinson, Shaw & Lawton (1982) use *R* for energy reflectance, which they call energy reflection coefficient, and they use *b* for pressure reflectance.

The device for the measurement is termed an acoustic otoscope for measurement of acoustic reflectometry. It is a hand-held device that resembles an otoscope, except that it has a built-in speaker and microphone. The probe of the device is placed into the orifice of the external auditory canal. No hermetic seal is required. The speaker generates in the ear canal a tone of 80 dB SPL across several frequencies (2000 to 4500 Hz) in a brief period (100 ms). A certain portion of the sound is reflected at the tympanic membrane. The built-in microphone receives the reflected sound wave. The level of the reflected sound is indicated in the units of reflectivity, which ranges from 0 to 9. The higher the reflectivity, the more likely is the presence of fluid. The angle of the reflectivity may positively contribute to more accurate differentiation between normal versus abnormal ears (Block et al., 1999; Katz, 1994).

Resistance (R) of an Electrical Line

Distributed resistance.

The distributed resistance of a line represents the imperfection of the conductor. It is expressed in ohms per unit length (Ω/m) (Johnson, 1950).

Series resistance.

On an infinitesimally small section of the line, Δx, the series resistance, will be $R\Delta x$, expressed in ohms (Ω) (Johnson, 1950).

Sound

Sound is said to exist if a disturbance propagated through an elastic material causes an alteration in pressure or a displacement of particles of the material that can be detected by a person or an instrument. Pressure in the gas is a scalar (non-dimensional) quantity (Beranek, 1954). (See also ***Pressure****.)*

Transmission of Energy via Auditory System

Human sound perception results from a complex process of transmission and transduction of acoustical energy via the auditory system, which comprises the outer, middle, and inner ears, auditory nerve and central auditory pathway. The outer, middle, and inner ears represent the peripheral auditory system. The process of transmission and transduction of sound energy is not, even in a healthy ear, a simple process. Reflections, amplification, losses and distortions at several instances accompany the transmission and transduction of the energy of the original sound wave. The air-propagated sound wave travels through the ear canal until it reaches the termination of the ear canal at the tympanic membrane. At the tympanic membrane, the energy of the sound is divided. Part becomes a reflected sound wave (see APPENDIX A, Figure A3). The remainder sets the tympanic membrane into a vibratory motion. Through this process, acoustical energy is converted into mechanical energy. The vibration is transferred further along the malleus, incus and stapes, bones of the ossicular chain, into the stapes footplate, which is in direct contact with the membranous labyrinth of the cochlea at the oval window. The cochlea may be conceptualized as a transducer that converts the vibratory stimulus into a form usable by the nervous system. It also is an organ, which performs substantial amount of analyses (Gelfand, 1998).

Uniformity of the Ear Canal

The cross-sectional and/or directional changes of the ear canal are so gradual that no significant energy of the sound traveling through the ear canal is scattered back before it reaches the tympanic membrane (Voss & Allen, 1994).

Velocity of Sound Wave Propagation (Speed of Sound)

The velocity of sound wave propagation, *c*, is expressed in meters per second (m/s), and varies with temperature and water vapor in the air. Calibration of many clinical and laboratory acoustic devices is performed at room temperature, approximately circa 20 ˚C (293.15 K) and velocity is corrected according to the equation below. The correction for the water vapor in the air is nearly negligible (Popelka, 1981).

$c = 331.45 (T/273.15)^{1/2}$, where c = velocity of sound in m/s, and T = temperature (in K).

So, for example, in room air temperature of 20˚C (293.15 K), the velocity of sound equals 343,37 m/s (Beranek, 1954).

Wideband Reflectance

See ***Reflectance and Energy Reflectance.***

CHAPTER II: BACKGROUND AND RATIONALE

The topic of investigation of the ARTs in younger and older adults for BBN and tonal activators obtained via acoustic-immittance and wideband reflectance techniques was inspired by several areas of research. The interest is in the intersection of the main themes as follows: the ART, acoustic immittance, wideband reflectance, and aging. Therefore, the following sections in this chapter focus on and draw conclusions from research in these fields.

The ART: Traditional Acoustic-Immittance Technique

Effects of Stimulus Spectrum, Duration and Age on the ART

Most of what is nowadays known about the acoustic reflex comes from the experiments using acoustic-immittance based techniques. The measurement of the acoustic reflex is an important component of the standard audiological evaluation. The most frequently employed clinical application of acoustic-reflex assessment is ART estimation.

Numerous studies have shown that the lowest intensity for eliciting a minimal change in middle-ear acoustic immittance, in other words, ART, may range from 70 to 100 dB HL in normal hearing subjects. Already early acoustic-reflex research had shown that there cannot be established direct relationship between the ART level and the degree of the hearing loss (Metz, 1946). Earlier studies utilizing the traditional acoustic-immittance based technique for measurement of the ART revealed the effect of activating stimulus bandwidth on the ART. As stimulus bandwidth increases around the center frequency, the ART in normal young adult ears remains unchanged until stimulus bandwidth reaches critical bandwidth; thereafter, the ART decreases in a curvilinear

fashion as the bandwidth increases beyond the critical band (Popelka, 1981). The BBN ARTs are approximately 15 to 20 dB lower than the tonal ARTs for normal young adults (Deutsch, 1972; Djupesland, Flottorp & Winther, 1967; Margolis & Popelka, 1975; Popelka, 1981; Silman, Popelka & Gelfand, 1978).

The relation between the ART and hearing threshold level is complex as the ARTs for tonal and BBN activators are related to hearing threshold level in different ways. The tonal ARTs remain constant in normal ears and ears with hearing losses up to 30 to 40 dB HL and increase as the hearing loss increases beyond 40 dB HL. For BBN activators, the ARTs for persons with hearing impairment not exceeding about 60 dB HL increase with hearing level at a rate of approximately 0.4 dB per 1 dB of hearing level. When the hearing thresholds exceed 60 dB HL, the BBN ARTs do not increase any further and remain relatively constant (Popelka, 1981) (See Appendix A, Figure A5). Jerger et al. (1978) reported that aging was associated with a decrease in the tonal ARTs and no change in the BBN ARTs. In contrast, the results of Silman's study (1979) on the contralateral ART for younger and older adults revealed higher BBN ARTs for older than younger adults and the absence of significant differences in the tonal ARTs between younger and older adults. Silman related these findings to Bredburg's theory (1968) regarding degeneration of outer hair cells as a function of aging.

Similar to Silman (1979), Gelfand and Piper (1981), Osterhammel and Osterhammel (1979) and Thompson et al. (1980) did not observe any aging effect for the tonal ARTs. The findings of Gelfand and Piper (1981), Thompson et al. (1980) and Wilson (1981) corroborated Silman's findings regarding the aging effect on the BBN ART.

The methodological differences between Silman's (1979) and Jerger et al's (1978) studies on the effect of age on the ART were examined by Silverman et al. (1983). The contralateral ARTs for BBN and tonal activators (500, 1000, 2000, 4000 Hz) were obtained under clinical and research conditions for 72 normally hearing subjects ranging in age from 20 to 69 years. In the clinical measurement condition, the ascending-descending procedure was employed with 5-dB increments and visual monitoring of the response (needle deflection on the balance meter), following Jerger et al. The ART was defined as the response at the lowest intensity level at which needle deflection on the balance meter was observed three times in consecutive ascending order. In the research measurement condition, 1-dB intensity increments and a strip-chart recorder were employed following Silman. The ART was defined as the lowest stimulus intensity level at which deflection was noted on the strip-chart recorder. The deflection pattern had to be time-locked within one second after the stimulus presentation and distinguishable from random pen deflections.

Silverman et al's (1983) results showed that the participant's age was correlated with the BBN ART for both conditions but not the tonal ART for either condition. The correlation between age and the BBN ART was more robust under the 1-dB than 5-dB condition. Participants were divided into five groups according to their age, with 14 or 15 subjects representing each of the five age decades. The mean BBN ARTs for the youngest three age decades, with ages ranging from 20 to 49 years, formed one homogenous subset, and the means for the oldest three age decades, ranging in age from 40 to 69 years, formed a second homogenous subset. The group of the subjects between 40 and 49 years of age exhibited mean BBN ARTs common to both age subsets. Thus,

Silverman et al. concluded that changes in the BBN ART associated with the aging process have their onset in the fifth decade of life, even when hearing sensitivity is within normal limits. This conclusion appeared to be in good agreement with other literature on auditory aging. For example, as the authors pointed out, Marston and Goetzinger (1972) and Sticht and Gray (1969) reported aging associated decrements in time-compressed speech recognition ability in adults with normal hearing sensitivity.

Jakimetz, Silman, Miller and Silverman (1989) studied the effects of spectral density and the effects of bandwidth on the ART in older adults. Two groups, 20 young (20-30 years of age) and 20 older (60-71 years old) normal-hearing adults, were tested using multicomponent tonal complexes of varying density and bandwidth. For the investigation of spectral density, the number of components varied from 3 to 53 and the bandwidth was 500 to 3920 Hz (centered at 1420 Hz). The bandwidth effect was assessed with multitonal complexes having components equally spaced in log frequency; bandwidth varied between 320 and 3420 Hz with a low frequency cut-off at 500 Hz and a high-frequency limit at 3920 (the stimuli were centered at 1420 Hz).

Jakimetz et al.'s (1989) spectral density findings revealed that as spectral density increased, the ART decreased as the number of components increased up to 7 components in the younger adults and up to 5 components in the older adults. With more than 7 components in the younger adults and more than 5 components in the older adults, the ART remained unchanged. The mean ART decrease with increase in number of components until no further changes in ART were observed was 8.1 dB for the younger adults as contrasted with 5.6 dB for the older adults. These findings indicated that older adults have reduced ability to summate the sound energy from a multitonal complex

signal, implying diminished frequency resolution ability. Jakimetz et al.'s bandwidth findings revealed a substantially reduced bandwidth effect for the older as compared with younger adults. Increase in bandwidth from 320 to 3420 led to a decrease in the ART of only 3 dB as compared with 9 dB in the younger subjects. Jakimetz et al. explained these findings in light of critical band theory, suggesting that the number of the critical bands is reduced and their width is increased in older adults. The absence of the bandwidth effect in older adults resembles the absence of this effect in young adults with sensorineural hearing impairment Popelka et al. (1976).

Emmer's (2000) investigation of relationship between the subject's age and temporal integration of the BBN ART and 1000-Hz ART for stimuli durations from 12 ms to 1000 ms (12, 25, 50, 100, 200, 300, 500, and 1000 ms) indicated interaction between age and stimuli duration for the BBN ART. A large NTD of about 10 dB was noted between the younger (10 men and 10 women, 18 to 29 years old) and older subjects (10 men and 10 women, 59 to 75 years old) at the three longest durations. At durations less than 200 ms, the NTDs in older subjects were similar to those in younger adult subjects

Diagnostic Applications of Acoustic-Reflex Measurement

The diagnostic significance of acoustic-reflex measurement is well recognized. Detection of retrocochlear pathology and prediction of hearing loss with the bivariate plotting procedure represent two major areas of ART applications

Detection of Retrocochlear Pathology

Numerous studies have indicated that the ART is an essential tool for detecting retrocochlear pathology (Gelfand, Schwander, & Silman, 1990). There is an expected

range of ARTs that is associated with normal-hearing sensitivity or cochlear impairments. Normative ART data, as a function of hearing sensitivity in normal and sensorineural hearing-impaired ears (cochlear origin of the impairment) have been established by several investigators (Gelfand & Piper, 1984); Gelfand, Piper, Silman, 1983; Silman & Gelfand, 1981.

The distinguishing characteristic of retrocochlear abnormalities is a contralateral tonal ART that is elevated relative to the normative data or absent. A preponderance of ears with retrocochlear pathology has tonal ARTs that exceed the 90th percentile-ranges (Gelfand, 1984; Olsen, Bauch, & Harner, 1983; Sanders, 1984). Thus, the 90th percentile values frequently are used as cutoff values to determine the risk of retrocochlear pathology. There are, however, two issues which must be taken into consideration when applying 90th percentile values for the prediction of retrocochlear involvement. One of them is related to the magnitude of the hearing loss at the activator frequency. The other is concerned with the inclusion versus exclusion of *no responses* in the calculation of the 90th percentile values. Gelfand, Schwander, and Silman (1990) showed that cutoff values based on the calculations including "no responses" (absent reflexes were coded at 125 dB HL for activator frequencies 500, 1000, 2000 Hz) are higher than those excluding "no responses" for hearing losses greater than about 55 dB HL. The 90th percentiles including the effects of no responses were able to identify ears with retrococochlear pathology for hearing losses as great as about 75 dB HL. When the hearing loss at the activator frequency exceeds 75 dB HL, however, the no-response rate for both cochlear and retrocochlear impaired ears becomes so high that it precludes differentiation between cochlear and retrocochlear pathologies.

Prediction of Hearing Loss with the Bivariate Plot Procedure

Because of the initially observed "lack of definitive [ART's] dependence on the degree of the loss of hearing" (Metz, 1946), the potential use of the acoustic reflex for detection of hearing loss was not explored until much later (Popelka, 1981). The first attempts of hearing loss prediction from ART were made by Niemeyer and Sesterhenn (1974), followed by Jerger et al. (1974) using the SPAR (Sensitivity Prediction from Acoustic Reflex). Niemeyer and Sesterhenn (1974) attempted to divide the subjects into groups according to the anticipated hearing sensitivity (normal, mild, moderate to severe, and profound). Using the SPAR procedure, which represented a modification of Niemeyer and Sesterhann's method (1974), Jerger et al. tried to predict the hearing threshold levels. The SPAR method was further revised by Jerger (1975) and Jerger, Hayes, Anthony, and Mauldin (1978).

Although these aforementioned methods represented innovative exploration of the relations among the ART, stimulus bandwidth, and magnitude of hearing impairment, these approaches incorrectly assumed that the NTD decreases as the hearing impairment increases. This incorrect assumption led to large false-negative rates. The results of research on the ARTs for BBN vs. tonal activators suggest that the NTD does not decrease as the hearing impairment increases beyond about 60 dB HL. The described prediction procedures were plagued by high false-positive rates as well. These errors most likely stem from the large variability in the NTD in normally-hearing adults and adults with mild- or high frequency- impairment (Popelka, 1981; Silman et al., 1984).

Efforts to overcome the limitations of the early predictive methods of Niemeyer and Sesterhann and the revised versions of the SPAR (Jerger, 1975; Jerger, Hayes,

Anthony & Mauldin, 1978) led to the *bivariate-plot method* developed by Popelka, Margolis and Wiley (1976) and Popelka (1981) (which, hereafter, will be referred to as the *traditional bivariate plot*). The bivariate-plot method displays two reflex-related quantities, X and Y, on the coordinates of the bivariate plot. Quantity X, the ratio of the BBN ART to the average of the tonal ARTs (multiplied by 100) is shown on the abscissa, while the ordinate displays the second quantity, Y, which is the average of the tonal ARTs. Since these two quantities increase as the hearing sensitivity declines, presence or absence of hearing loss may be determined from the bivariate plot. The traditional bivariate plot is constructed by plotting of the X and Y quantities based on the ART data from young, normal-hearing adults. Two line segments, one vertical and one with the slope of –1.0, are drafted, so that at least 90% of the data for the normally-hearing young ears are situated to the left of the line segments (Popelka, 1981).

The graph with the line segments then serves as a template for the detection of hearing impairment. To determine whether someone has hearing impairment, the individual's ARTs are obtained, and the ART-related quantities are calculated and then plotted. If the data point falls to the left of the line segments, normal hearing sensitivity is predicted. If the data point falls to the right of the line segments, hearing impairment is predicted. The bivariate plot method is employed with difficult-to-test individuals. The results of research indicate relatively good predictive accuracy for ears with normal hearing or with more significant losses, when mild or high- frequency impairments are absent. The accuracy of the aforementioned traditional bivariate plotting procedure appeared to be affected by subject's age as well (Hall & Koval, 1982).

The effect of age on accuracy of prediction of hearing impairment with the traditional bivariate plotting procedure was thoroughly evaluated by Silman, Silverman, Showers and Gelfand (1984) in their study on 72 normal-hearing subjects (20-69 years of age) and 86 adults with sensorineural hearing impairment of cochlear etiology (20-83 years of age). Analysis of the results revealed age 44 years to be a critical cut-off point on the traditional bivariate plot. Accuracy of prediction was reduced when subjects more than 44 years of age were included. Exclusion of subjects who were 45-years old or older resulted in significant improvement of predictive accuracy of the traditional bivariate plot. This finding was in excellent agreement with observation of Silverman et al. (1983) that the BBN ARTs are increased beginning with the fifth decade of life. Silman et al. obtained further decreases in the false-positive and false-negative rates following modification in the construction of the bivariate plot: The line segments were constructed only after the data points for all the subjects (those with hearing impairment as well as those with normal-hearing sensitivity) were plotted. The line segments were placed (and the slope of the diagonal line segment adjusted) such that 90% or more of the data for the subjects with the mild or high-frequency sloping hearing fell to the left. Improvement of the modification is illustrated by the contrast between the rates obtained via traditional (Popelka, 1981) and modified (Silman, Silverman, Showers, & Gelfand, 1984) bivariate plot (see Table 3).

Table 3

Predictive Accuracy of the Traditional and Modified Bivariate Plots

	Traditional bivariate plot				Modified bivariate plot	
	Subject age: 20-83		Subject age: 20-44		Subject age: 20-44	
	False-Positive	False-Negative	False-Positive	False-Negative	False-Positive	False-Negative
Subjects with ***Normal Hearing Sensitivity***	12 %		3 %		14 %	
Subjects with ***Mild Loss/ High Frequency Sloping Loss***		57 %		42 %		4 %
Subjects with ***Significant Loss*** (Moderate and ***Worse***)		31 %		21 %		4 %

Summary and Conclusions

In summary, acoustic-immittance-based ART research showed aging effects on the ART for a complex signal. Higher BBN ARTs were obtained for older than younger adults (Silman, 1979; Thompson et al., 1980; Gelfand & Piper, 1981; Wilson, 1981; Silverman et al, 1983) This aging effect on the BBN ART is first observed in the fifth decade (Silverman et al, 1983) The effects of spectral density on the ART of a multitonal complex differs with age (Jakimetz et al., 1989). Similarly, the bandwidth effect on the ART of a multitonal complex also differs with age (Jakimetz et al.). Decreased frequency resolution may explain the spectral density findings whereas reduced number and increased width of the critical bands may explain the bandwidth findings in older

adults (Jakimetz et al., 1989). For auditory perception, aging effects first are observed for complex signals, such as speech, before being observed for pure-tone signals.

The utility of the use of the 90th percentiles to detect retrocochlear pathology from acoustic-immittance based ARTs in persons with normal-hearing sensitivity or sensorineural hearing impairment becomes limited when the magnitude of the hearing impairment exceeds about 75 dB HL because the no-response rate for the acoustic reflex for both cochlear and retrocochlear impaired ears becomes high when the hearing impairment exceeds that level. The use of the bivariate-plot method for detection of hearing impairment from acoustic-immittance-based ARTs becomes limited when used on older adults more than 44 years of age (Silman, Silverman, Showers, & Gelfand, 1984). The ART NTD is not adequate for the prediction of hearing impairment in young adults when the duration is shorter than 200 ms and should not be used for this purpose in older subjects regardless of the AR stimulus duration (Emmer, 2000)

For accurate and valid measurement of the ART with the acoustic-immittance-based technique, the highest probe-tone frequency that can be employed is approximately 2000 Hz. At higher probe-tone frequencies, the variations in acoustic pressure along the external auditory canal are large, and sound pressure at a single location no longer defines an acoustic input into the auditory system. At these higher probe-tone frequencies, acoustic immittance provides unreliable assessment of middle-ear function (Khanna & Stinson, 1985; Stinson, Shaw & Lawton, 1982; Wiener & Ross, 1946). Two major factors play role in the observed acoustic pressure variations: First, interference between incident and reflected acoustic pressure waves leads to standing waves resulting in the sound pressure variation as a function of ear canal measurement location; secondly,

the ear-canal and tympanic membrane anatomy such as irregular shape of ear canal with overall taper, or ear canal termination with an oblique tympanic membrane, cause acoustic pressure variations along the canal and even across the tympanic membrane (Khanna & Stinson, 1985).

With the traditional acoustic-immittance based technique, the frequency domain is very restricted, as the probe-tone frequency employed is a single frequency, such as 226 or, less commonly, a higher frequency such as 678 Hz. The results of some studies have shown lower ARTs, on the order of 2-6 dB, when a higher (e.g., 678 Hz) probe-tone frequency is employed as compared with a lower frequency (e.g., 226 Hz) probe tone (Beattie & Leamy, 1975; Burke & Herer, 1973; Porter, 1972; Wilson & McBride, 1978). Thus, it may be interesting and beneficial to evaluate the acoustic reflex related physical changes (impedance, admittance or other quantities) as a function of frequency, rather than at singular frequency. The expansion of the frequency domain for measurement of the ART might unmask the most sensitive frequencies or frequency region for ART measurement. Wideband reflectance, on the other hand, would allow examination of the immittance changes caused by the stapedial reflex with step size as small as 47 Hz in a broad frequency range, such as 200 to 8000 Hz, thereby the investigator to select those frequencies yielding the lowest ART.

The acoustic-immittance based ART procedures in the clinical setting usually employ one or few stimuli presentations at a given intensity level, rather than signal averaging. Signal-averaging has been successfully used, however, to reduce the signal-to-noise ratio in many areas of health technology. Signal-averaging in ART measurement has been employed in research settings. The ARTs obtained with signal

averaging are generally improved as compared with those elicited without signal averaging (Hayes & Jerger, 1983; Jerger et al., 1977; Stach & Jerger, 1984; Terkildsen et al., 1973; Zito & Roberto, 1980). Thus, signal averaging represents a method for enhancement of the ART.

Thus, ART measurement techniques which are based on a broad frequency domain (e.g., wideband reflectance), and which use signal-averaging technology, may yield ARTs at lower thresholds than those based upon a restricted frequency domain and the absence of signal averaging. Consequently, these techniques should be used to re-evaluate aging, hearing loss, spectral density, bandwidth, and other effects on the tonal and BBN ART. Additionally, ART measurement using wideband reflectance may provide additional information about the ear function over a broad frequency domain. If ART differences are seen with the enhanced techniques as compared with acoustic-immittance based procedures without signal averaging, then clinical methods for detection of retrocochlear pathology (e.g., 90^{th} percentiles) and hearing impairment (bivariate plot procedure) need to be revised. In light of the theoretical and clinical results obtained in the past decade, it appears that wideband reflectance method may overcome shortcomings and ambiguities of the earlier acoustic-immittance-based ART research.

ART: Wideband Reflectance Technique

The wideband reflectance technique is based on the transmission line model of ear canal and middle ear, rather than on the lumped elements' concept employed in the acoustic-immittance instrumentation. The transmission line model allows wide range of human ear canal measurements, reaching frequencies as high as 8000 Hz, or perhaps

even higher. The transmission line theory and its wideband reflectance application are explained in detail in APPENDIX B. APPENDIX C provides the wideband reflectance method summary (method by J.B. Allen).

The wideband reflectance technique has been used in number of scientific as well as clinical investigations. The body of wideband reflectance literature can be divided into several categories: (a) research primarily dedicated to the concepts and methodology of wideband reflectance (Allen, 1985; Keefe, 1984; Keefe, 1997; Keefe, Ling & Bulen, 1992; Voss & Allen, 1994); and (b) studies focusing on clinical applications of wideband reflectance (Burns, Harrison, Bulen & Keefe, 1993; Burns, Keefe & Ling, 1998; Feeney & Keefe, 1999; Feeney & Keefe, 2001; Feeney, Keefe & Marryott, 2003; Feeney, Keefe & Sanford, 2004; Feeney & Sanford, 2004; Jeng, Levitt, Wei & Gravel**,** 1999**;** Keefe, Bulen Hoberg Arehart & Burns, 1993; Keefe, Folsom., Gorga, Vohr, Bulen & Norton, 2000; Keefe, Gorga, Neely, Zhao & Vohr, 2003; Keefe & Levi, 1996; Keefe & Simmons, 2003; Keefe, Zhao, Neely, Gorga & Vohr, 2003; Margolis, Saly & Keefe, 1999; Piskorski, Keefe, Simmons &Gorga,1999). As the main focus of this investigation is directed at the ARTs, the foregoing section will concentrate on the wideband reflectance studies concerned with the acoustic reflex.

Burns and his colleagues (1993) obtained pre-contraction and peri-contraction wideband reflectance measurements in a young female with voluntary contraction of middle ear muscles. The wideband reflectance increased for frequencies below about 4000 Hz during the voluntary contraction of the middle-ear muscles. The acoustic-immittance changes associated with the voluntary contraction of the middle-ear muscles were judged to be comparable to those reported in literature for the acoustic reflex.

Feeney and Keefe (1999) successfully used the wideband reflectance system (Keefe, Ling, & Bulen, 1992) to obtain tonal ARTs from three young normal-hearing female subjects at levels that were at least 8 dB lower than those obtained with the traditional immittance-based clinical method. The wideband reflectance technique allowed not only a wide frequency range of measurements, but also evaluation of acoustic-reflex induced changes in the domains of admittance, reflectance and power.

The tonal activator signals of 1000 and 2000 Hz were generated by a Madsen 622 diagnostic audiometer and were delivered via an ER-3A insert earphone into the subject's left ear. The right ear served as the probe ear. This arrangement was used for both acoustic-immittance based (using a GSI 33 middle-ear analyzer) and wideband-reflectance-based ART measurements. With the traditional clinical acoustic-immittance technique, measurement parameters included an ascending intensity method starting at 70 dB HL, activator duration of 1-2 seconds, and a 2-dB intensity step size. The ART was defined as the first activator level to produce a 0.03 mmho or greater change in acoustic admittance on three ascending runs.

The wideband reflectance measurements consisted of two types of data collection: baseline measurements using chirp stimuli in probe ear in the absence of an activating stimulus in the contralateral ear, and measurements using chirp stimuli in the probe ear with activating stimuli in the contralateral ear. The instrumentation arrangements are depicted in Figure 1. The activating stimuli were presented using 2-dB steps at levels within ± 8 dB of the ART as measured earlier in the experiment, using the traditional acoustic-immittance technique. Two ascending runs were completed at each activating stimulus frequency for each subject. The activator duration varied from 2-3 seconds,

depending on the levels of the noise associated with the measurement. A time-averaged wideband reflectance response was obtained based on 8 chirp stimuli in the probe ear. The wideband reflectance response was measured between 200 and 8000 Hz, in 1/12-octave steps. The wideband reflectance technique allowed computation of physical quantities of admittance/impedance, reflectance and power.

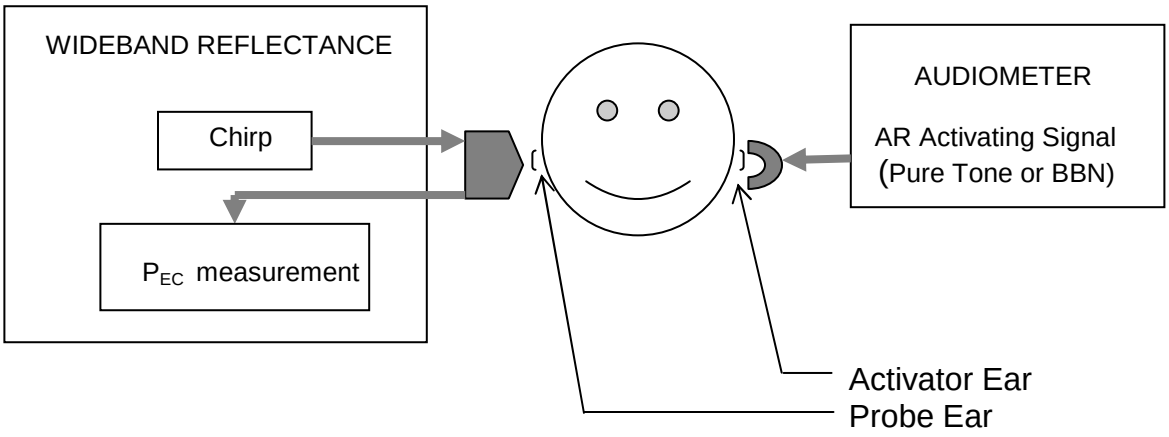

Figure 1. Schematic drawing of instrumentation arrangements for contralateral ART measurement via wideband reflectance; p_{EC} is the ear-canal acoustic pressure used to compute impedance Z, admittance Y, reflectance R and power π, quantities that describe peripheral ear response (The admittance and impedance measurements were normalized by ear canal's cross-sectional area).[Based on Feeney& Keefe (1999, 2001)].

The results of the wideband reflectance measurements were displayed in their report as reflectance-, normalized admittance magnitude- and power level-changes between the baseline condition and the activating signal condition as a function of frequency. The results for wideband measurement for the 1000-Hz activating stimulus were similar to those for the 2000-Hz activating stimulus. Systematic admittance

magnitude and wideband reflectance changes as a function of activator intensity were noted. The most significant acoustic-reflex elicited reflectance changes were observed at the low frequencies below 1000-1200 Hz, with several peaks and notches at higher frequencies. The instrumentation set-up used by Feeney and Keefe (1999) demonstrated that the wideband reflectance method not only can be successfully employed for ART measurement but also that the method yields ARTs for tonal activators at levels that are at least 8 dB lower than those based on traditional acoustic-immittance techniques.

Feeney and Keefe (2001) and Feeney, Keefe and Marryott (2003) used essentially the same instrumentation set-up as in their earlier study (Feeney & Keefe, 1999) for evaluation of the ART. In contrast with their earlier investigation, Feeney and Keefe (2001) examined the ART in response to the BBN activating stimulus using wideband measures of admittance, and power as well as wideband reflectance. (All three quantities are measured across wide range of frequencies, rendering them wideband measures.) The investigation was divided into two experiments. The first experiment was conducted on the same three female participants as in the preceding research (Feeney & Keefe, 1999). The ART was defined using a magnitude and correlation technique. The baseline responses to eight chirps were combined to obtain a time-averaged baseline. The acoustic reflex was tested with activator levels starting at 32 dB below the traditional acoustic-immittance-based threshold and ending at 8 dB beyond that value. The activator was presented in ascending order using 2-dB steps. With the correlation approach, the shape of the wideband reflectance responses was evaluated, whereas with the magnitude method, the shifts in magnitude of the wideband reflectance responses were assessed. With the magnitude approach, the activator-baseline difference was compared with the

baseline variability and an acoustic-reflex was assumed to be present if the former was larger than the latter. Also, in order to be considered acoustic reflex effect, the wideband reflectance shift had to exceed 2 SDs beyond the mean of the absolute difference between baseline conditions over half octave range (equivalent of at least 6 six consecutive frequencies). The lowest level of activator that met these conditions was accepted as ART. The correlation method approach was based on the observation that the response shifts preserved the same basic configuration while the intensity of the activator was decreased. Cross-correlations between the shifts for the highest activator with those elicited by lower-intensity activators were calculated. High positive cross-correlation values were attributed to the acoustic reflex effect. The cross-correlations were transformed via Fisher's Z transformation. And the correlations were assessed using a one-tailed test at a 0.05 level of significance. The lowest activator level whose correlation with the highest activator level response exceeded criterion value ρ_0 was accepted as ART ($\rho_0 = \sqrt{0.3} = 0.548$). (In a regression mode, the corresponding linear regression between two variables with correlation value of 0.548, would be estimated to account for 30% of overall variance).

Only the wideband response data between 250 and 2000 Hz were examined in the analysis. The average difference (across the 3 participants) between the experimental wideband ART and the traditional acoustic-immittance ART ranged from 12.3 dB (average ART difference between the wideband admittance magnitude method and traditional admittance method) to 16.3 dB (when wideband power correlation method results were compared with traditional admittance approach). Comparison between the ARTs obtained via experimental wideband reflectance correlation method and the

traditional admittance technique yielded difference of 14.3 dB. The difference between averaged wideband reflectance magnitude method ARTs and averaged traditional admittance measurements was 13.7 dB.

As it was unclear which analysis technique (magnitude or correlation) yielded lower ARTs, the goal of the second experiment was to improve the design of both techniques and to determine whether a combined test would be superior over either technique. Eventually, the magnitude approach was modified to include an F-test (ratio of the variance in the presence of the activator to the baseline variance) and the correlation method focused on correlations between the responses to successively lower activator presentations rather than the first experiment's cross-correlations between the response to the most intense activator, and a particular lower activator presentation.

The participants of the second experiment were two young adult females and two young adult males. Three wideband response bandwidths were analyzed: 250 Hz to 2000 Hz (range used in the first experiment), 250 Hz to 4000 Hz, and 250 Hz to 8000 Hz. The magnitude method was revised (revised magnitude method) to include an F test to evaluate whether mean-square amplitude of activator response shift was greater than the corresponding baseline change. With the magnitude method, for each wideband response bandwidth, three baseline measurements were obtained to account for baseline variability (i.e., baseline differences among the 3 pairs of baseline measures were computed). In a given wideband response bandwidth, the baseline yielding the smallest baseline difference among the 3 baselines was determined to represent the baseline variance. These three baseline differences were then summed to form a single baseline variance estimate *VARb*. Variance in the presence of the activator, *VARa*, was determined as the

variance across frequency based on the wideband reflectance shift. VARb and VARa were calculated for wideband admittance and wideband power. VARbs and VARas were used to calculate the F ratios, defined as VARa/VARb. A one-tailed F test was assessed with $\alpha = 0.001$. ARTs were determined evaluating the F ratios in descending order, starting from the highest level of activator ART was defined as the lowest activator level associated with a significant F ratio.

The previously used correlation method was modified so that each activator response was correlated with the response from the activator at the next higher level, rather than with the response to the very highest activator. This method was denoted as consecutive correlation method.

The revised magnitude method ARTs and consecutive correlation method ARTs were compared, and the higher (i.e., poorer) from each pair of estimates was chosen as the final ART.

When the most restricted bandwidth was employed, agreement across the three types of measurements (wideband admittance, reflectance, and power) was good. With increasing analysis bandwidth, there was a trend of increasing wideband reflectance ARTs and wideband admittance ARTs, but unchanging wideband power ART. The wideband power ARTs were slightly lower (more sensitive) than the wideband reflectance and admittance ARTs. On the other hand, the false-positive rate (misidentification of a baseline as an acoustic reflex response) was better for the wideband reflectance ARTs than the wideband power or wideband admittance ARTs. The wideband reflectance ARTs for the 250-2000 Hz and 250-4000 Hz bandwidths and with wideband admittance for the former bandwidth were judged to possess good

sensitivity as well as specificity. The average traditional acoustic-immittance ART was 81 dB and the average wideband reflectance ART was 62.5 dB (when the cross-correlation analysis was based on the 250-2000 Hz bandwidth). This improvement in ART for the wideband reflectance as compared with the traditional acoustic-admittance measurement technique was attributed to the combination of improved hardware, noise reduction through computerized signal averaging and the use of a wideband measurement technique (Feeney & Keefe, 2001).

Using a similar methodological and analytical approach, Feeney, Keefe and Marryott (2003) examined the wideband reflectance ARTs, wideband admittance ARTs and traditional acoustic-immittance ARTs using the 1000-Hz activator in 17 young adult subjects and the 2000-Hz activator in a different group of 17 young adult subjects. The activator intensity varied in each run from 24 dB below the acoustic admittance ART to 4 dB above that threshold, with 4-dB step sizes and random order of presentation of intensities. Two runs were completed for each activator frequency. To determine whether response bandwidth affected the ART, the wideband reflectance and admittance responses were evaluated under four bandwidth conditions: with the upper limit cut-off frequencies of 1000, 2000 and 4000 Hz, and with the full bandwidth (250-8000 Hz). The responses were analyzed using the magnitude method utilizing an F-test and the consecutive-correlation method. Following Feeney and Keefe (2001), the higher of the two ART estimates (correlation or magnitude) in the given intensity run was accepted as the ART.

The results from the two intensity runs for each tonal activator were averaged and the averaged value was accepted as the final ART. The wideband admittance and

reflectance ARTs were about 12 dB lower than the traditional acoustic-immittance ARTs. It should be noted that in several subjects both wideband reflectance and wideband admittance acoustic-reflex responses were obtained at the lowest activator level, suggesting that these responses were obtained at suprathreshold levels. When the response bandwidth of analysis was 250-2000 Hz, specificity was 96%, indicating that 96% of baseline responses were correctly rejected (i.e., not accepted as ART-elicited responses). With the cross-correlation statistical method, robust responses occurring from noise rather than the acoustic reflex are accurately rejected. "Conversely, the magnitude method functioned to eliminate sub-reflex-threshold activator conditions for which small changes in middle-ear stiffness occurred that were indistinguishable in magnitude from normal baseline variability" (p. 131, Feeney et al., 2003). The authors also reported that the traditional acoustic immittance ARTs were more narrowly dispersed whereas those obtained using wideband reflectance and wideband admittance measurements are more widely dispersed in normal young adult subjects (Feeney, Keefe, & Marryott, 2003).

Feeney, Keefe and Sanford (2004) investigated ipsilateral and contralateral ARTs for high-frequency tonal activators in 27 young adult subjects with normal-hearing sensitivity using the traditional acoustic immittance-based technique, as well as the wideband reflectance and wideband admittance methods. With the traditional acoustic-immittance technique, only CARTs were measured, and only the 4000-Hz activator was used (maximum intensity used was 92 dB SPL). As the largest acoustic-reflex elicited shift in wideband reflectance and admittance previously was noted to occur at frequencies below 2000 Hz (Feeney, Keefe & Marryott, 2003) care was taken to separate the

frequency distance between the activator and probe stimuli by using a 4000-Hz octave band-filtered click (rather than the broad 250-10,000 Hz chirp used in several previous studies) with an upper cut-off frequency of 2000 Hz for the response bandwidth. Reflectance recordings in a Zwislocki coupler confirmed that the highest activator level produced negligible artifacts. The presumed activator-elicited shifts were evaluated in the frequency range from 314 to 2000 Hz using a statistical method that analyzed both the magnitude of the shifts in reflectance and admittance as well as the correlation of shifts at the lower levels with those at higher activator levels. Traditional acoustic-immittance ARTs and wideband reflectance and wideband admittance ARTs were obtained under all conditions for 9 of the 27 subjects (traditional acoustic-immittance contralateral, wideband reflectance contralateral, wideband reflectance ipsilateral, wideband admittance contralateral, and wideband admittance, ipsilateral). The wideband reflectance and admittance CARTs were comparable and both were lower than the (traditional acoustic immittance-based CARTs by approximately 3 dB. Similar findings were obtained for the ipsilateral and contralateral activator conditions.

Greater acoustic-reflex adaptation to high frequency activators as compared with lower frequency activators was proposed by the authors as possible explanation for this relatively small difference between the traditional and wideband ARTs. It was observed, for example that two subjects had adaptation to the baseline within 2.4 seconds with wideband measures. Adaptation would be more pronounced with wideband than traditional acoustic-immittance measures as the activator duration is longer for the former than latter measure. Another factor in the 3-dB difference might be the intensity and the type of probe stimulus. Feeney, Keefe & Sanford (2004) used a filtered click stimulus

(200–2000 Hz) at 70 dB peSPL. Earlier studies (Feeney & Keefe, 2001; Feeney, Keefe & Marryott, 2003) used a 40-ms chirp having an overall level of 65 dB SPL as measured in a Zwislocki coupler. The authors hypothesized that "it is possible that if the probe were presented at a level slightly below reflex threshold that it could facilitate an acoustic reflex in combination with the activator stimulus, thus lowering the reflex threshold" (Feeney, Keefe & Sanford, 2004, p.427). This phenomenon might be the reflection of the width of the auditory filter for the acoustic reflex.

In summary, the recent ART research has employed the experimental method of wideband reflectance as well as the wideband reflectance-related methods of wideband admittance and wideband power to re-examine the conclusions of the earlier ART research utilizing the traditional acoustic-immittance technique. All of the wideband reflectance studies have shown CARTS that are improved with the wideband reflectance technique as compared with the traditional acoustic-immittance technique. The results of studies are inconsistent regarding the amount of improvement. The difference between wideband reflectance and traditional acoustic-admittance CARTs varied from as low as 3 dB, when 4000 Hz tonal activator and band-filtered click as probe stimulus were used (Feeney, Keefe & Sanford, 2004), up to differences well over 10 dB. For example, Feeney & Keefe (2001) documented CART improvement of 13.7 dB for BBN activator and 250-2000 Hz probe bandwidth when magnitude statistical method was used; 14.3 dB in the same study when correlation approach was applied; 18.5 dB when cross-correlation method was employed. The large improvements in CARTs appeared to hold a promise for improving the diagnostic and predictive capabilities of the ART. Variety of factors may account for these large differences between the wideband reflectance CARTs.:

statistical analysis approach, activator stimulus, probe band width, acoustic-reflex adaptation to high frequency activators, number of participants. Possibility of binaural summation of the BBN activator and probe chirp stimulus should be examined in future as well. None of the studies examined the wideband versus traditional acoustic-immittance NTD or the CART age effects. Future research needs to resolve the existing controversies using larger sample sizes and to evaluate the wideband reflectance versus traditional acoustic-immittance NTD using appropriate criteria for defining the ART.

Theoretical Concepts and Models underlying Acoustic Immittance and Wideband Reflectance Techniques

In order to be able to apply the techniques of traditional acoustic-immittance and wideband reflectance and interpret the obtained results correctly within the realm of the peripheral ear function, it is imperative to understand the underlying theoretical concepts, limitations and assumptions of different models of the ear as well as those of the applied techniques. Moreover, good understanding of the acoustical behavior of the peripheral ear is essential in other areas as well. To name just few: design and calibration of earphones and hearing aids, diagnosis of middle ear pathologies, prediction of the outcomes of auditory (re)habilitation and surgical outcomes, application of current and development of new medical technologies The degree of required precision in the model representing the external auditory canal and tympanic membrane is dictated by the measurement frequency (Stinson & Lawton, 1989).

Lumped Element Model

In the lower range of frequencies, below approximately 2000 Hz, measurements of ear-canal acoustic immittance are valid indicators of the middle ear behavior at the

level of the tympanic membrane (Lawton & Stinson, 1986). At these frequencies, various mechanical components, such as the ossicular chain and the tympanic membrane, can be treated as lumped elements and the middle ear is generally well understood (Stinson, Shaw & Lawton, 1982). The assumption underlying the lumped element approach is that specification of acoustic pressure at a single location uniquely defines the acoustic input into the ear. At 1000 Hz, for example, the diameter of the tympanic membrane is only about 2.5% of the wavelength of the 1000-Hz tone, and the longest dimension of the external auditory canal, about 25 mm, is significantly less than the quarter-wavelength of that pure tone. In other words, under the lumped element concept based upon measurement with the traditional acoustic-immittance technique, the acoustic pressures at the ear-canal measurement point and at the level of tympanic membrane are identical. Equality of acoustic pressures at these sites occurs only at the low frequencies below approximately 2000 Hz, depending on the specific ear-canal anatomy. (Stinson, Shaw & Lawton, 1982; Khanna & Stinson, 1985). At 10,000 Hz, on the other hand, if a specific point in the ear canal has been chosen for measurement of traditional acoustic immittance, and the impedance value at that point is measured to be (300 + 200i) cgs acoustic ohms, then it may be shown that ± 1 mm change in the measurement location would cause the resistance to vary between 100 and 600 ohms and the reactance to vary between 0 and 400 ohms (Stinson, Shaw, & Lawton, 1982).

Transmission Line Model

At higher frequencies, where the lumped element representation breaks down, a more complicated approach is required. As mentioned earlier, large variations of acoustic pressure along the external auditory canal occur at high frequencies, and the magnitude

and frequency dependence of a reference signal would depend upon the position chosen for the reference measurement (Khanna, Stinson, 1985; Wiener & Ross, 1946).

Up to 4000 Hz, transmission line theory predicts the pressure variations along the entire ear canal length when the ear canal is represented by a straight tube of uniform cross-section area with the tympanic membrane terminating the tube perpendicularly (Stinson & Lawton, 1989). If the measurements are limited to the central axis, this model is appropriate for frequencies as high as 8000 Hz. (Stinson & Lawton, 1989). At frequencies above approximately 10,000 Hz in humans, significant spatial variations in acoustic pressure can be expected in the immediate vicinity of the tympanic membrane (Stinson & Shaw 1982). The external auditory canal acoustic pressure variations must be considered when specifying the acoustical input to the ear at high frequencies. The main factors and relationships influencing ear-canal acoustic pressure variations (Khanna & Stinson, 1985) are as follows: (a) reflection of substantial portion of the energy entering the external auditory canal; (b) standing waves produced by the interference between incident and reflected waves that may yield strong acoustic pressure variation along the ear canal, especially near a standing wave pattern minimum; (c) ear canal geometry, the ear canal taper in particular, which affects the acoustic pressure distribution so that the acoustic pressure extrema shift and the altered height of adjacent maxima produce modifications in the pressure distribution because of external auditory canal geometry;(d) the oblique rather than perpendicular termination of the external auditory canal by the tympanic membrane causes variation in acoustic pressure over the tympanic membrane as well as along the main body of the ear canal; (e) vibration of the tympanic membrane in sections rather than as a single unit at the high frequencies (Khanna & Tonndorf,

1972); the acoustic pressure measurement will depend upon how the particular section of the tympanic membrane contributed to the middle-ear motion (Khanna & Stinson, 1985).

Wideband Reflectance Technique

Based on transmission line theory (see APPENDIX B), energy reflectance $\mathcal{R}$, is a quantity that is less ambiguous than impedance or admittance because it is more stable along the length of the ear canals; it is computed from the acoustic pressure in the ear canal. The energy reflectance magnitude is essentially the same at the beginning as at the termination of the ear canal. The error is negligible (Allen, 1985; Voss & Allen, 1994). Thus, the acoustic pressure measurement in the beginning of the ear canal allows estimate of energy reflectance magnitude at the tympanic membrane. For detailed information see APPENDIX B. Energy reflectance $\mathcal{R}$ is related to the pressure reflectance coefficient (sometimes simply referred to as reflectance) K, ratio of reflected acoustic pressure p_r to incident acoustic pressure p_i ($K = p_i / p_r$) . In a given frequency, energy reflectance $\mathcal{R}$ equals to reflectance K squared ($\mathcal{R} = K^2$). At frequencies essentially up to about 8000 Hz, energy reflectance $\mathcal{R}$ and pressure reflectance coefficient K can be determined using the previously mentioned wideband reflectance technique (Allen, 1985; Voss & Allen, 1994). For detailed information on the technique see APPENDIX C.

Standing Wave Ratio (SWR) Technique

Another approach, allowing measurements of energy reflectance $\mathcal{R}$ or pressure reflectance coefficient K even in the frequencies above 8000 Hz, going up to about 13 kHz, is the standing wave ratio method (Lawton Stinson, 1986; Stinson, 1990). Incident acoustic waves traveling towards the tympanic membrane are met by reflected waves propagated outward from the tympanic membrane. Their interactions produce standing

wave patterns in the canal. These patterns may be described by standing wave ratios, SWRs, defined as the difference between the acoustic pressure maximum, L_{max} and acoustic pressure minimum L_{min}. The energy reflectance $\mathcal{R}$ then may be calculated from SWR (Stinson, Shaw & Lawton, 1982) as follows

$$SWR \equiv L_{max} - L_{min}$$

$$SWR = 20 \log [(1+ \mathcal{R}^{1/2}) / (1 - \mathcal{R}^{1/2})] \quad dB$$

Series of measurements of sound pressure distribution in thirteen normal ear canals have shown the SWR range to be between 18 and 24 dB at 8000 Hz, and corresponding energy reflectance to range from 60% to 78 % (Stinson, Shaw & Lawton; 1982).

Above 8000 Hz, the tympanic membrane is no longer small when compared with the wavelength of the stimulus. The inclination of the tympanic membrane, its non-planar shape, and the extreme non-uniformity of its vibration pattern cannot be disregarded. Studies have already demonstrated that wideband reflectance measurement of the middle ear is speedy. Although wideband reflectance measurement largely is an experimental technique, it has the potential for becoming a clinical technique for measurement of middle-ear function. The standing wave ratio method is tedious and time consuming. However, it has the potential to validate results of wideband reflectance investigations

CHAPTER III: METHODS

Participants

Participants were recruited from flyers distributed in Graduate School University Center, CUNY and Brooklyn College, CUNY. All test sessions were scheduled at days and times that were convenient for the participants. Participants were briefed about the purpose of the study and counseled regarding their audiologic findings. (The subject informed consent form appears in APPENDIX D, Figure D1.)

To rule out any possible gender effect, gender was restricted to females. For the independent variable of age, participants were classified dichotomously as younger versus older adult females. The younger adult group comprised 10 women between twenty and thirty years of age. The older adult group comprised 10 women between sixty and seventy years of age.

All participants met the following criteria for study inclusion: (a) normal otologic and audiologic history; (b) normal otoscopic findings; (c) pure-tone air-conduction thresholds ≤ 20 dB HL (re: ANSI 1996) at 250, 500, 1000, 2000, and 3000 Hz; and ≤ 25 dB HL at 4000 Hz; (d) air-bone gaps not exceeding 10 dB at all frequencies between 250 and 4000 Hz; (e) peak-compensated static-acoustic admittance (SAA) between 0.3 and 1.6 mmho; (f) tympanometric peak pressure (TPP) > -50 daPa); (e) CARTs for 500, 1000 and 2000 Hz tonal activators measured using clinical acoustic-immittance approach (5-dB steps) not exceeding the 90th percentiles (Silman & Gelfand, 1981); (g) equivalent ear-canal volume not exceeding 2.5 mmho; (h) BBN CART measured using clinical acoustic-immittance approach (5-dB steps) ≤ 95 dB HL to avoid loudness discomfort during testing.

Instrumentation

Participants were tested in a single-walled Industrial Acoustics Company, Inc., series 400, sound-attenuating booth. The ambient noise in the sound-attenuating booth was measured using digital sound level meter (Quest Model 2900) with octave-band analyzer. The levels of the ambient noise were as follows: 26.3 dB SPL at 250 Hz, 20.5 dB SPL at 500 Hz, 16.3 dB SPL at 1000 Hz, 14.8 dB SPL at 2000 Hz, 15.8 dB SPL at 4000 Hz, 17.2 dB SPL at 8000 Hz.

Pure-tone air- and bone-conduction testing was performed with a two-channel diagnostic audiometer (Grason-Stadler GSI 61) with insert earphones (Etymotic ER 3-A) periodically calibrated using an HA-2 (2-cc) coupler with rigid tube attachment according to ANSI (S3.6-1996) standards. Bone-conduction calibration was performed periodically according to ANSI S3.6-1996 standards using a mechanical coupler that meets ANSI S3.13-1987 (R 1997) design specifications. Biologic checks of the audiometer were performed each day that it was used, prior to assessment of any participant.

Traditional acoustic-immittance tympanometric and acoustic-reflex assessment using the 226-Hz probe tone were performed with a Grason Stadler Middle-Ear Analyzer (GSI 33). Calibration was performed in accordance with ANSI S3.39-1987 (R2002) standards. For CART testing, the activating signals were generated by the acoustic-immittance device and presented into the activator ear through an insert receiver. The CARTs were inferred from changes in acoustic admittance of the ear the middle ear admittance (during presentation of the activating stimuli) that were assessed using a 226-Hz probe tone in the probe ear, which was contralateral to the ear receiving the activating

stimuli. Activator duration was 3000 ms and the interstimulus interval was at least six seconds (Jerger & Oliver, 1987).

Wideband reflectance assessment of the CARTs was performed using a Grason Stadler (GSI 16) diagnostic audiometer with an insert earphone, wideband reflectance device, and synchronization switch. The instrumentation set-up is shown in Figure 2.

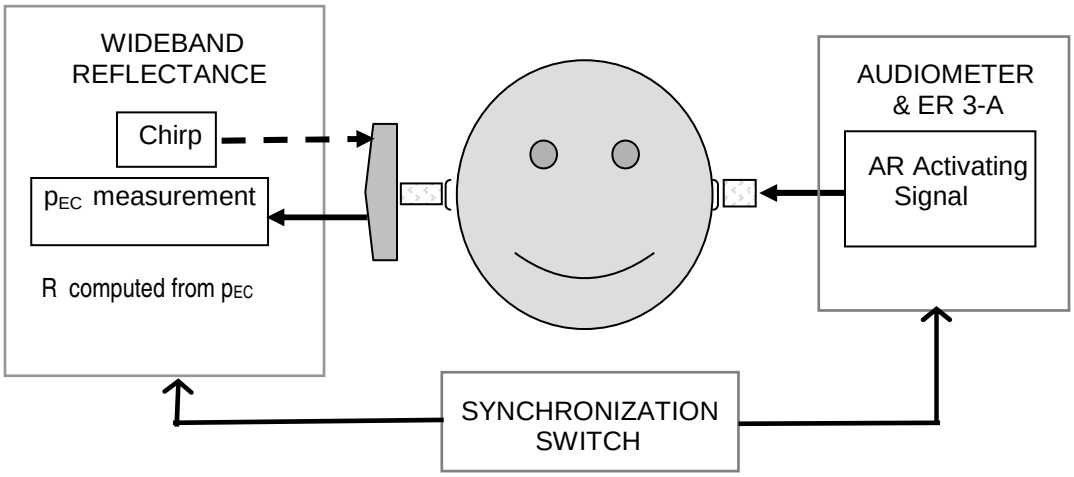

Figure 2. Schematic drawing of instrumentation set-up for CART measuring using wideband reflectance

Wideband reflectance measurements of the CART for BBN and tonal activators in the frequency range of 200-6000 Hz were obtained with the Mimosa Acoustics Clinical Reflectance System. The instrumentation consisted of a laptop computer with a PCMCIA (Personal Computer Memory Card International Association) driver/adapter, personal computer printed circuit board (type II PCMCIA card for audio data acquisition and delivering, and for digital signal processing), probe interface cable (to connect the probe to the personal computer printed circuit board) and ER-10CP probe (same as DP 2000, with two output transducers and one input transducer), and a four-cavity calibration device. The probe interface cable also functioned as a pre-amplifier for the probe.

First, during calibration, a sequence of chirps delivered through an ER 10CP probe fitted with compressible foam ear-tip was used to obtain the signal-averaged in-situ pressure frequency responses in four calibration cavities. Then, the system automatically computed the transducer source pressure and source impedance that were later used by the system, along with the ear canal pressure measurements, for the ear-canal wideband reflectance computations.

The chirps were also delivered into the ear canal during the ear-canal measurements. The intensity level of the chirps was estimated to be 60 dB SPL and was verified during the ear-canal calibration measurement that preceded the actual ear-canal wideband reflectance measurement. The chirp intensity was sufficiently high to minimize otoacoustic emissions and sufficiently low to preclude acoustic-reflex activation (Voss & Allen, 1994). The chirp stimulus is a short-duration click signal that is all-pass filtered with a group delay proportional to the signal's overall frequency range during a period of about 50 ms. "The output chirp is akin to a rapidly swept sine wave with frequency dependent amplitude" (Burns, Keefe, & Ling, 1999, p. 464). Twenty-four chirps were presented over two seconds.

The four-cavity calibration of the probe was performed prior to testing of each subject. (The principles of the calibration procedure are described in detail in APPENDIX B and APPENDIX C). The compressible foam ear-tip of the probe was inserted into the calibration cavities during calibration or into the ear canal during the testing, so that the rear of the foam plug was flush with the tube entrance, or ear-canal entrance. The length of the foam plug was about 12 mm. On some earlier versions of the wideband reflectance device (which had a broader frequency range than the device used

in this study), the microphone probe tip protruded about 3 mm beyond the edge of the foam plug to reduce evanescent mode coupling between the flow source and probe tip (Voss & Allen; 1994). In the wideband reflectance device used in this study, the microphone probe tip terminated together with the tip of the earphone's microphone's plane at the so-called sending point, which was located at the same plane as the earphone's measurement point. (For a further description, see APPENDIX A, Figures A4. and A5.). The nominal ear-canal length from the entrance to the tympanic membrane, based on Fletcher's measurements, was assumed to be 23.5 mm (Voss & Allen, 1994). Depending on the exact probe tip insertion and individual anatomical variation, the distance between the microphone probe tip and the tympanic membrane was in the vicinity of 8.5 mm. Acoustic pressure measurements obtained at this ear-canal measurement point served as the basis for the computations of the wideband reflectance magnitude that describe events at the level of the tympanic membrane, where direct measurement is impossible (Voss & Allen, 1994).

A synchronization switch was employed to time-lock the presentation of the acoustic-reflex activating stimulus with the onset of the wideband reflectance measurement, so that the acoustic-reflex response would be elicited during chirp stimuli presentation for measurement of p_{EC}. The chirp presentation and p_{EC} measurement lagged behind the onset of the acoustic-reflex activator by one second. The time relations among presentations of the acoustic-reflex activating stimuli (pure tone and BBN) and the wideband chirp stimuli and measurement of ear canal pressure (p_{EC}) are depicted in Figure 3.

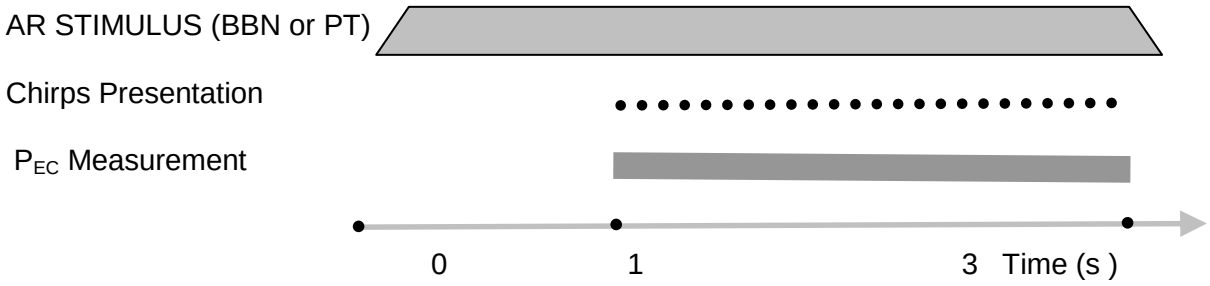

Figure 3. Time relations among presentations of the acoustic-reflex activating and wideband chirp stimuli and measurements of p_{EC}.

Design and Variables

The study design was a mixed, repeated-measures design (combined between-subjects design and within-subjects design). For the between-subjects design, the classification variable was age, which was bivalent (younger vs. older adults). For the repeated measures, within-subjects design, the independent variables were as follows: (a) measurement technique (traditional acoustic-immittance vs. wideband reflectance); and (b) acoustic-reflex activating stimulus (1000-Hz tonal activator vs. BBN activator). The design types, independent variables, and their values and symbols are listed in Table 4.

The dependent variables, for both the between-subjects and within-subjects designs, were the CART (dB HL) and NTD (dB). The CART that was measured using traditional acoustic admittance was labeled AI-CART, and the CART that was measured using wideband reflectance was labeled WBR-CART. Similarly, the WBR-NTD referred to the NTD based on the wideband reflectance, and AI-NTD referred to the NTD based on traditional acoustic immittance.

Table 4

Study Design and Variables

Independent variable	Independent variable	Value/type of Independent variable	Symbol / Abbr.
Within subjects	Measurement approach	Acoustic immittance	AI
		Wideband reflectance	WBR
Within subjects	Activating signal	Tonal (1000 Hz)	1000 Hz
		Broad-band noise	BBN
Between subjects	Age	20-30 years	
		60-70 years	

Procedures

The principal investigator read out the consent form to each potential participant and then gave the informed consent form to the potential participant to read. The principal investigator advised each participant to read the form carefully and encouraged each participant to ask any questions he or she may have relating to the study and participation in it. Testing commenced upon obtaining informed consent. All testing was performed in the audiometric booth (previously described in the ***Instrumentation*** section) of the hearing science laboratory.

Screening was administered to determine if the potential participant met the inclusion criteria. Based on the results of the screening, if the potential participant met the inclusion criteria she was enrolled in the study and underwent CART assessment using the traditional acoustic immittance versus the wideband reflectance approaches. The screening comprised elicitation of a history, inspection of the ear canals with

otoscopy, pure-tone air- and bone-conduction threshold tests, tympanometry, and acoustic-immittance CART (AI ART) testing using pure-tone and BBN stimuli (5-dB step size) with the 226-Hz probe tone. The screening CART was defined as the lowest stimulus intensity in dB HL yielding the smallest detectable change in middle-ear acoustic admittance. The experimental CART was determined using the traditional acoustic-immittance technique (AI CART) and wideband reflectance (WBR CART). The order of the CART measurement approach, AI versus WBR, was counterbalanced. The CARTs for the tonal (1000-Hz) and BBN activators were obtained from one ear (ear selected was counterbalanced) of each participant. The activator presented (tonal vs. BBN) was counterbalanced.

The CART measured using the traditional acoustic-immittance technique was determined using ascending runs with 2-dB intensity steps and a starting level at circa 8 dB below the screening CART. The CART was defined as the first activator to yield a 0.02 mmho change in SAA on two ascending runs. In order to confirm the CART, the measurement was repeated with an activator presented at 2- and 4- dB above the CART. Equivalent or greater changes in acoustic admittance magnitude were obtained at these suprathreshold levels.

The WBR CARTs were obtained for the 1000-Hz tonal activator and BBN activator presented during the test and retest sessions, yielding a total of altogether four WBR CARTs. The WBR CARTs were obtained through the analysis of differences between the WBR response in the presence of a contralateral activator (WBR activator response) and WBR responses in the absence of an activator (WBR baseline measurements with the activator set at -10 dB HL). The order of baseline and activator-

response measurements was alternated. The activator starting level was about 26 dB below the AI CART determined during the screening procedure. The maximum level of the activator did not exceed the screening AI CART by more than about 4 dB unless visual observation during the collection of WBR ART responses suggested that WBR CART was not reached. In those cases the activator level may have exceeded AI CART by up to circa 8 dB. For example, for a participant whose screening AI CART was 80 dB HL, the activator range during WBR CART testing was 54-84 dB HL. If the WBR response at 84 dB appeared to be identical to the preceding baseline, an additional 1 to 2 baselines and 1 to 2 activator responses at 86 dBHL and 88 dBHL, respectively, would be obtained. As for the traditional acoustic-immittance CART, the activating stimuli were presented using ascending runs with 2-dB intensity steps. The 30-dB activator range (16 highest WBR activator responses and their preceding 16 WBR baselines) during the test and retest sessions were used to determine the four WBR CARTs (test tonal WBR CART, test BBN WBR CART, retest tonal WBR CART and retest BBN WBR CART). Resultantly, across both activators and sessions, a total of 64 baselines and 64 activator responses were obtained for each participant for the computation of 4 WABR CARTs for each participant. The computations of the WBR CARTs were performed post testing and are discussed in the results section.

Upon completion of the testing, the principal investigator debriefed the participant about the audiologic findings. A summary of the study findings was submitted to the participants upon the conclusion of this investigation.

Data Recording

The *consent* form is shown in APPENDIX D, Figure D1. The screening procedure results were documented on the individual *Otologic and Audiologic History and Otoscopy Record* (See APPENDIX D, Figure D2) and the individual audiometric results were marked on the individual *Audiogram* form (see APPENDIX D, Figure D3). A summary of the individual pure-tone air- and bone-conduction thresholds for all participants is shown in Table 5. Records of the individual GSI-33 tympanometric and AI-CART results were retained. A summary of the individual TPPs, SAAs, , and 500-, 1000-, 2000-Hz and BBN screening CARTs for all participants is displayed in Table 6.

Experimental younger and older group AI CART results are presented in the *Results* section. Each individual experimental AI CART testing GSI 33 instrumentation print-out was retained and the individual results could be reviewed together with the WBR-CART results in the *Appendix E* section.

The WBR baselines and activator responses were stored in the Mimosa laptop for off-line analysis. An example of baseline and activator responses is presented in Figure 4. These baseline and activator responses show the absence of the acoustic reflex as these curves overlapped nearly completely.

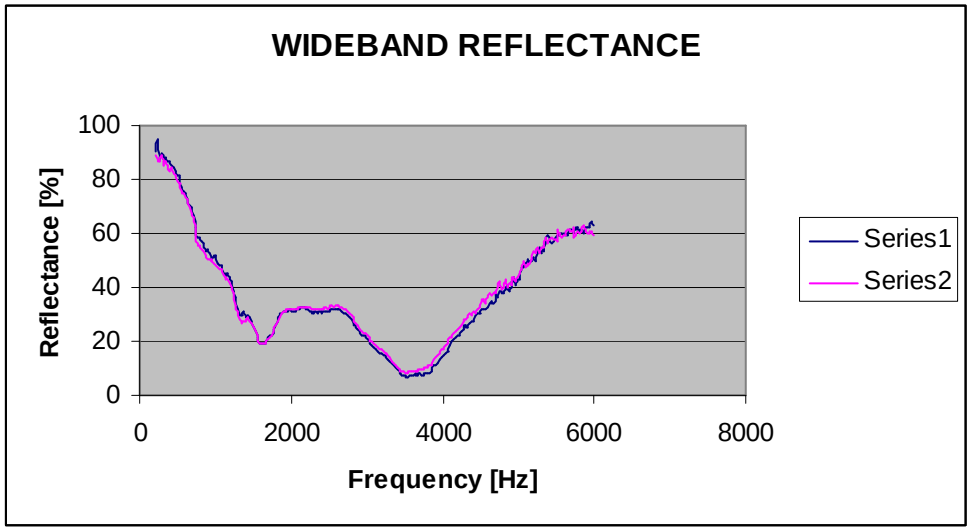

LEGEND

Series1: Baseline response

Series 2: Activator response

Figure 4. Baseline and activator response recordings for BBN retest in Subject 001. The BBN activator was presented at 48 dB HL.

One Mimosa file captured 8 WBR measurements: 4 baseline responses and 4 activator responses. So, four files captured responses for a single activator and eight files captured all responses for both activators; and sixteen files captured all the responses for both activators under both the test and retest conditions used for the WBRCART determination. One baseline or activator response encompassed measurements across about 250 frequencies. Thus, one participant's recordings across 250 frequencies for sixteen baselines and sixteen activators, for both activators, in both the test and retest conditions included 32,000 measurements. The raw data for the sixteen Mimosa files for each participant were labeled and exported to Excel for reformatting so they could be statistically analyzed using SAS statistical software. An example of raw test data as recorded in Microsoft Excel File is presented in APPENDIX A, Figure F1.

Statistical Analysis

Several series of statistical comparisons were performed using AI CARTs and WBR CARTs obtained from the younger and older participant groups. When WBR CARTs were employed only test CARTs were used, except when test-retest reliability was examined. Also, comparisons were drawn between the obtained AI CARTs and NTDs, and those obtained by Silman (1979). Grubb's test [Extreme studentized deviation (ESD) method] was used to identify CART and NTD outliers. Paired two-tailed t-test and Wilcoxon signed ranks test were used for within-subjects comparisons. Unpaired two-tailed t-test (independent groups two-tailed *t*-test) and Mann-Whitney test were used for between-subject comparisons. The parametric *t*-test was used when the data were assumed to be normally distributed. The Wilcoxon signed ranks test and Mann-Whitney test were used for non-parametric analyses when outliers were included.

CHAPTER IV: RESULTS

This study focused on three main goals :(a) development of the working criterion for the wideband CART identification; (b) comparison of the tonal (1000-Hz) and BBN CART obtained with the two measurement approaches (CARTs obtained with traditional acoustic immittance technique versus wideband CARTs); (c) to examination of the effect of age on the wideband reflectance and traditional tonal and BBN CARTs. In order to achieve these goals series of tests on the participants as well as mathematical computations had to be performed before the actual CARTs were available and could be analyzed. The *Results* chapter presents the younger and older group results in a logical order that allows the reader to see the rationale behind the WBR CART criterion and The *Results* chapter is divided into 2 sections: *Results* and *Analysis*. The *Results* section is then divided into 3 parts: *Audiometric Results, Acoustic Immittance Results, Wideband Reflectance Results*. The last part is then subdivided into subsections. The individual results are presented in APPENDIX E.

Audiometric Results

The Younger and Older group audiometric results are presented in Table 5. All the individual thresholds were within normal clinical limits and met the inclusion criteria (See CHAPTER III, Methods, Participants). Individual audiometric results may be seen in APPENDIX E, Table E1.

Table 5

Younger and Older Group Mean Pure-Tone Air-Conduction Thresholds (dB HL), Standard Deviations (S.D.), Standard Errors of Mean (SEM) and 95% Confidence Intervals (95% CI) at the Test Frequencies 250 through 4000 Hz in the Right and Left Ear

Group	Parameter	Right ear air-conduction thresholds						Left ear air-conduction thresholds					
		250 Hz	500 Hz	1000 Hz	2000 Hz	3000 Hz	4000 Hz	250 Hz	500 Hz	1000 Hz	2000 Hz	3000 Hz	4000 Hz
Younger	N	10	10	10	10	10	10	10	10	10	10	10	10
	Mean	5.50	5.50	5.50	5.50	3.00	4.50	7.0	6.50	4.50	3.50	3.50	4.50
	S.D.	5.50	4.38	4.97	6.43	6.32	3.69	4.22	6.26	5.99	7.09	5.80	4.38
	SEM	1.74	1.38	1.57	2.03	2.00	1.17	1.33	1.98	1.89	2.24	1.83	1.38
	95% CI	1.6 - 9.4	2.4 – 8.6	1.9 – 9.1	0.9 – 10.1	-1.5 – 7.5	1.9 – 7.1	4.0 – 10.0	2.0 – 11.0	0.2 – 2.8	-0.6 – 7.6	-0.7 – 7.7	1.4 – 7.6
Older	N	10	10	10	10	10	10	10	10	10	10	10	10
	Mean	13.50	13.00	12.00	10.50	12.50	16.50	13.50	12.00	11.50	11.50	12.00	17.0
	S.D.	4.12	4.22	5.37	4.97	5.40	7.09	4.12	4.22	4.12	2.42	6.32	6.32
	SEM	1.30	1.33	1.70	1.57	1.71	2.24	1.30	1.33	1.30	0.76	2.00	2.00
	95% CI	10.6 – 16.4	10.0 – 16.0	8.2 – 15.8	6.9 – 14.1	8.6 – 16.4	11.4 – 21.6	10.6 – 16.4	9.0 - 15.0	8.6 – 14.4	9.8 – 13.2	7.5 – 16.5	12.5 – 21.5

Acoustic Immittance Results

A summary of the younger and older group mean TPPs (daPa), SAAs (mmho), and 500-, 1000- and 2000-Hz tonal and BBN- CARTs (dB HL) and their standard deviations (S.D.), standard errors of mean (SEM) and 95% Confidence Intervals (95% CI) as obtained via the acoustic-immittance method (AI-CART) is presented in Table 6. When the right ear was the test ear, the probe was in the right ear for the TPP and SAA but was in the left ear for the CART (activator was in the test ear). Similarly, when the left ear was the test ear, the probe was in the left ear for the TPP and SAA, but was in the right ear for the CART. Comparison of this study results with the same type of

measurements by other investigator is presented in *Analysis* section of this chapter. Individual participants' TPPs (daPa), SAAs (mmho), and 500-, 1000- and 2000-Hz tonal and BBN- CARTs (dB HL) as obtained via the acoustic-immittance method (AI-CART) may be reviewed in APPENDIX E, Table E2, E3.

Table 6.

Younger and Older Group Mean TPPs (daPa), SAAs(mmho), and Tonal and BBN CARTs (dB HL) and their Standard Deviations (S.D.), Standard Errors of Mean (SEM) and 95% Confidence Intervals (95% CI) with the Acoustic-Immittance Method

		Right ear						Left ear					
Group	Parameter	TPP	SAA	500-Hz AI CART	1000-Hz AI CART	2000-Hz AI CART	BBN AI CART	TPP	SAA	500-Hz AI-CART	1000-Hz AI CART	2000-Hz AI CART	BBN AI CART
Younger	N	10	10	10	10	10	5	10	10	10	10	10	5
	Mean	6.00	0.60	95.50	89.30	92.50	76.40	5.00	0.66	91.50	89.50	89.00	74.80
	S.D.	9.37	0.19	6.85	4.74	5.99	2.61	5.27	0.32	4.12	4.50	6.58	2.28
	SEM	2.96	0.06	2.17	1.50	1.89	1.17	1.67	0.10	1.30	1.42	2.08	1.02
	95% CI	-0.7 – 12.7	0.5 – 0.7	90.6 – 100.4	85.9 – 92.7	86.2 – 94.8	73.1 – 79.6	1.2 – 8.8	0.4 – 0.9	88.6 – 94.4	86.3 – 92.7	84.3 – 93.7	72.0 – 77.6
Older	N	10	10	9	10	10	5	10	10	10	10	10	5
	Mean	1.50	0.76	92.22	88.50	86.00	78.00	9.50	0.67	94.50	89.18	87.50	80.40
	S.D.	16.67	0.40	7.55	7.15	6.58	8.12	12.57	0.35	8.32	5.16	6.77	5.73
	SEM	5.27	0.13	2.52	2.26	2.08	3.63	3.98	0.11	2.63	1.63	2.14	2.56
	95% CI	-10.4 - 13.4	0.5 – 1.0	86.4 – 98.0	83.4 – 93.6	81.3 – 90.7	67.9 – 88.1	0.5 – 18.5	0.4 – 0.9	88.6 – 100.5	86.1 – 93.5	82.7 – 92.3	73.3 – 87.5

Wideband Reflectance Results

Wideband Reflectance CART (WBR-CART) Definition

The WBR CART was defined as the lowest activator level which resulted in a computed change in the activator-elicited reflectance from the baseline reflectance in the absence of the activator. The threshold is determined for specified criteria relating to the frequency range of the change and the magnitude of the difference between the baseline and activator-elicited reflectance responses.

Activator-Baseline Difference (ABD)

The term activator-baseline difference (ABD) refers to the shift in reflectance $\Delta\mathcal{R}$ (f) calculated as a difference between the baseline reflectance and activator reflectance at a given frequency. The ABDs were computed at all WBR frequencies for all activator levels as the difference between the activator WBR value $\mathcal{R}_{\text{ACTIVATOR}}$ (f) and the immediately preceding baseline WBR value $\mathcal{R}_{\text{BASELINE}}$ (f):

$$\text{ABD (f)} = \Delta\mathcal{R}\,(\text{f}) = \mathcal{R}_{\text{ACTIVATOR}}\,(\text{f}) - \mathcal{R}_{\text{BASELINE}}\,(\text{f})$$

WBR CART Definition

The WBR CART represents the lowest activator level that was associated with an ABD outside the ± 1 standard deviation (SD) of the mean reflectance baseline for at least ten adjacent frequencies, and that produced greater ABDs at all higher activator levels. A response occurring only at the highest level was accepted as a CART if corroborated by consistent pattern of ABD change in ABD graphs (See *ABD Graphs*). This approach was designed to prevent the misidentification of ABDs associated with natural baseline variance as acoustic-reflex responses.

Baseline SD

The baseline SDs were calculated as follows: WBR baseline values, $\mathcal{R}_{BASELINE}$, was used to determine four mean baselines, $\overline{\mathcal{R}}_{BASELINE}$, for each of the four tests, at every WBR frequency (248 frequencies) for each participant: BBN CART Test, BBN CART Retest, 1000-Hz WBR CART Test, 1000-Hz-WBR and CART Retest. Each of these tests involved 16 baseline measurements (associated with each of the 2-dB intensity steps) for

each of the 248 frequencies. So, for example, the mean baseline values for the BBN CART Test, $\mathcal{R}_{BASELINE\ TEST\ BBN}(f)$, were calculated as follows:

$$\overline{\mathcal{R}}_{\text{BASELINE TEST BBN}}(f) = \frac{\sum_{1}^{16} \mathcal{R}_{\text{BASELINE TEST BBN}}(f)}{16}$$

where the reflectances at each of the 16 baselines are averaged at a given frequency. The baseline variance value, $SD_{BASELINE}$, was computed for each of the four tests at each WBR frequency. For instance, the SD value for the BBN-CART Test, $SD_{BASELINE\ TEST\ BBN}(f)$, was computed using the following formula:

$$\text{SD}_{\text{BASELINE TEST BBN}}(f) = \sqrt{\sum_{1}^{16} \{[\mathcal{R}_{\text{BASELINE TEST BBN}}(f) - \overline{\mathcal{R}}_{\text{BASELINE TEST}}(f)]^2\}/(16-1)}$$

where the 16 squared differences betweens the baseline reflectance and the mean baseline reflectances are summed at a given frequency.

Graphs depicting ± 1 SD (illustrated in blue) of the mean baseline reflectance and the individual ABDs at a specific intensity and activator (BBN vs. 1000-Hz) were constructed for all tests and presentation levels. A sample graph is shown in Figure 5.

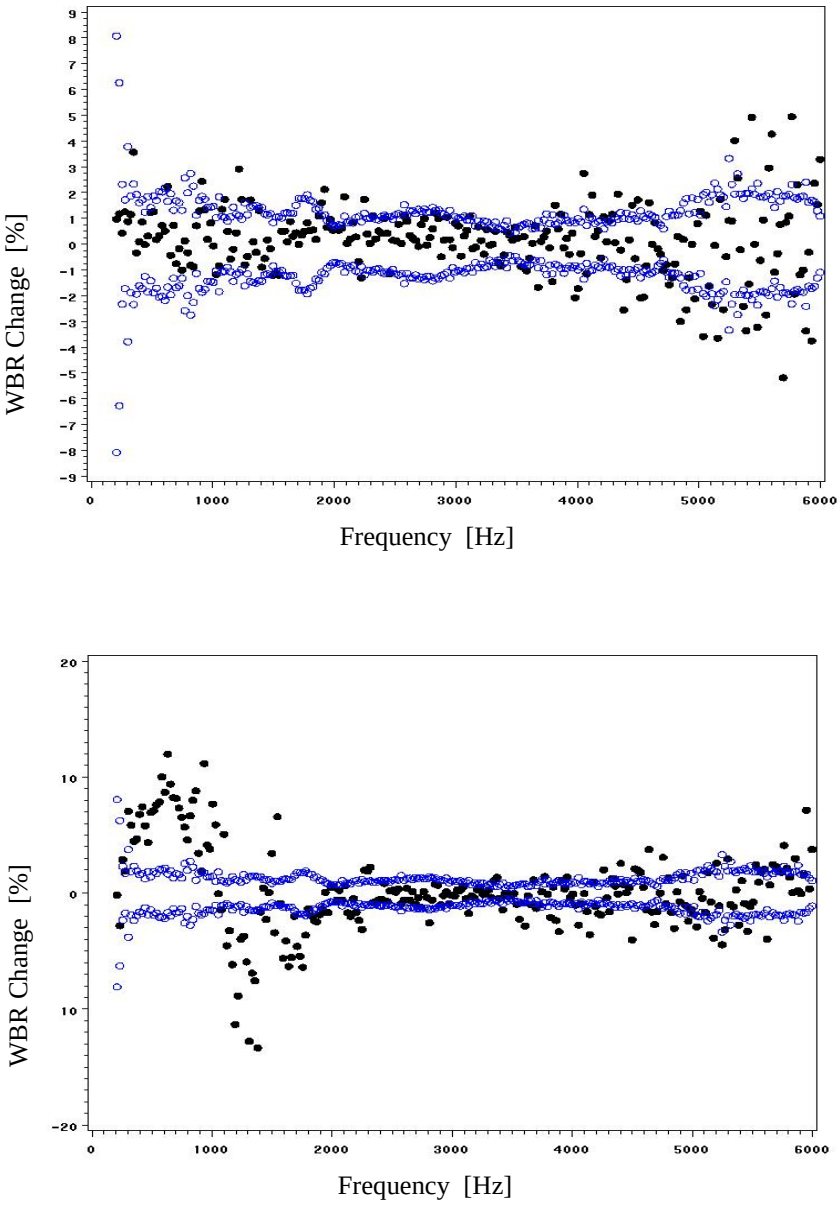

Figure 5. ABDs for 52-dB HL BBN activator (upper graph) and 72-dB HL BBN activator (lower graph) obtained during the Test of subject 003. The probe stimulus frequency is shown on the horizontal axis. The ABD (%) is shown on the vertical axis. The ± 1-SD limits (from the baseline means) are shown in blue.

Graphs showing the ± 1-SD limits from the baseline means (shown in blue) and individual ABDs at the CART level and at specified levels below and above the CART for each participant are shown in APPENDIX F.

Algorithm for the WBR-ART Criterion

The algorithm for the WBR-CART criterion in the SAS® program was constructed as follows:

For each subject, a data file was created with the following fields/variables:

- *Frequency*
- *Intensity*
- *Baseline*
- *Response*
- *Shift*, which equaled (activator associated response – baseline)
- *Baseline Mean*, which was the mean across all 16 baseline measurements at that frequency
- *Baseline SD*, which represented ± 1 SD of the Baseline Mean at that frequency
- *Above*, which was an indicator of whether the reflectance shift (ABD) was greater than a certain multiple of the SD.

2. The data set first was sorted by intensity, and then (within each value of intensity) was sorted by frequency.

3. At each level of intensity, the data was stepped through and a running count was kept (initially set to zero) of the number of consecutive frequencies for which “above” was true. This variable was called “*abovecount*”. At a given frequency, it was checked

whether "*above*" was true. If true, then the count was incremented by one. If not true, then the count was reset to zero. After doing this, then a check whether "abovecount" was greater than the threshold criterion was performed (this was set to 10 consecutive frequencies—this parameter can also be changed). If so, the indicator variable "*abovecrit*" was set equal to one (initially, abovecrit was set to zero). When the last frequency within this particular intensity was reached, then the information in "abovecrit" was output to a new data file. This procedure was repeated at each intensity level, producing a new (smaller) data file with one row for each intensity, and an indicator of whether, at each intensity, the criterion number of consecutive frequencies above the threshold criterion was achieved.

4. Now, starting with this new data file, each intensity was stepped through and an indicator was maintained of whether or not the ART has been met and, if so, another variable indicating the intensity at which this occurred. The indicator was called "*ARTreached*" and the intensity at which it was reached was in a variable called "*ART*". This was achieved by doing the following:

- Initialize "ARTreached" to be zero (meaning no, or false).
- Initialize "ART" to be missing (unknown).
- Then, at each intensity, do the following:
- If ARTreached=0, then:
- If abovecrit=1 (true), then:
- Change ARTreached to be one (true)
- Change ART to be equal to the current value of intensity
- Next, if ARTreached=1, then:
- If abovecrit=0 (false), then:

- Change ARTreached back to zero
- Change ARTreached back to missing

This last step relating to abovecrit=0 (false) ensured that if intensity was reached at which the criterion was met, but was not sustained at a higher intensity, then it would not have been identified as the threshold. But if at every subsequent intensity the criterion was still met, then the value of the intensity at which that first occurred would have been saved.

5. At the very end, a single record was put out to a new data file that contained the values of ART reached and "CART".

The ART criterion denoted as Criterion 1SD/10f, used multiplier 1 (1standard deviation of the mean baseline) as the condition for "above" and 10 consecutive frequencies for "abovecount".

WBR-CART Results

The WBR data for all the subjects were assessed via visual inspection and mathematically using the WBR-CART criterion of 1SD/10f. Visual inspection of the ABD graphs provided the so-called *visually estimated WBR-CARTs*. Mathematical approach yielded the *computed WBR-CARTs*. Mean group results for both visually estimated and computed WBR-CARTS in younger and older groups of participants are presented in Table 7. Individual participants' results may be viewed in APPENDIX E, Table E3.

Table 7

Younger and Older Group Experimental Mean AI-CARTs (dB HL), Mean Visually Estimated WBR-CARTS (dB HL) and Mean Computed WBR-CARTs (dB HL and Their Standard Deviations (S.D.), Standard Errors of Mean (SEM) and 95% Confidence Intervals (95% CI). No BBN and 1000 Hz Retest Data Were Collected for AI-CART.

Group	Test	Parameter	AI-CART [dB HL]	Visually Estimated WBR-CART [dB HL]	Computed WBR-CART 1SD/10f [dB HL]
Younger	BBN Test	N	10	10	10
		Mean	75.60	61.60	61.60
		S.D.	2.46	8.68	9.32
		SEM	0.78	2.75	2.95
		95% CI	73.84 - 77.36	55.39 – 67.81	54.93 – 68.27
	BBN Retest	N		10	10
		Mean		65.20	65.20
		S.D.		4.73	4.92
		SEM		1.50	1.55
		95% CI		61.81 – 68.59	61.68 – 68.72
	1000-Hz Test	N	10	10	8
		Mean	89.80	92.40	92.75
		S.D.	3.19	4.09	4.65
		SEM	1.01	1.29	1.64
		95% CI	87.52 – 92.08	89.49 – 95.32	88.86 – 96.64
	1000-Hz Retest	N		7	6
		Mean		92.00	92.67
		S.D.		5.16	5.01
		SEM		1.95	2.04
		95% CI		87.22 – 96 78	87.41 – 97.92
Older	BBN Test	N	10	10	9
		Mean	79.20	66.40	63.78
		S.D.	6.75	14.78	13.76
		SEM	2.13	4.67	4.59
		95% CI	74.37 – 84.03	55.83 – 76.97	53.20 – 73.46
	BBN Retest	N		10	10
		Mean		67.00	67.20
		S.D.		9.49	10.12
		SEM		3.00	3.20
		95% CI		60.21 – 73.79	59.96 – 74.44
	1000-Hz Test	N	10	9	8
		Mean	89.20	89.56	89.75
		S.D.	6.20	4.88	5.70
		SEM	1.96	1.63	2.02
		95% CI	84.77 – 93.63	85.81 – 93.30	84.98 – 94.52
	1000-Hz Retest	N		10	10
		Mean		90.80	91.00
		S.D.		8.65	8.18
		SEM		2.74	2.59
		95% CI		84.61 – 96.99	85.15 -96.85

ABD Graphs

Visual inspection of the ABD graphs showed a distinct pattern of ABDs as a function of frequency. The pattern tended to emerge just below or at the CART level of the activator and became more pronounced as the activator level increased. The pattern typically had two or more peaks: a positive peak at the low frequencies that was consistent with the increase in the reflectance in the presence of the activator; and a mid-frequency ABD peak that was suggestive of decrease in the reflectance. These findings were consistent with Feeney & Keefe (1999), Feeney & Keefe (2001). The two peaks often were followed by additional positive and negative peaks in mid-to-high frequency region. The formation of the pattern and its progression is illustrated in Figure 6.

(a) (b)

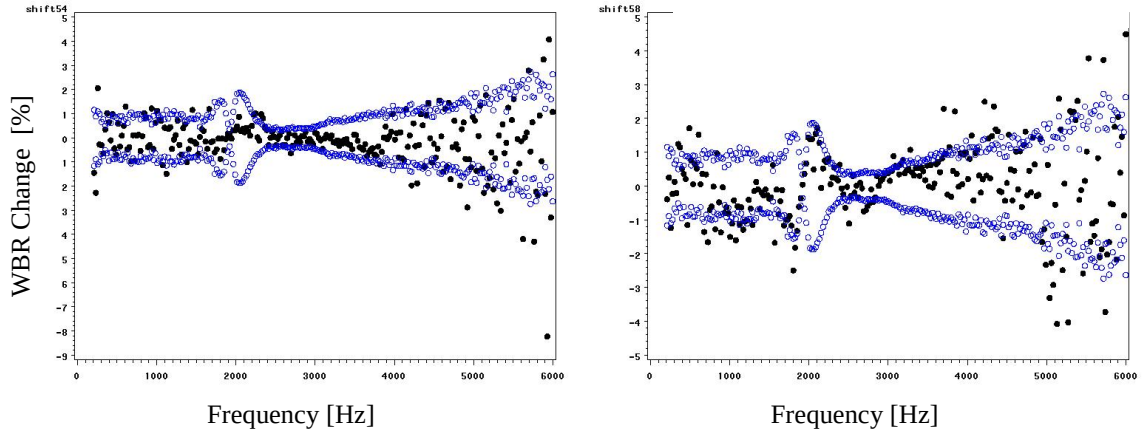

Figure 6. ABDs for BBN activators: 54 dB HL BBN (a), 58 dB HL BBN (b) obtained during the test of subject 010. The visually estimated WBR-CART was 66 dB HL. Probe stimulus frequencies are shown on horizontal axis. The ABD (%) is shown on the vertical axis. The ± 1-SD limits (from the baseline variances) are shown in blue.

(c) (d)

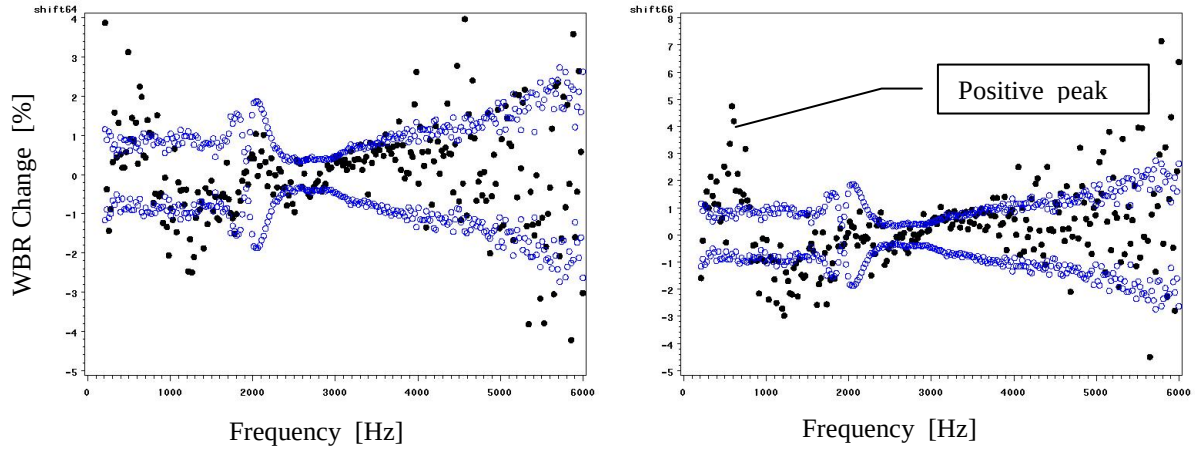

(e) (f)

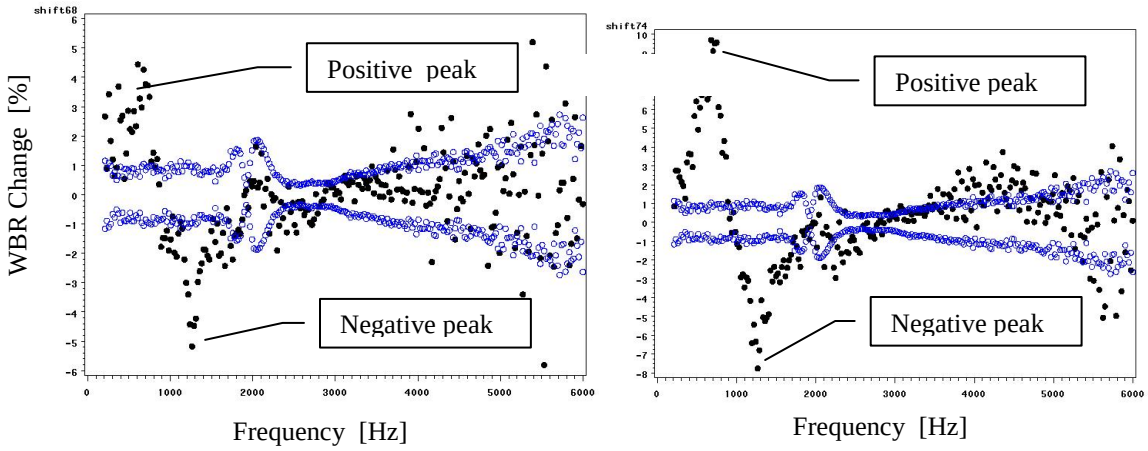

Figure 6. (continued) ABDs for BBN activators: 64 dB HL BBN (c), 66 dB HL (d), 68 dB HL (e), 74 dB HL (f) obtained during the test of subject 010. The visually estimated WBR-CART was 66 dB HL. Probe stimulus frequencies are shown on horizontal axis. The ABD (%) is shown on the vertical axis. The ± 1-SD limits (from the baseline variances) are shown in blue.

(g)

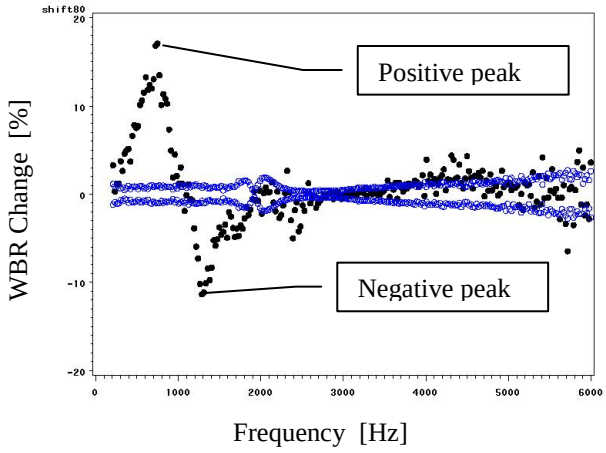

Figure 6. (continued) ABDs for BBN activator 80 dB HL (g) obtained during the test of subject 010. The visually estimated WBR-CART was 66 dB HL. Probe stimulus frequencies are shown on horizontal axis. The ABD (%) is shown on the vertical axis. The ± 1-SD limits (from the baseline variances) are shown in blue.

The level of activator at which ABDs were greater than 1SD of the mean baseline over a discernable range of frequencies and formed a "peak-like" pattern was labeled as the visually estimated WBR-CART. The "peak-like" pattern became more pronounced at subsequently higher activator levels.

Computed WBR CARTS

Computations in SAS® using the algorithm for WBR CART criterion (1SD/10f) yielded 8 WBR CARTs for each participant (4 test and retest WBR CARTs for both the BBN and 1000-Hz activators for both criteria) were denoted as the *Computed WBR CARTs*.

The visually estimated WBR CARTs based on 1SD/10f criterion and computed WBR CARTs using criterions of 1SD/10f are presented together with the experimental AI CARTs in Table 7. It may be noted that some of the visually estimated WBR CARTs and computed WBR CARTs were identified only at the highest activator level (WBR CARTs marked with "[C]" in Table 7). Although the presence of the acoustic reflex could not be verified at higher activator level in these cases, the clear emergence of the characteristic pattern was accepted as reliable confirmation of the WBR CART. An example of WBR CART that was obtained at the highest activator level is presented in Figure 7.

(a) (b)

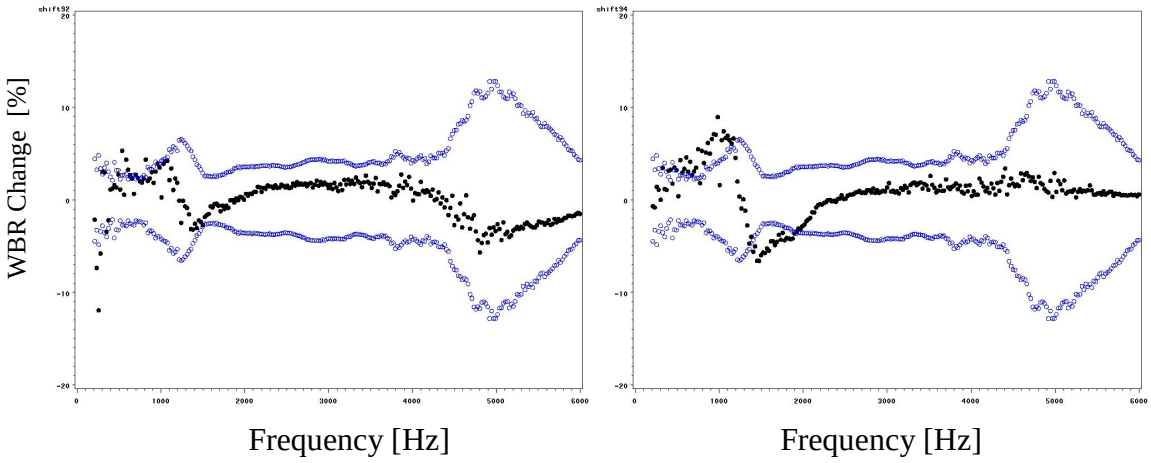

Figure 7. ABDs for 1000-Hz activator during the retest of subject 102: (a) activator level at 92 dB HL, (b) activator level 94 dB HL. Both WBR CARTs - the visually estimated WBR CART and computed WBR CART for criterion 1SD/10f, were at 94 dB HL. The probe stimulus frequency is shown on the horizontal axis. The ABD (%) is shown on the vertical axis. The ± 1 SD limits (from the baseline means) are shown in blue.

Statistical Analyses Results

The results of the paired two-tailed *t*-test (N = 10) revealed the AI BBN CARTs to be significantly better than the AI 1000-Hz CARTs in the younger group ($t[9] = 15.50$, $p < 0.0001$). The mean difference = 14.2 dB (95% CI = -16.3 - -12.1, SE = 9.2). (The individual AI BBN and AI 1000-Hz CARTs and resultant AI NTD data for the younger group are shown in Appendix E, Table E4.) The results of the descriptive analysis are presented in Table 8.

Table 8

The AI BBN CARTs, AI 1000-Hz CARTs, and Resultant AI NTDs for the Younger Group

Parameter	AI BBN CART	AI 1000-Hz CART	AI NTD
N	10	10	10
	8[a]	8[a]	8[a]
	7[b]	7[b]	7[b]
Range	72 - 80	84 - 94	10 - 18
	74 - 80[a]	84 - 94[a]	10 - 18
	74 - 80[b]	86 - 94[b]	
Mean	75.6	89.8	14.2
	76.0[a]	89.5[a]	13.5[a]
	76.3[b]	90.3[b]	14.0[b]
S.D.	2.5	3.2	2.9
	2.4[a]	3.5[a]	2.8[a]
	2.4[b]	2.9[b]	2.6[b]
95% CI	73.8 - 77.4	87.8 - 91.8	12.1 - 16.3
	74.0 - 78.0[a]	86.6 - 92.4[a]	11.2 - 15.8[a]
	74.0 - 78.5[b]	87.6 - 93.0[b]	11.6 - 16.4[b]

[a]Excluded S003 & S006
[b]Excluded S003, S006, & S007

Comparisons between the mean AI BBN Test CARTs and AI 1000-Hz Test CARTs in the older adult group performed using the nonparametric paired Wilcoxon signed ranks test with all participants included revealed a mean AI BBN CART that was significantly lower than the mean AI 1000-Hz CART (n_s / r = 10, W = - 55, z =-2.78, $p = 0.0054$). When S102 was excluded from the sample,, the results of the paired two-tailed *t*-test revealed similar findings regarding the relation between the mean AI BBN CART and the mean AI 1000-Hz CART ($t[8] = 11.63$, $p < 0.0001$) with the mean difference = 8.7 dB (95% CI = -10.4 - -7.0, SE = 0.8). (The individual AI

BBN and AI 1000-Hz CARTs and resultant AI NTD data for the OLDER group are shown in Appendix E, Table E5).The results of descriptive analysis for the AI BBN and 1000-Hz CARTs in the older group are presented in Table 9.

Table 9

The AI BBN CARTs, AI 1000-Hz CARTs, and Resultant AI NTDs for the Older Group

Parameter	AI BBN Test CART	AI 1000-Hz Test CART	NTD
N	10	10	10
	9[a]	9[a]	9[a]
Range	72 - 92	80 - 98	6 - 22
	72 - 92[a]	80 - 98[a]	6 - 12[a]
Mean	79.2	89.2	10.0
	80.0[a]	88.7[a]	8.7[a]
S.D.	6.8	6.2	4.7
	6.6[a]	6.3[a]	2.2[a]
95 % CI	74.4 - 84.0	84.8 - 93.6	6.6 - 13.4
	74.9 - 85.1[a]	83.8 - 93.5[a]	7.0 - 10.4[a]

[a]Excluded S102

Grubb's test [Extreme Studentized Deviation (ESD) Method] was employed to identify the outliers. The results are shown in Table 10.

Table 10

Participants with Outlier CARTs or NTDs as Identified with Grubb's Test

Measure	Younger group	Older group
AI BBN CART	No outliers	No outliers
AI 1000-Hz CART	No outliers	No outliers
AI NTD	No outliers	S102[a]
WBR BBN Test CART	S007[a]	No outliers
WBR BBN Retest CART	No outliers	No outliers
WBR 1000-Hz Test CART	No outliers	No outliers
WBR 1000-Hz Retest CART	No outliers	No outliers
WBR Test NTD	S007[a]	S109[a]

[a]$p < 0.05$.

The mean AI NTDs in the younger and older adult groups were compared using the unpaired two-tailed *t*-test. The results revealed significantly greater AI NTDs in the younger than older group ($t[18] = 2.40$, $p = 0.0274$). The mean difference = 4.2 (95% CI = 0.5 - 7.9, SE =

1.8). With S102 excluded because the AI-NTD CART was an outlier, the results of the unpaired (independent groups) two-tailed *t*-test revealed a greater mean AI NTD in the younger than older group ($t[17] = 4.61$, $p < 0.0002$). The mean difference = 5.5 (95% CI = 3.0 – 8.1, SE = 1.2). The descriptive AI NTD data are shown in Table 11.

Table 11

AI NTDs in Younger and Older Adult Groups

Parameter	AI NTD younger group	AI NTD older group
N	10	10 9[a]
Range	10 – 18	6 – 22 6 – 12[a]
M	14.2	10.0 8.7[a]
SD	2.9	4.7 2.2[a]
95% CI	-16.3 – -12.1	6.6 - 13.4 7.0 - 10.4[a]

[a]Excluded S102

Using the unpaired two-tailed *t*-test, the mean AI CARTs from this study were compared with those obtained by Silman (1979). The results revealed no statistically significant difference between studies ($t[28] = 0.81$, $p = 0.4256$) for the AI BBN CART in the younger adult group. The mean difference = 3.0 (95% CI = -4.52 – 10.4, SE = 3.7). No statistically significant difference for the AI 1000-Hz CART occurred between studies in the younger group ($t[28] = 0.22$, $p = 0.8297$). The mean difference = 0.4 (95% CI = -3.0 – 3.7, SE = 1.6). Similar findings were obtained with respect for the AI BBN CART in the older group ($t[28] = 1.35$, $p = 0.1771$) . The mean difference = -3.70 (95% CI = -9.2 – 1.8, SE = 2.7). When S102 was excluded from the analysis, the findings remained essentially unchanged for the AI BBN CART in the older group ($t[27] = 1.05$, $p = 0.3023$) . The mean difference = -2.90 (95% CI = -8.6 – 2.8, SE = 2.8).And similar findings were obtained with respect for the AI 1000-Hz CART in the older group ($t[28] = 0.34$, $p = 0.7388$). The mean difference = 0.8 (95% CI = -5.7 – 4.1, SE = 2.4);

when S102 was excluded, the findings remained essentially unchanged (t[28] = 0.54, p = 0.5823). The mean difference = -1.33 (95% CI = -6.4 – 3.8, SE = 2.5). The descriptive AI CART data for younger and older participants are shown in Tables 12 and 13.

Table 12

AI CARTs for Current Study and from Silman (1979) in Younger Adults

Parameter	Current Study AI BBN CART	Silman (1979) AI BBN CART	Current Study AI 1000-Hz CART	Silman (1979) AI 1000-Hz CART
N	10	20	10	20
Range	72-80	55-96	84 – 94	82 – 99
Mean	75.6	72.65	89.80	89.45
S.D.	2.5	11.3	3.19	4.55
95 % CI	73.8 – 77.4	67.4 – 77.9	87.8- 91.8	87.3 – 91.6

Table 13

AI CARTs for Current Study and from Silman (1979)in Older Adults

Parameter	Current Study AI BBN CART	Silman (1979) AI BBN CART	Current Study AI 1000-Hz CART	Silman (1979) AI 1000-Hz CART
N	10 9[a]	20	10 9[a]	20
Range	72 – 92 72 – 92[a]	66 – 98	80 – 98 80 – 98[a]	82 – 107
M	79.2 80.0[a]	82.9	89.2 88.7[a]	90
SD	6.8 6.6[a]	7.0	6.2 6.3[a]	6.1
95 % CI	74.4 – 84.0 74.9 – 85.1[a]	79.6 – 86.2	84.8 – 93.6 83.8 – 93.5[a]	87.2 – 92.9

[a]Excluded S102

Test-retest reliability was assessed with the paired two-tailed t-test for the WBR CART in the younger and older adult groups. The results of this statistical analysis revealed the absence of statistically significant differences between the test and retest WBR BBN CARTs in the younger adult group (t[9] = 1.69, p = 0.1245). The mean difference = -3.6 (95% CI = -8.4 – 1.2, SE = 2.1). With S007 excluded (WBR BBN Test CART was identified as an outlier) absence of statistical difference became stronger (t[8] = 1.23, p = 0.2367). The mean difference = -2.0 (95%

CI = -5.6 – 1.6, SE = 1.56). Similar findings were obtained for the older adult group (t[8] =0 .32, $p = 0.7589$) when S104 was excluded (for no response for WBR 1000-Hz Test); the mean difference = -1.1 (95% CI = -9.2 – 7.0, SE = 3.5). When both S104 and S109 (WBR NTD outlier) were excluded from the data analysis, no statistically significant differences between the test and retest WBR BBN CARTs were obtained in the older adult group ($t[7] = .77$, $p = 0.4681$); the mean difference = 1.75 (95% CI = -3.64 – 7.14, SE = 2.3). (The individual test and retest WBR BBN CARTs are presented in Appendix E, Table E6). Thedescriptive analysis relating to test-retest reliabili for the WBR BBN CART is shown in Table 14.

Table 14

Test and Retest WBR BBN CARTs in the Younger and Older Adult Groups

Parameter	Younger adult group		Older adult group	
	WBR BBN CART Test	WBR BBN CART Retest	WBR BBN CART Test	WBR BBN CART Retest
N	10	10		10
	9[a]	9[a]	9[b]	9[b]
			8[c]	8[c]
Range	38 – 70	56 – 74	34-80	58-84
	56 – 70[a]	60 –74[a]	34-80[b]	58-82[b]
			56-80[c]	58-82[c]
M	61.6	65.2		67.2
	64.2[a]	66.2[a]	64.2[b]	65.3[b]
			68.0[c]	66.3[c]
SD	9.3	4.9		10.1
	4.5[a]	3.9[a]	14.3[b]	8.7[b]
			9.3[c]	8.8[c]
95% CI	54.9 – 68.3	61.7 – 68.7		59.9 – 74.4
	60.8 – 67.7[a]	63.2 – 69.2[a]	53.3-75.2[b]	60.9 – 73.5[b]
			60.3 – 75.4[c]	58.9 – 73.6[c]

[a]Excluded S007.
[b]Excluded S104.
[c]Excluded S104, S109.

As for the WBR BBN CART, test-retest reliability was assessed with the paired two-tailed *t*-test for the WBR 1000-Hz CART in the younger and older adult groups. With S003, S006, and S008 (for no response for some of the tests) excluded from the data, the results of this statistical analysis revealed no statistically significant differences between the test and retest

WBR 1000-Hz CARTs in the younger adult group (t[6] = .55, *p* = .0604). The mean difference = -0.6 (95% CI = -3.1 – 2.0, SE = 1.0). Similar findings were obtained for the older adult group (t[7] = 0.27, p = 0.7939), with S104 and S105 excluded. The mean difference = 0.5 (95% CI = -3.9 - 4.9, SE = 1.8). (The individual test and retest WBR 1000-Hz CARTs are presented in Appendix E, Table E7). The descriptive measures relating to test-retest reliability for the WBR 1000-Hz CART are shown in Table 15.

Table 15

Test and Retest WBR 1000-Hz CARTs in the Younger and Older Adult Groups.

	Younger adult group		Older adult group	
Parameter	Test	Retest	Test	Retest
N	8[a]			10
	7[b]	7[b]	8[c]	8[c]
Range	84 - 98[a]			78 – 102
	84 - 96[b]	84 - 98[b]	84 – 100[c]	78 – 100[c]
M	92.6[a]			90
	92.0[b]	92.6[b]	89.8[c]	89.3[c]
SD	4.7[a]			8.4
	4.5[b]	4.6[b]	5.7[c]	8.0[c]
95% CI	88.9 - 96.7[a]			84.0 – 96.0
	89.5 - 96.0[b]	89.18 - 95.96[b]	84.98 – 94.52[c]	82.6 – 95.9[c]

[a]Excluded S003, S006.
[b]Excluded S003, S006, S008.
[c]Excluded S104, S105.

To examine whether an age effect was present on the WBR CARTs, the unpaired two-tailed *t*-test was applied. The non-parametric Mann-Whitney U test was also employed for the examination of the age effect on the WBR BBN CART. The differences are deemed to be statistically insignificant. The results of descriptive analysis are shown in Table 17. No significant age effect was present for the WBR BBN CART (*t*[17] = 0.48, *p* = 0.6378) when S104 (no response) was excluded; the mean difference = -2.6 (95% CI = -14.2 – 8.9, SE = 5.5). Similar findings were obtained when S007 (outlier), S104 (no response), and S109 (WBR NTD outlier) were excluded (*t*[15] = 1.09, *p* = 0.2930); the mean difference = -3.8 (95% CI = -11.2 – 3.6, SE = 3.5). Also Mann-Whitney U test produced insignificant difference (pair of S003

{highest BBN CART in the younger group] and S104 was excluded due to the absent S104 WBR BBN CART) (U=40.5, z = 0.04, p =0.9681) Similarly, for the test WBR 1000-Hz CART, no significant age effect was present (t[14] = 1.15, p = 0.2681) when S003, S006, S104, and S105 were excluded; the mean difference = 3.0 (95% CI = -2.6 – 8.6, SE = 2.6). The results of descriptive statistics also are shown in Table 16.

The results of the paired two-tailed t test revealed a mean WBR CART that was significantly lower for the BBN than for the 1000-Hz activator in the younger adult group when S003 and S006 (for no response in WBR 1000-Hz Test) were excluded from the analysis (t[7] = 13.56, p <0.0001); the mean difference = -31.5 (95% CI = -37.0 - -26.0, SE = 2.3). Similar findings were obtained when S003, S006, and S007 (outlier) were excluded from the analysis (t[6] = 24.28, p < .0001); the mean difference = -29.4 (95% CI = -32.4 - -26.5, SE = 1.2). When S007 (outlier) was included (S003 and S006 were excluded due to the absent WBR 1000-Hz CARTs) the results of statistical analysis using the non-parametric Wilcoxon signed ranks test (W = -36, n_s/r = 8, p = 0.01) revealed statistically significant difference as well. In the older group, as for the younger group, the results of the paired two-tailed t test revealed a mean WBR CART that was significantly lower for the BBN than for the 1000-Hz activator in the younger adult group when S104 and S105 were excluded from the analysis (for no response) (t[7] = 6.05, p < .0005); the mean difference = -24.5 (95% CI = -34.1 - -14.9, SE = 4.1). Similar findings for the older group were obtained when S104, S105 (no response), and S109 (WBR NTD outlier) were excluded from the analysis (t[6] = 10.2, p < .0001); the mean difference = -20.9 (95% CI = -25.9 - -15.9, SE = 2.0). The results of the descriptive analyses are shown in Table 16.

Table 16

Test WBR BBN and 1000-Hz CARTs in the Younger and Older Adult Groups

Parameter	WBR BBN CART		WBR 1000-Hz CART	
	Younger group	Older group	Younger group[d]	Older group[e]
N	10	9[b]		
	9[a]	8[c]	8	8
Range	38 - 70	34 – 80[b]	84 – 96	84 – 100
	56 - 70[a]	56 – 80[c]		
M	61.6	64.2[b]	92.75	89.8
	64.2[a]	68.0[c]		
SD	9.3	14.3[b]	4.65	5.7
	4.5[a]	9.3[c]		
95% CI	54.9 – 68.3	53.3 - 75.2[b]	88.86 – 96.64	85.0 – 94.5
	60.8 – 67.7[a]	60.3 – 75.7[c]		

[a]Excluded S007.
[b]Excluded S104.
[c]Excluded S104 and S109.
[d]Excluded S003 and S006.
[e]Excluded S104 and S105.

The resultant mean WBR NTDs in the younger and older adult groups are shown in Table 17, along with the results of descriptive statistical analyses. Comparison of the mean WBR NTDs between the younger and older groups using the paired two-tailed t-test (excluding S003, S006, S007, S104, S105, and S109) revealed that the mean WBR NTD was significantly smaller in the older than younger adult group ($t[12] = 3.61$, $p < .0036$); the mean difference = 8.6 (95% CI = 3.4 – 13.7, SE = 2.4).

Table 17

WBR NTD in the Younger and Older Adult Groups

Parameter	Younger group	Older group
N	8[a]	8[c]
	7[b]	7[d]
Range	24 – 46[a]	10 – 50[c]
	24 – 34[b]	10 – 26[d]
M	31.5[a]	24.5[c]
	29.4[b]	20.9[d]
SD	6.6[a]	11.5[c]
	3.2[b]	5.4[d]
95% CI	26.0 – 37.0[a]	14.9 – 34.1[c]
	26.5 – 32.4[b]	15.9 – 25.9[d]

[a]Excluded S003, S006.
[b]Excluded S003, S006, and S007.

[c]Excluded S104, S105..
[d]Excluded 104, S105, and S109.

The CART measurement methods, AI method and WBR method, were assessed with regards to participants' age and activator type. Paired two-tailed t-test had shown the WBR to yield highly significantly lower CARTs for BBN activator than for the AI activator in the younger group regardless of whether S007 (WBR BBN CART was identified as an outlier for S007) was included. (t[9] = 5.28, p = 0.0005); the mean difference = 14.0 (95% CI = 8.0 - 20.0, SE = 2.65), or excluded (t[8] = 10.10, p < 0.0001); the mean difference = 11.56 (95% CI = 8.9 to 14.2, SE = 1.14). Wilcoxon signed ranks test (non-parametric paired analysis) with all participants included confirmed the statistically significant improvement with the WBR method (W = 55, n_s/r =10, z= 2.78, p = 0.0054). Similarly, WBR produced highly significantly lower CARTs for BBN activator in the older group (t[8] = 3.56, p = 0.0074); the mean difference = 14.0 (95% CI = 4.9 - 23.1, SE = 3.93) (S104 was excluded for no response to the WBR 1000-Hz activator) . All the analysis details for the BBN CART comparisons by method are displayed in Table 18.

Table 18

Comparison between AI BBN CARTs and WBR BBN Test CARTs in Younger and Older Adult Groups

	Younger group		Older group	
Parameter	AI BBN CART	WBR BBN Test CART	AI BBN CART	WBR BBN Test CART
N	10	10		
	9[a]	9[a]	9[b]	9[b]
Range	72 – 80	38 – 70		
	72 – 80[a]	56 – 70[a]	72 – 92[b]	34 – 80[b]
M	75.6	61.6		
	75.8[a]	64.2[a]	78.2[b]	64.2[b]
SD	2.5	9.3	6.4[b]	14.3[b]
	2.5[a]	4.5[a]		
95% CI	74.1 – 77.1	55.8 – 67.4		
	73.8 – 77.4[a]	60.8 – 67.7[a]	73.3 – 83.1[b]	53.3 – 75.2[b]

[a]Excluded S007.
[b]Excluded S104 No Response.

. No method (WBR versus AI) difference was observed for 1000-Hz activator in the older group (t[7] = 0.94, p = 0.3776); the mean difference = -1.5 (95% CI = -5.3 – 2.3, SE = 1.59). AI produced slightly better CARTs than WBR for 1000-Hz activator in the younger group (t[7] = 3.05, p = 0.0185); the mean difference = -3.25 (95% CI = -5.8 - -0.7, SE = 1.07) . All the analysis details for the 1000-Hz CART comparisons by method are displayed in Table 19.

Table 19

Comparison Between AI 1000-Hz CARTs and WBR 1000-Hz Test CARTs in Younger and Older Adult Groups

Parameter	Younger group AI 1-kHz CARTs	WBR 1-kHz Test CARTs	Older group AI 1-kHz CART	WBR 1-kHz Test CART
N	10		10	
	8[a]	8[a]	8[b]	8[b]
Range	84 – 94		80 – 98	
	84 – 94[a]	84 – 98[a]	80 – 98[b]	84 – 100[b]
Mean	89.80		89.20	
	89.50[a]	92.75[a]	88.25[b]	89.75[b]
S.D.	3.19		6.20	
	3.51[a]	4.65[a]	6.45[b]	5.70[b]
95% CI	87.5 – 92.1		84.77 – 93.63	
	86.6 – 92.4[a]	88.9 – 96.6[a]	82.9 – 93.6[b]	85.0 – 94.5[b]

[a]Excluded S003 and S006.
[b]Excluded S104 and S105 excluded.

Further, the AI – WBR method comparison focused on NTD using paired two-tailed t-test. WBR method produced highly statistically greater NTDs than AI method in the younger group, regardless whether S007 was included (t[7] = 6.36, p= 0.0004); the mean difference = -18.00 (95% CI = - 24.69 - – 11.31, SE = 2.83), or excluded (t[6] = 11.34, p< 0.0001); the mean difference = -15.43 (95% CI = -18.8 – 12.1, SE = 1.36). Wilcoxon signed rank test through the nonparametric approach analysis (with outlier S007 included) confirmed the significant difference (W= -36, n_s/r = 8, p = 0.01) between the AI NTD and WBR NTD in the younger group. The older group presented with similar findings: (t[7] = 2.93, p = 0.0220); the mean difference = -14.25 (95% CI =- 25.75 to – 2.75, SE = 4.86) with S109 included and (t[6] = 3.67,

p = 0.0105); the mean difference = -10.00 (95% CI = -16.7 - -3.3, SE = 2.73) without S109. Wilcoxon signed rank test again showed WBR NTD to be significantly greater than the AI NTD in the older group as well (W = -33, n_s /r = 8, p< 0.05) (Individual WBR NTD values are presented in Appendix E, Tables E8, E9). All the NTD-by-method comparisons are shown in Table 20.

Table 20

Comparison Between AI-NTD and WBR NTD in Younger and Older Adult Group

	Younger group		Older group	
Parameter	AI NTD	WBR NTD	AI NTD	WBR NTD
Sample	10			
	8[a]	8[a]	8[c]	8[c]
	7[b]	7[b]	7[d]	7[d]
Range	10 – 18			
	10 – 18[a]	24 – 46[a]	6 – 22[c]	10 – 50[c]
	10 – 18[b]	24 – 34[b]	6 – 22[d]	10 – 26[d]
Mean	14.20			
	13.50[a]	31.50[a]	10.25[c]	24.50[c]
	14.00[b]	29.43[b]	10.86[d]	20.86[d]
SD	2.90			
	2.78[a]	6.57[a]	5.28[c]	11.45[c]
	2.58[b]	3.21[b]	5.40[d]	5.40[d]
95% CI	12.1 – 16.3			
	11.2 – 15.8[a]	26.0 – 37.0[a]	5.8 – 14.7[c]	14.9 – 34.1[c]
	11.6 – 16.4[b]	26.5 – 32.4[b]	5.9 – 15.9[d]	15.9 – 25.9[d]

[a]Excluded S003, S006.
[b]Excluded S003, S006, S007.
[c]Excluded S104, S105.
[d]Excluded S104, S105, S109.

CHAPTER V: DISCUSSION

The general purpose of the study was to evaluate a new method of WBR for the measurement of CARTs, as well as to gain a better understanding of the effects of the aging process on the auditory mechanism, specifically, the CART. The findings of this experiment represent a contribution to the ongoing efforts to build a precise functional model of the ear. The results of the investigation also have implications for clinical acoustic-reflex assessment of individuals with sensorineural hearing impairment, particularly CART-based prediction of hearing status in older adult subjects. The specific purposes of the study were (a) development of criteria for defining the WBR CART; (b) comparison of the WBR versus AI tonal (1000-Hz) and BBN CARTs; and (c) examination of the effect of age on the WBR and AI tonal and BBN CARTs.

The set of criteria for defining the WBR CART that were developed and refined by this investigator in the course of this investigation aided in the obtaining of sensitive and specific WBR CARTs that then were compared with the traditional AI CARTs. The WBR and AI noise-tone differences (NTDs), that reflect the difference between the tonal and BBN CARTs, were compared in this investigation as the NTD has implications for prediction of hearing loss from the acoustic-reflex threshold (e.g., the bivariate plot procedure) in younger and older adults.

Visual Observations of the WBR ABD Graphs

Visual inspection of the WBR ABD graphs often revealed a pattern showing a positive peak in the low-frequency region, typically below 1000 Hz, and a negative peak in the mid-to-high frequency range, usually above 1000 Hz. This pattern of a positive peak followed by a negative peak in some cases was followed by additional one or more peaks in the mid-to-high frequency region. The positive peak at the CART activator level and at suprathreshold levels is

consistent with decreased energy flow through the middle ear; the negative peak at the CART activator level and suprathreshold levels is suggestive of energy gain (see Fig.6 and Fig.8)..

Areas above and below the mean baseline were estimated for the WBR-BBN test of subject 010 at the suprathreshold activator levels of 74 and 80 dB HL (see Fig. 6, panels f and g). The triangular areas were calculated using the frequency range below the peak in Hz as a base, and maximum ABD at the peak in percentage as the height. The positive area (estimated as triangular area between the curve of ABD and the horizontal axis representing the mean baseline WBR; expressed in Hertz multiplied by percentage) for the 74 dB HL activator was estimated as 3,800 and the negative area was estimated as 3,100. So, proportionately, the amount of overall WBR decrease at the mid frequencies reached about 82% (3100 divided by 3800) of the WBR increase at the low frequencies due to the effect of acoustic-reflex elicitation. The positive area for the 80 dB HL activator was estimated at 7,225 and the negative area was estimated at 5,100. So, proportionately, the amount of overall WBR decrease at the mid frequencies reached about 71% (5,100 divided by 7,225). Similar ratios were obtained even when the areas corresponding with 1 SD or 2 SD of the mean baseline were subtracted from the triangular peak areas. Thus, the acoustic reflex should not be viewed as an energy reducing mechanism, but rather as an energy redistributing system favoring the mid-frequency region, possibly decreasing the upward spread of masking, and thereby optimizing speech perception in the presence of transient, intense low-frequency noise.

The computed WBR-CARTs were, in the vast majority of cases, based on the responses in the low-frequency range where the positive peaks formed and, in all cases, were corroborated by the results of visual assessment at the CART stimulus level, as well as at subsequent stimuli intensities. Computations of the WBR-CARTs at higher frequencies were sometimes adversely

affected by the widening of the positive low-frequency peaks with increases in activator intensity. In other words, as activator intensity increased, the positive low- frequency triangular peak became higher and wider with ABD growth, thereby shifting the subsequent negative triangular peak upwards towards higher frequency region. This phenomenon is well illustrated in recordings for the WBR-BBN Test of Subject 002 in Figure 8.

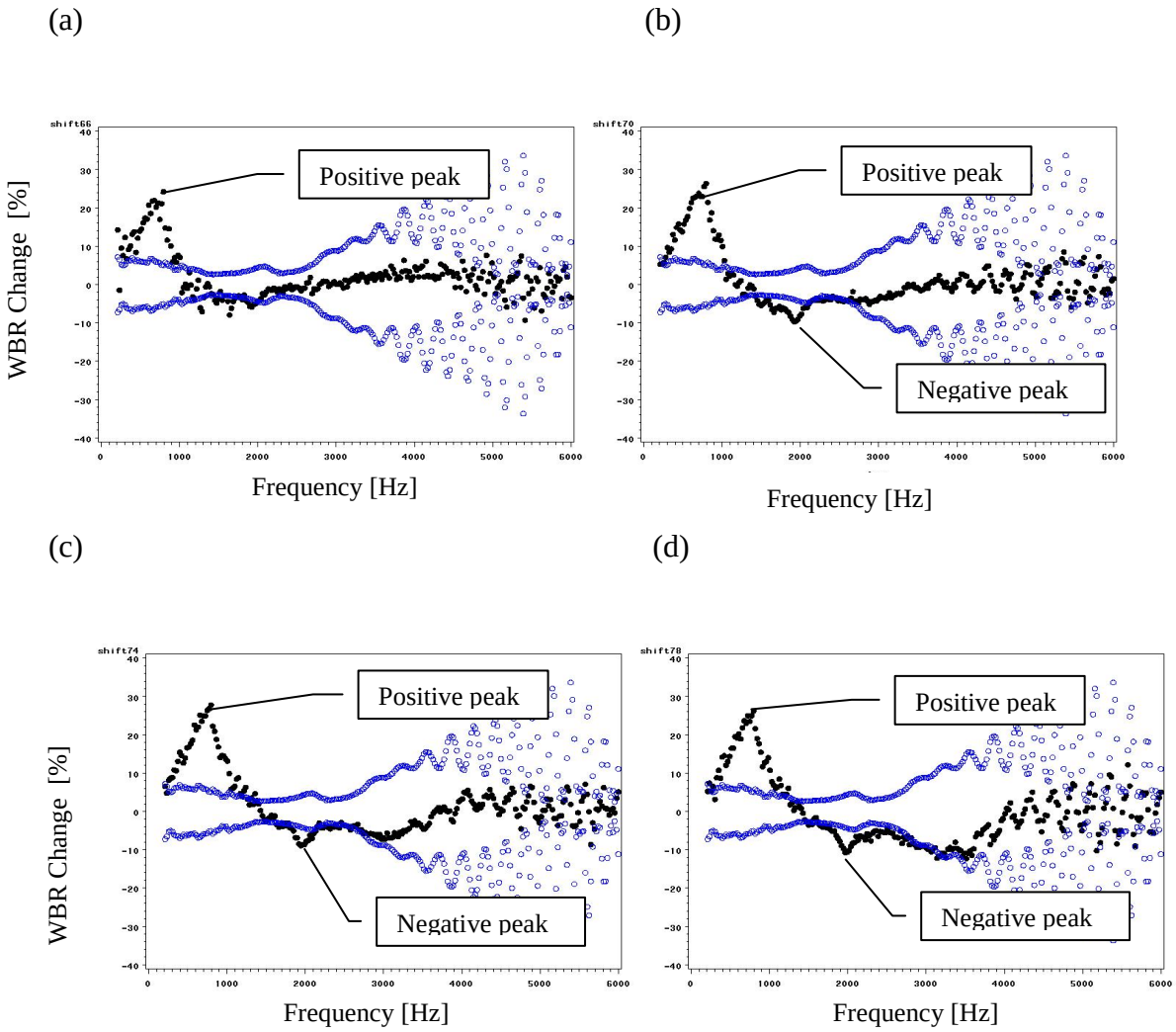

Figure 8. ABDs for BBN activators 66 dB HL (a), 70 dB HL (b), 74 dB HL (c), 78 dB HL (d) obtained during the test of subject 002; note the shift in the frequency range above the negative peak

The AI CARTs: This Investigation and Silman (1979)

This investigation's mean AI BBN and 1000-Hz CARTs for the younger and older adult participants were in good agreement overall with those obtained by Silman (1979). No statistically significant mean differences between the current and Silman AI BBN and 1000 CARTs were obtained for either of this study's groups. The current AI CARTs trended towards being lower for the BBN than for the 1000-Hz activators. The results of the unpaired two-tailed *t*-test comparison in the AI BBN CARTs between the younger and older adults in this investigation approached, but did not reach significance ($p = 0.064$). In contrast, Silman's findings revealed a significantly lower mean AI BBN CART for the younger than older adult group ($p = 0.001$). This slight difference between studies may reflect a smaller sample size in this study (n = 10 in this study vs. n = 20 in the Silman study) and greater stimulus step-size (2-dB in the current study vs. 1-dB in Silman's study). The role of the step-size in CART assessment was documented by Silverman et al. (1983) who showed a smaller difference in BBN ARTs between younger (20 to 29 years old) and older subjects (50 to 59 years old) with the 5-dB step size (2.5 dB difference between the groups) than with the 1-dB step size measurement condition (7.4 dB difference between the groups)

The mean AI NTD for the younger adult group (14.2 dB) exceeded that for the older adult group (10.0 dB when all 10 participants were included and 8.7 dB when outlier S102 was excluded). The difference in mean AI NTDs between the younger and older adults in the current study was 5.5 dB (with outlier S102 excluded). Silman (1979) obtained mean AI NTDs of 16.8 dB and 7.1 dB for the younger and older adult participants, respectively. Silman's 9.7 dB difference in the mean AI NTD between the younger and older adult groups was greater by 4.2 dB than that obtained in the current investigation. (The AI NTDs from the Silman and current

study cannot be statistically compared as Silman did not report the AI NTD SDs.) The differences between studies in sample size and step-size in CART measurement may explain these slight CART differences between the Silman and the current studies.

WBR CART Test-Retest Reliability

The WBR CART test-retest reliability was good as no statistically significant differences ($p > 0.05$) were observed for the test-retest comparisons (paired two tailed *t*-test) for the WBR BBN CARTs or WBR 1000-Hz CARTs in either the younger or older adult participants (see the *p* levels for each test-retest comparison in the *Analysis* section). Pooling of all test-retest WBR CART differences for both groups and both activators (yielding n = 34) produced a mean test-retest difference of 1.36 dB (SD = 7.0 dB, 95% CI = -3.79 to +1.08). These results indicate that the Mimosa WBR instrumentation yields reliable CART findings, which supports the use of the instrumentation in future research. Although the mean WBR CART test-retest differences were small, some larger individual test-retest differences were noted. They may reflect the following:

1. An apparently high sensitivity of the WBR Mimosa system to acoustico-mechanical disturbances. Individual WBR measurements appeared to be easily altered by participants' bodily sounds, very slight participant motion, and the Mimosa computer-generated sounds (cooling fan). Although this investigator was cognizant of the system's high sensitivity, it was virtually impossible to eliminate those disturbances in a test situation involving a lengthy test session for WBR data collection. Those disturbances were likely to influence the WBR measurements at some frequencies (or frequency ranges) and to have negative effects on the baseline variance and consistency of the series of measurements.

2. A possible Mimosa probe placement effect. Although the WBR concepts postulate that the ear canal functions as a lossless transmission line, in some of the participants, especially

in those with more pronounced ear canal curvature, the depth of the probe insertion affected the WBR measurement. It was observed during the pilot phase that in some curved ear canals, shallower insertion produced poorer WBR recordings. This investigator always attempted to achieve good secure placement of the probe tip. The expandable foam probe tip, however, sometimes led to outward movement of the probe during the long data collection sessions.

Comparison between the AI CARTs and the WBR CARTs

The mean BBN CART was significantly lower with the WBR than the AI approach in both groups. In the younger participants, the difference in mean BBN CART between the WBR and AI approaches was 11.6 dB ($p < 0.0001$; outlier S007 excluded). In the older group the difference in mean BBN CART between the two approaches was 14 dB (n = 9, $p = 0.0074$); it was 10.8 with exclusion of outlier S109 (n = 8, $p = 0.0036$). The finding that the BBN CART is lower with the WBR than the AI method for both groups of participants suggests that the former approach is more sensitive than the latter approach for BBN CART measurement.

In contrast with the finding for the BBN CART, the mean 1000-Hz CART was slightly, but significantly higher for the WBR methodologic approach than for the AI approach in the younger adults. The 1000-Hz CART was essentially the same for both approaches in the older adult participants; the difference in mean was 3.3 dB (n = 8 $p = 0.0185$) for the younger adults and 1.5 for the older adults (n = 8; $p = 0.3776$).

Age Effect on the WBR and AI CART

Comparison of the mean WBR BBN CARTs between the younger and older adults yielded a small, statistically non-significant difference of 3.8 dB ($p > 0.05$). With the AI approach, in the current study, the mean BBN CARTs trended lower in the younger than the older adult group; the mean difference in AI BBN CART between groups equaled 4.4 dB ($p >$

0.05).Previous studies using the AI approach yielded a significantly higher BBN CART for the older than younger adults (Gelfand & Piper, 1981; Osterhammel & Osterhammel, 1979; Silman, 1979; Thompson et al., 1980). The lack of age effect for the AI BBN CART in this study probably reflects the small sample size. In contrast, an age effect was strongly demonstrated for the NTD (see the later section on the WBR NTDs).

The mean difference in WBR 1000-Hz CART between the younger and older older adults equaled just 3 dB (p >0.05). This lack of age effect on the WBR tonal CART is consistent with previous research based on the AI approach (Silverman et al., 1983).

The AI and WBR NTDs

The mean difference in the NTD between the WBR and the AI measurement approaches was large for both age groups with the former approach yielding a significantly greater NTD than the latter approach. The difference in NTD between measurement approaches was 15.4 dB for the younger participants (n = 7, p < 0.000.1) and 10.0 dB for the older participants (n = 7, p = 0.0105). These findings show substantially greater NTD sensitivity for WBR than AI CART. The mean WBR NTD was significantly greater, by 8.6 dB, in the younger adults (29.4 dB) than in the older adults (20.9 dB) (n = 7, p = 0.0036).

This study represents the first investigation to explore age effects on the CARTs and NTDs using the WBR technique and it represents the first CART investigation using the Mimosa instrumentation. The substantially greater NTD with the WBR technique as compared with the AI technique suggests that the WBR method should be employed for NTD measurement, especially in the older adults, in whom the traditional AI approach often yields small or absent NTDs. Furthermore, this study's finding of large WBR NTDs has important implications for the application of WBR in estimating the hearing loss from the CART in the older population. It has

been demonstrated that the bivariate-plot method based on the AI CARTs is unsuccessful for detection of hearing impairment in older adults who are more than 44 years of age (Silman et al., 1984).

In summary, the BBN CART is substantially improved with the WBR method as compared with the AI method. The increased sensitivity of the WBR method to the BBN signal, together with a possible effect of the method itself may explain the observed large improvement in the WBR BBN CARTs in comparison with the AI BBN CARTs and consequently larger WBR NTD than AI NTD. The large improvement of WBR NTDs should be further investigated in adults with sensorineural hearing loss so a WBR bivariate-plot procedure can be developed for prediction of hearing sensitivity in older adults. The WBR CARTs and NTDs obtained in this study also can be combined with similar data from future investigations (assuming the same methods are employed), thereby contributing to the establishment of normative WBR ART data for WBR bivariate plots.

The WBR CARTs from the Current and Other Investigations

In the current study, the mean BBN CART was significantly improved, by 11.6 dB, with the WBR method as compared with the AI method in the younger adults. This improvement was a smaller than that measured by Feeney and Keefe (2001), whose WBR BBN CARTs in three young female adults were obtained at levels that were 12.3 to 16.3 dB (depending on the WBR CART statistical measurement approach) lower than the AI BBN CARTs. Additional measurements in four more subjects (two young males and two young females) yielded improvement of about 18.5 dB with the WBR than AI approach to the BBN CART.

In contrast with the current study's lack of improvement in the mean WBR 1000-Hz CART as compared with the AI 1000-Hz CART, Feeney and Keefe (1999) obtained tonal WBR

CARTs at levels that that were at least 8 dB lower than those obtained with the AI technique. The degree of improvement could not be precisely determined due to the restricted activator intensity range. Feeney et al. (2003) obtained tonal 1000-Hz and 2000-Hz CARTs that were about 12 dB lower than those measured via the AI technique. On the other hand, Feeney, Keefe, and Sanford (2004) observed improvements of only about 3 dB in the ipsilateral and contralateral high-frequency ARTs for the WBR as compared with the AI approach. In that study, a band-filtered click rather than chirp was used as the WBR probe stimulus, allowing separation between the frequencies of the probe stimulus and the activator. All of the other studies (Feeney & Keefe, 1999, 2001; Feeney et al., 2003) used a sequence of eight chirps as the probe stimulus.

The outcome differences between the current investigation and the other studies may be related to differences in the instrumentation and procedure, statistical method for computing the WBR CARTs, and sample size. The WBR CARTs in the current study were based on sample sizes of 7 or 8 within a particular age group. The sample sizes in the other WBR CART investigations had sample sizes of only 3-4. The Mimosa WBR system (used in the current investigation) employs 24 chirps for WBR measurement in contrast with the WBR system employed by Feeney and his colleagues which uses only 8 chirps. Thus, each Mimosa WBR response reflects signal averaging of the responses to 24 chirp probe stimuli. Additionally, the baseline variance was computed based on 16 baseline measurements in the current study as compared with only 6 baseline measurements in the Feeney et al. studies. An increased number of baseline samples provides more precise estimates of baseline variance.

Criterion Selection

The 1SD/10f criterion applied in the current investigation produced WBR BBN CARTs significantly better than those measured via the AI technique. Additional refinement of the WBR

CART criterion may yield additional decreases in the WBR CARTs. The current criterion balanced the width of the frequency range (where the minimal ABD had to be observed for the response to be considered a CART effect) with the requirement of a minimum ABD of 1 SD. Furthermore, the criterion was stringent, as the general theoretical probability of the response meeting the 1SD/10f criterion for just one activator level is 1.03477×10^{-5} (0.0000103477). Also, when comparing the WBR CARTs and AI CARTs, the typical research as well as clinical criterion employed for assessment of the AI ART either is the smallest noticeable immittance change, or a 0.2 mmho manufacturer-defined acoustic-immittance change. In this study the criterion was the smallest noticeable immittance change. The AI change occurs at a singular probe tone frequency and the ABD is not evaluated statistically (no SD requirement for threshold determination is used). Future research is needed to further refine the WBR CART criterion.

The WBR Method Effect for the BBN Activator

The significant improvement in the WBR BBN CARTs in comparison with the AI BBN CARTs may result from summation of the energy of the BBN activator and the circa 65-dB SPL chirp probe stimulus. Both stimuli encompass a wide range of frequencies and their energy is greater than the energy of the BBN activator in combination with singular probe tone of the AI instrumentation. Since the 1000-Hz activator has a single rather than wide range of frequencies, summation of its energy with the energy of the chirp probe stimulus is not expected, and in fact, did not occur for the WBR 1000-Hz CARTs obtained with the Mimosa instrumentation (in contrast with the results received in the other tonal WBR CARTs investigations with other instrumentation). This explanation of the WBR method summation effect is supported further by the reduction in the WBR CART improvement when the frequency ranges of the probe stimulus and activator were separated as found in the research by Feeney, Keefe, and Sanford (2004).

Future research is needed to examine the WBR CARTs for the BBN and tonal activators using both instruments (Mimosa and that used by Feeney and his colleagues) with 16 baselines averaged.

A method artifact, rather than the presence of summation effect, was ruled out by obtaining WBR measurements with the Mimosa instrumentation in young adult female with a bilateral, profound sensorineural hearing loss during the pilot phase of this study. No WBR changes from baseline were noted in the presence of the contralateral 1000-Hz or BBN activator for the young, adult female, consistent with the profound degree of hearing loss. Future WBR research employing lower-intensity probe stimuli together with designs ensuring activator-probe stimulus separation may yield better understanding of the ART activator-probe stimulus summation phenomenon.

Because the WBR approach yielded an expanded NTD that primarily is attributable to the improved WBR BBN CART as compared with the AI BBN CART and to the summation effect, future research needs to re-examine all other parameters of the acoustic reflex that is related to the BBN stimulus, such as latency, magnitude, and temporal integration and aging effects upon these parameters. Thus, the findings of this investigation have far-reaching implications for understanding many aspects of the acoustic reflex and may lead to changes in the existing basic concepts of the acoustic reflex.

The study was limited by the restricted available upper range of activator output from the measurement system. As a result, a WBR-CART was not obtained in some instances. Possible factors in the restricted activator level upper range are as follows:

1. Based on the review of the literature, it was projected that an upper range limit of 4 dB above the AI-CART would suffice to capture the WBR-CART. With the WBR

approach, the presence of the acoustic reflex is not apparent during measurement collection; it becomes apparent only after exporting and analyzing the WBR-CART data. Future studies should obtain WBR-CARTs using a higher upper range of activator output.

2. In some cases, the crossover of the higher levels of the activator stimulus interfered with the WBR instrumentation measurement mechanism in this study as the equipment indicated excessive levels of noise. That precluded valid measurement even at the levels below the activator's upper range. Thus, the WBR measurement could not be made and consequently, the CART could not be computed.

APPENDIX A: SUPPLEMENTARY FIGURES AND TABLES

List of supplementary figures

List of supplementary tables

Supplementary Figures

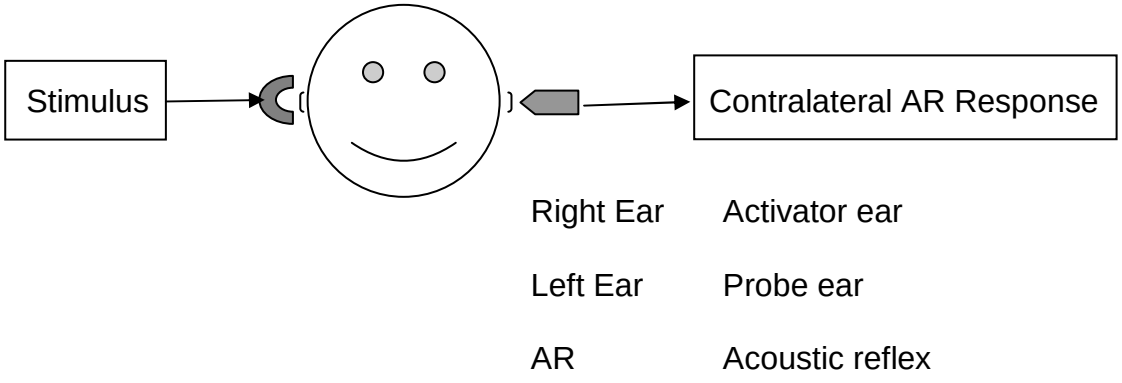

Figure A1. Schematic of the right contralateral reflex test set-up (based on Silman & Silverman, 1991).

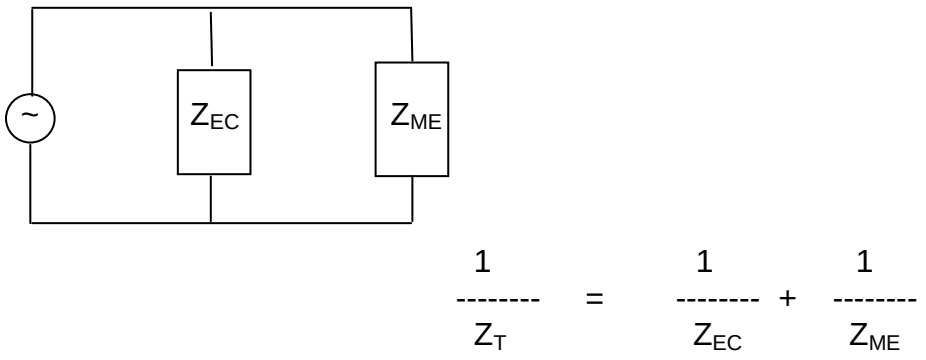

Figure A2. Parallel system: Z_T represents total ear impedance, Z_{EC} is ear canal impedance and Z_{ME} refers to middle ear impedance (based on Silman & Silverman, 1991).

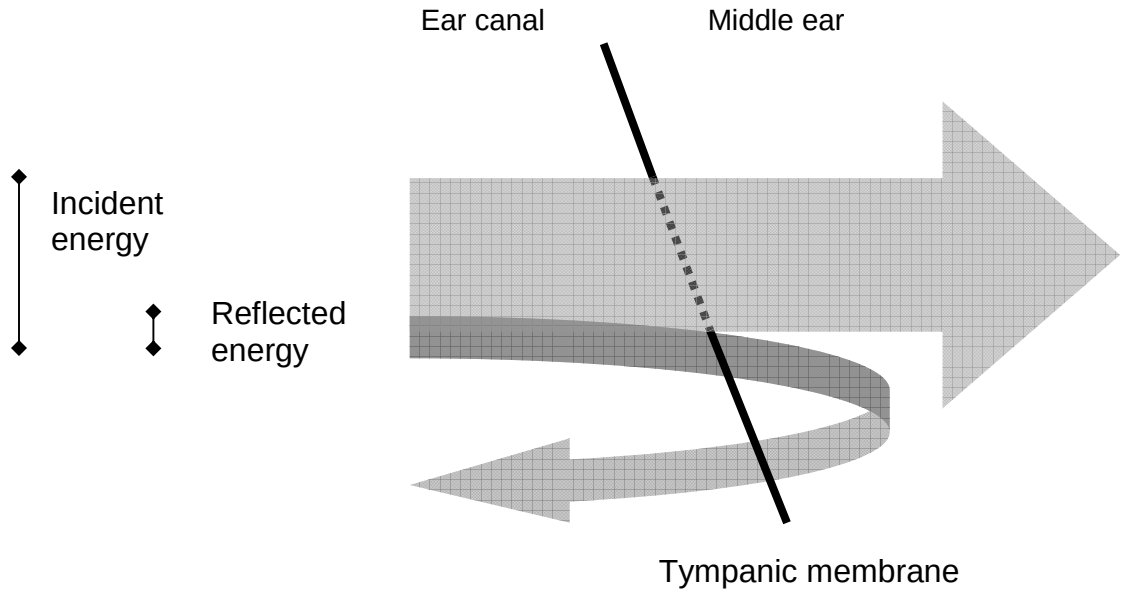

Figure A3. Idealized diagram of the energy distribution at the tympanic membrane; the ear canal is conceptualized as a lossless transmission line in human adult ears up to circa 8000 Hz (Stinson et al., 1982)

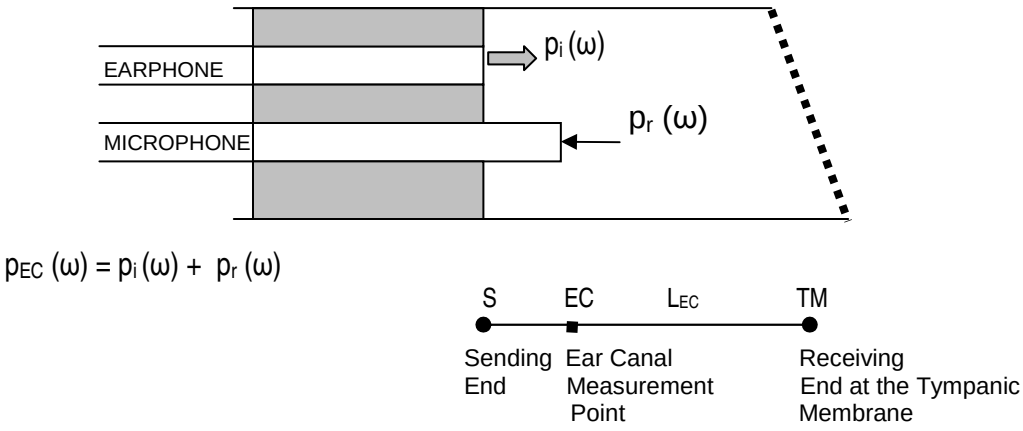

Figure A4. Ear canal as acoustic transmission line (schematic drawing).

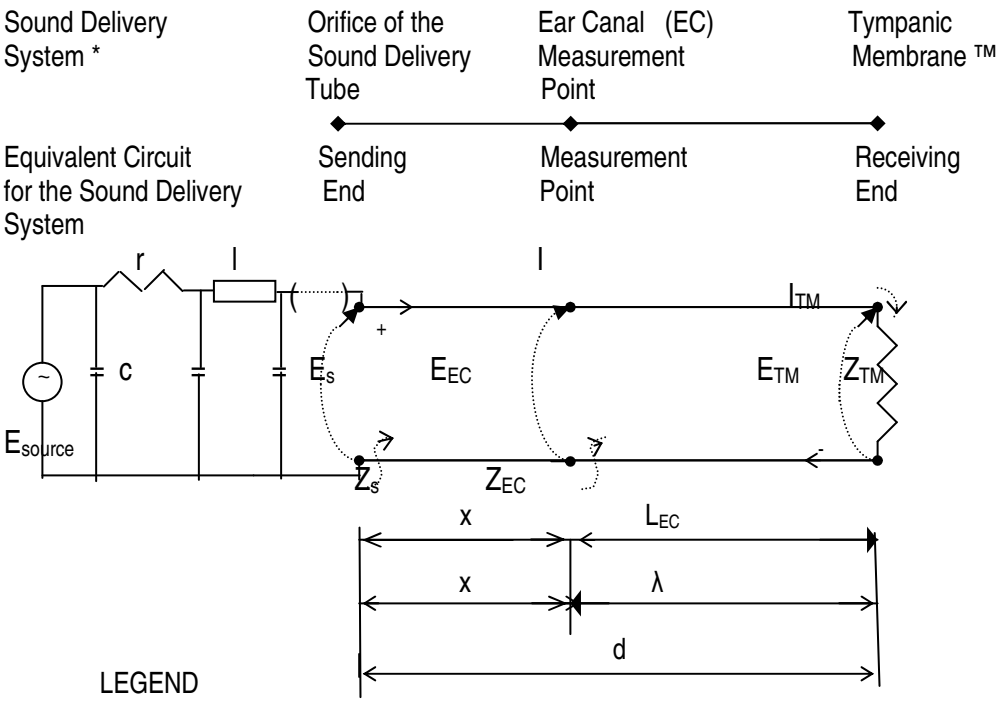

LEGEND

Physical quantities

Z_s sending end impedance

Z_{TM} terminating impedance representing impedance at tympanic membrane at the receiving end

Z_{EC} measurement point ear canal impedance

Z_0 characteristic impedance

d distance from the sending end to the receiving end

L_{EC} distance from the measurement point along the line (measured from left to right)

λ distance from the receiving end at the TM to the measurement point along the line

* The sound delivery system consists of the input sound source connected to a sound delivery tube through a porous screen. The sound delivery tube may be represented as a mass-compliance transmission line. The porous screen which acts as an acoustic resistor "r" is created by cascading several screens together.

Figure A5. Model of human ear canal as electrical uniform transmission line with the reflection at the termination of the line (based on Allen, 1985, and Johnson, 1950)

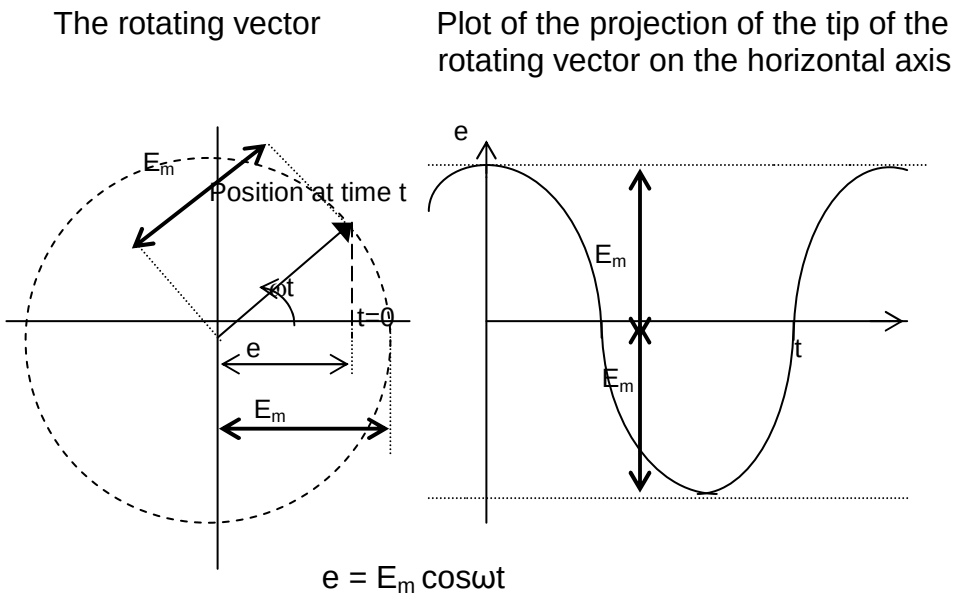

Figure A6. The generation of sinusoid by rotating vector [Based on Johnson (1950)]

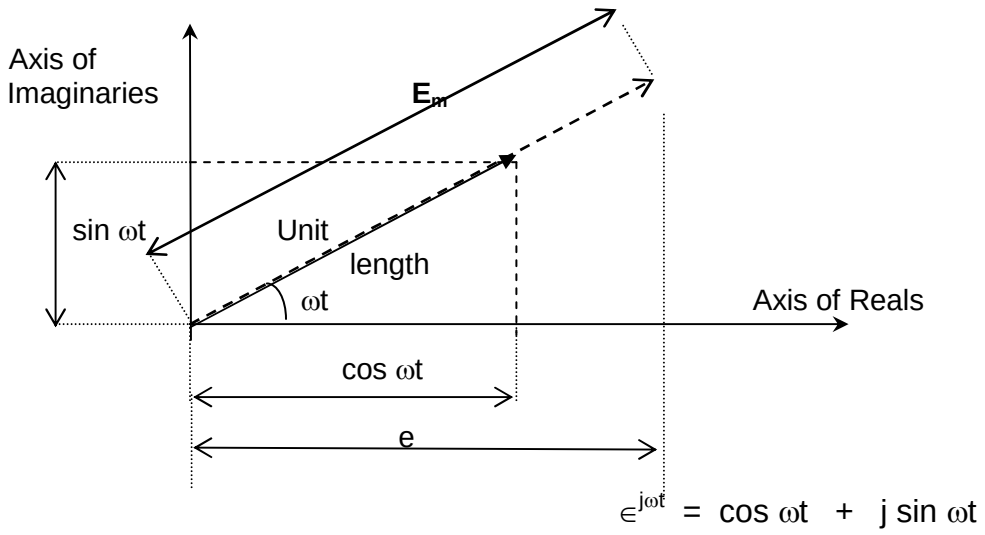

*Figure A7***.** Representation of $\in^{j\omega t}$ on the complex plane [Based on Johnson (1950)].

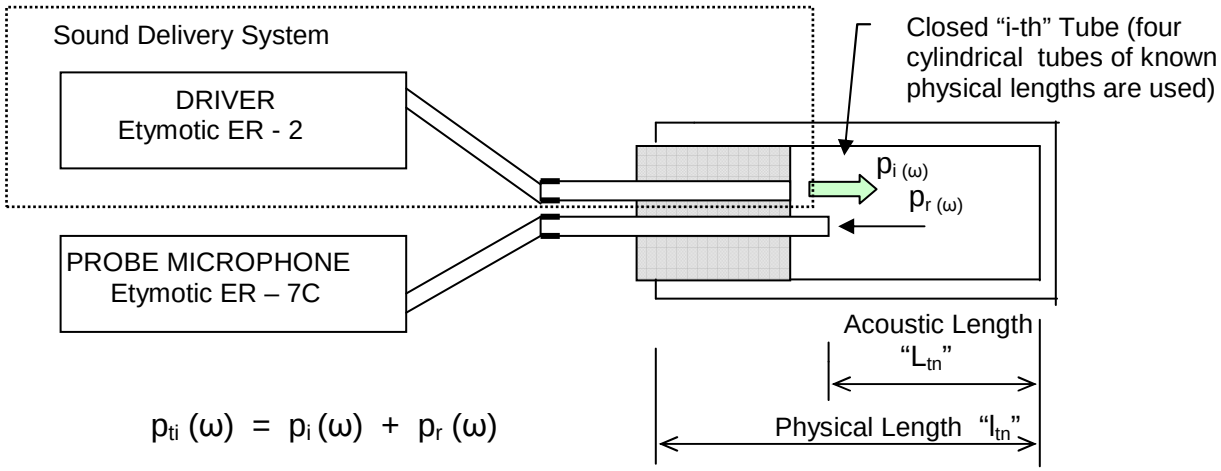

Figure A8. Schematic drawing of the calibration assembly

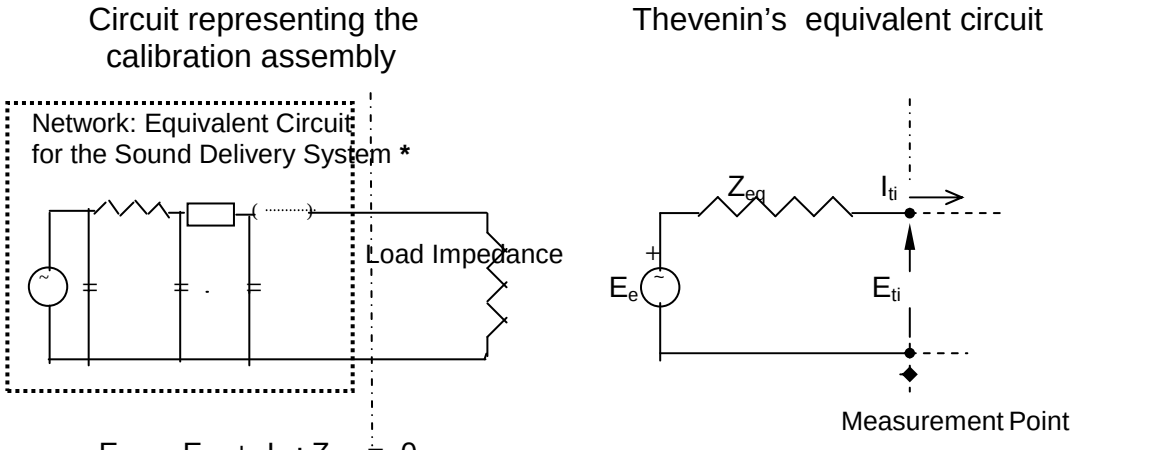

$$E_{tn} - E_{eq} + I_{tn} \cdot Z_{eq} = 0$$

$$E_{tn} + \frac{E_{tn}}{Z_{tn}} \cdot Z_{eq} = E_{eq}$$

$$E_{tn} \cdot \left(1 + \frac{Z_{eq}}{Z_{tn}}\right) = E_{eq}$$

$$\frac{E_{tn}}{E_{eq}} = \frac{Z_{tn}}{Z_{eq} + Z_{tn}}$$

The sound delivery system consists of the input sound source connected to a sound delivery may be represented as a mass-compliance transmission line. The porous screen which acts as an acoustic resistor “r” is created by cascading several screens together (Allen, 1985)

Figure A9. Equivalent circuit for the calibration assembly (based on Allen, 1985, and Johnson, 1950)

	A	B	C	D	E	F	G	H	I
1	% RMS-Data Export (RMS 4.3.3.3 -- Mimosa Acoustics)								
2	% Name: 001		Date: 8/11/2006 1:00:09 PM						
3	% Power Reflectance as |R|^2 [%]								
4	% Column 1: frequency / Hz								
5	Column 2: [Data] Right Ear:	Tip 14A	Measured 0h 27m after Probe Calibration	SPL = 60.1 dB @1kHz	equ. vol.: 1.30 ccm				
6	Column 3: [Data] Right Ear:	Tip 14A	Measured 0h 32m after Probe Calibration	SPL = 59.8 dB @1kHz	equ. vol.: 1.37 ccm				
7	Column 4: [Data] Right Ear:	Tip 14A	Measured 0h 33m after Probe Calibration	SPL = 59.8 dB @1kHz	equ. vol.: 1.39 ccm				
8	Column 5: [Data] Right Ear:	Tip 14A	Measured 0h 34m after Probe Calibration	SPL = 59.8 dB @1kHz	equ. vol.: 1.37 ccm				
9	Column 6: [Data] Right Ear:	Tip 14A	Measured 0h 34m after Probe Calibration	SPL = 59.9 dB @1kHz	equ. vol.: 1.40 ccm				
10	Column 7: [Data] Right Ear:	Tip 14A	Measured 0h 35m after Probe Calibration	SPL = 59.7 dB @1kHz	equ. vol.: 1.37 ccm				
11	Column 8: [Data] Right Ear:	Tip 14A	Measured 0h 35m after Probe Calibration	SPL = 59.8 dB @1kHz	equ. vol.: 1.42 ccm				
12	Column 9: [Data] Right Ear:	Tip 14A	Measured 0h 36m after Probe Calibration	SPL = 59.8 dB @1kHz	equ. vol.: 1.41 ccm				
13	2.11E+02	9.07E+01	8.90E+01	8.88E+01	9.09E+01	8.98E+01	9.20E+01	8.89E+01	8.97E+01
14	2.34E+02	9.48E+01	8.74E+01	8.79E+01	8.82E+01	8.55E+01	9.06E+01	8.73E+01	8.68E+01
15	2.58E+02	8.73E+01	8.69E+01	8.63E+01	8.37E+01	8.58E+01	9.16E+01	8.55E+01	8.43E+01
16	2.81E+02	8.97E+01	8.90E+01	8.50E+01	8.56E+01	8.72E+01	8.70E+01	8.48E+01	8.68E+01
17	3.05E+02	8.70E+01	8.52E+01	8.63E+01	8.57E+01	8.46E+01	8.54E+01	8.32E+01	8.49E+01
18	3.28E+02	8.75E+01	8.64E+01	8.50E+01	8.46E+01	8.56E+01	8.53E+01	8.68E+01	8.33E+01
19	3.52E+02	8.79E+01	8.66E+01	8.54E+01	8.71E+01	8.40E+01	8.72E+01	8.25E+01	8.34E+01
20	3.75E+02	8.66E+01	8.52E+01	8.17E+01	8.42E+01	8.33E+01	8.43E+01	8.18E+01	8.23E+01
21	3.98E+02	8.67E+01	8.33E+01	8.34E+01	8.30E+01	8.41E+01	8.44E+01	8.42E+01	8.27E+01
22	4.22E+02	8.50E+01	8.46E+01	8.08E+01	8.34E+01	8.27E+01	8.22E+01	8.14E+01	8.19E+01
23	4.45E+02	8.47E+01	8.23E+01	8.18E+01	8.23E+01	8.27E+01	8.08E+01	7.87E+01	8.20E+01
24	4.69E+02	8.28E+01	8.12E+01	8.01E+01	8.13E+01	8.14E+01	7.94E+01	7.70E+01	7.93E+01

Figure A11. Example of MIMOSA RMS raw data recording for subject 001, Test BBN, Frequency range 211 to 469Hz; lines 13 thru 24 show in column A: frequency; column B: baseline response; column C: 48 dB HL activator response; column D: baseline response; column E: 50 dB HL activator response; column F: baseline response; column G: 52 dB HL activator response; column H: baseline response; column I: 54 dB HL activator response

Supplementary tables

Table A1

Impedance and Admittance and Their Components (Based on Popelka, 1981; Silman & Silverman, 1991)

	Impedance	Admittance
Physical quantities	Z Complex impedance	Y Complex admittance
	|Z| Magnitude of the impedance	|Y| Magnitude of the admittance
	X_M Mass reactance	B_M Mass susceptance
	X_S Stiffness Reactance	B_S Stiffness susceptance
	X_T Total reactance = imaginary component of complex impedance	B_T Total susceptance = imaginary component of complex admittance
	R Resistance = real component of complex impedance	G Conductance = real component of complex admittance
	θ Phase angle in degrees	Θ Phase Angle in degrees
Geometrical vector relationships	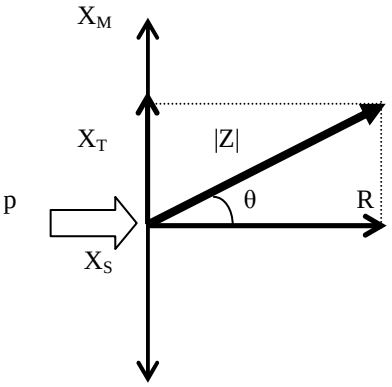	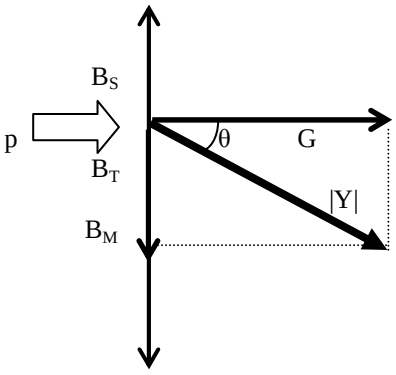

Table A.1 *Continued*

	Impedance	Admittance
Mathematical relationships	$\lvert Z\rvert^2 = R^2 + X_T^2 =$ $= R^2 + (X_M - \lvert X_S \rvert)^2$	$\lvert Y\rvert^2 = G^2 + B_T^2 =$ $= G^2 + (B_S - \lvert B_M \rvert)^2$
	$\lvert Z\rvert = \sqrt{R^2 + X_T^2} =$ $= \sqrt{R^2 + (X_M - \lvert X_S \rvert)^2}$	$\lvert Y\rvert = \sqrt{G^2 + B_T^2} =$ $= \sqrt{G^2 + (B_S - \lvert B_M \rvert)^2}$
	$\sin\theta = \frac{X_T}{\lvert Z\rvert} = \frac{X_M - \lvert X_S \rvert}{\lvert Z\rvert}$	$\sin\theta = \frac{B_T}{\lvert Y\rvert} = \frac{B_M - \lvert B_S \rvert}{\lvert Y\rvert}$
Rectangular notation of immittance	$Z = R + jX_T$ j represents complex numbers and can be treated mathematically as $j = \sqrt{-1}$	$Y = G + jB_T$ j represents complex numbers and can be treated mathematically **as $j = \sqrt{-1}$**
Polar notation of immittance	$Z = \lvert Z\rvert \angle\theta$	$Y = \lvert Y\rvert \angle\theta$
Impedance – Admittance Relationship	From equations $\lvert Z\rvert = 1/\lvert Y\rvert$ and $\sin\theta = X_T/\lvert Z\rvert = -B_T/\lvert Y\rvert$ we obtain following relationships: $X_T = \frac{-B_T}{G^2 + B_T^2}$ $B_T = \frac{-X_T}{R^2 + X_T^2}$	 $R = \frac{G}{G^2 + B_T^2}$ $G = \frac{R}{R^2 + X_T^2}$

APPENDIX B:

TRANSMISSION LINE THEORY AND ITS

WIDEBAND REFLECTANCE APPLICATION

B.1 Energy reflectance and reflectance

B.1.1 Introduction

Experimental wideband reflectance devices utilize transmission line theory, concept originally developed in the electrical engineering.

Wideband reflectance measurement consists of two parts:

- Calibration
- Ear-canal wideband reflectance measurement.

Typical wideband reflectance instrumentation set-up is briefly described in the following paragraph.

The wideband reflectance device has several parts: computational device, probe containing two transducers (acoustic pressure source (earphone) and microphone) and, so called calibration tubes which are used during calibration procedure. Compressible foam eartip of the probe is inserted into the ear canal when the ear-canal measurement is conducted or into the calibration tubes during the calibration procedure. The ear-tip is inserted into the orifice, so that the rear of the foam plug is flush with the tubal edge when the calibration is performed, or ear canal entrance during the ear-canal measurement. The length of the foam plug is about 12 mm. This design In order to reduce evanescent mode coupling between the flow source and probe tip, when high frequency stimuli are used, On some versions of the wideband reflectance device, the microphone probe tip protrudes about 3 mm beyond the edge of the foam plug. (Voss & Allen; 1994) The point of the microphone tip termination will be described in this text as the *ear canal measurement point* (see Figure A7). Acoustic pressure source presents at the, so called, *sending end*, a chirp signal in to the ear canal. The chirp signal is a complex frequency signal.

B.1.2 Acoustical Transmission Line

The ear canal functions as a *transmission line*. The complex sound-wave travels from the sending end through the ear canal and would be characterized at particular point on the line by so called *incident pressure* p_i. This complex sound-wave progresses until it reaches the tympanic membrane at the so-called *receiving end*, or, in other words, *termination of the line*.
At the receiving end, part of the energy of the sound-wave is transferred in to the middle ear and part is reflected and travels as a *reflected sound-wave* in the opposite direction. The reflected sound-wave would be described at particular location on the transmission line by the complex *reflected pressure* p_r. The probe microphone at the ear canal measurement point obtains value of the *ear canal pressure* p_{EC} which is complex frequency pressure sum of incident pressure and reflected pressure at the measurement point (see Figure A7).

B.1.3 Definition, Physical Relationships

The acoustical energy reflectance $\mathcal{R}$ at angular frequency ω may be defined as the square magnitude of the pressure reflection coefficient K at the same angular frequency ω. The pressure reflection coefficient K is often called simply, reflectance.

$$\mathcal{R}(\omega) = |K(\omega)|^2$$

Equation 1.3/1 (Voss & Allen, 1994; Johnson, 1950)

The reflectance K at angular frequency ω is a transfer function that is defined by the ratio of the reflected pressure p_r to the incident pressure p_i:

$$K(\omega) = \frac{p_r(\omega)}{p_i(\omega)} \quad \text{[dimensionless]}$$

Equation 1.3/2 (Voss & Allen, 1994; Johnson, 1950)

where ω is angular frequency and is described by following equation:

$\omega = 2 \Pi f$ [rad / s]

B.1.4 Reflectance-Impedance Equation

Direct measurements of incident pressure p_i and reflected pressure p_r are problematic. Ear canal reflectance K_{EC}, however, may be computed from the ear canal impedance Z_{EC} or from normalized ear canal impedance $\mathcal{Z}_{EC}$. Ear canal impedance Z_{EC} may be obtained from the measured ear canal pressure p_{EC}.

$$K_{EC}(\omega) = \frac{Z_{EC}(\omega) - Z_0}{Z_{EC}(\omega) + Z_0} = \frac{\frac{Z_{EC}(\omega)}{Z_0} - 1}{\frac{Z_{EC}(\omega)}{Z_0} + 1} = \frac{Z_{EC}(\omega) - 1}{Z_{EC}(\omega) + 1}$$

Equation 1.4/1 "Reflectance-Impedance Equation" [Based on Voss & Allen (1994); Johnson, (1950)])

Note, that the ear canal impedance Z_{EC} was normalized using the characteristic impedance Z_0 and normalized ear canal impedance $\mathcal{Z}_{EC}$ was obtained.

Z_0 is the ear canal characteristic impedance:

$$Z_0 = \frac{\rho . c}{A}$$, where ρ is the air density

c speed of the sound

A nominal cross-sectional area of the ear canal

B.1.5 Reflectance-Reflectance Equation

It is believed that the energy losses due to wave propagation in the ear canal are relatively small and that the nonuniformity is gradual, so, that the soundwave propagation through the ear canal is planar. With these assumptions the ear canal may be conceptualized as a uniform lossless transmission line with the termination at the level of the tympanic membrane. The impedance at the termination at the tympanic membrane may be modeled by load impedance Z_{TM}. (Voss & Allen, 1994)

In a uniform transmission line the reflectance at the termination of the line at the receiving end at the tympanic membrane K_{TM} and the reflectance at the ear canal measurement point K_{EC} differ only by a phase factor. (Voss & Allen, 1994; Johnson, 1950) That means that the magnitudes of the reflectance K_{TM} and K_{EC} at particular angular frequency ω are equal and may be computed from the ear canal pressure measurement obtained at a convenient measurement point in the ear canal

The distance L_{EC}, defined as the distance from the ear canal measurement point to the termination point at the tympanic membrane, determines the reflectance phase factor. This relationship is expressed by "reflectance-reflectance equation":

$$K_{TM}(\omega, L) = K_{EC}(\omega, 0) \cdot \in^{-2\Gamma(\omega) LEC}$$

Equation 1.5/1: "Reflectance-Reflectance Equation" (based on Voss & Allen, 1994; Johnson, 1950)

$K_{TM}(\omega, L_{EC})$ is the tympanic membrane reflectance
at the termination point (receiving end)
in response to the stimulus with
angular frequency ω;
$L_{EC} > 0$

$K_{EC}(\omega, 0)$ is the ear canal reflectance obtained at the measurement point for stimulus with angular frequency ω;
L = 0

$\in^{-2\Gamma(\omega)LEC}$ is a complex number, representing the vector of the acoustic pressure at the level of tympanic membrane in distance L_{EC} from the ear canal measurement point
It is based on Euler's formula.
Better understanding of this complex number will be gained when the electrical transmission line model will be explained. (Section B.2)

$\Gamma(\omega)$ is complex wave number of the line
In a lossless uniform line $\Gamma = i\omega/c$
c is the velocity of the sound, and
$i = \sqrt{-1}$

The above "reflectance-impedance" and "reflectance-reflectance" equations for the acoustical transmission line {Equations 1.4./1. and 1.5./1.) were adopted from the electrical transmission line theory. The acoustical transmission lines are analogous with the electrical transmission lines. This allows us to substitute acoustical elements by the electrical ones and to model acoustical events in the electrical world. Electrical transmission line theory, presented in the next section, section 2, explains how the formulas describing the relationships of reflectance and impedance (Equation 1.4/1.) and of reflectance at two different points on the line (Equation 1.5/1.), at the tympanic membrane and ear canal measurement point, were deduced.

B.2 Electrical Transmission Line Theory

B.2.1 Acoustical and Electrical Correlates

Analogy between elements of acoustical transmission line and the components of electrical line is apparent from Table B1.

Table B1

Analogy of Acoustical and Electrical Elements

Acoustico-Mechanical Quantities			Electrical Quantities		
Quantity & Symbol	Relations	Physical units & Relations	Quantity	Symbol & Relations	Physical units & Relations
Instantaneous Sound pressure p_{inst}	$p = \frac{F}{A}$ (Force over area)	Pa (Pascal) [Pa = $N \cdot m^{-2}$]	*Instantaneous Voltage / emf* e	$E = E_m / \sqrt{2}$ $= 0.707\ E_m$	V (Volt)
Amplitude Sound Pressure (peak amplitude) p_{ampl}		([N] Newton [m^2] square area	*Amplitude Voltage* E_m		
Effective Sound Pressure p	$p = p_{ampl} / \sqrt{2}$ $= 0.707\ p_{ampl}$	[10^{-5} N = dyne])	*Effective Voltage* E		
Volume velocity U		$m^3 \cdot s^{-1}$	*Current* I		A (Amper)
Acoustic impedance Z	$Z = \frac{p}{u}$ $Z^2=[X_M+(X_S)]^2+R^2$	Ω (Ohm) [Ω = 10^5 Pa·s·m^{-3}]	*Impedance* (for parallel connections of elements with R, X_L, X_c) Z	$Z = \frac{E}{I}$	Ω {Ohm) [Ω = V·A^{-1}]

Table B1 *Continued*

Acoustico-Mechanical Quantities			Electrical Quantities		
Quantity & Symbol	Relations	Physical units & Relations	Quantity	Symbol & Relations	Physical units & Relations
Acoustic mass reactance $+X_M$	$X_M = 2\Pi f \cdot M = \omega \cdot M$ (angular frequency by mass)	Ω $[\Omega = 2\Pi \cdot s^{-1} \cdot kg]$	*Inductance reactance* $+ X_L$	$X_L = 2\Pi f \cdot L = \omega \cdot L$ (angular frequency by inductance) $L \cdot \frac{di}{dt} = e_L = E_m \cdot \sin \omega t$	Ω $[\Omega = 2\Pi \cdot s^{-1} \cdot H]$ ([H] Henry)
Acoustic stiffness reactance $- X_s$	$X_S = \frac{S}{2\Pi f}$ (stiffness over angular frequency) $S = \frac{F}{x}$ (force over displacement)	Ω $[\Omega = N \cdot rad^{-1} \cdot s \cdot m^{-1}]$ ([N] Newton)	*Capacitance Reactance* $- X_c$	$X_c = \frac{1}{2\Pi \cdot f \cdot C} = \frac{1}{\omega \cdot C}$ (inverse value of angular frequency by capacitance) $C \cdot \frac{de_c}{dt} = i_c = \omega C E_m \cos \omega t$ $= \omega C E_m \sin(\omega t + \Pi/2)$	Ω $[\Omega = rad^{-1} \cdot s \cdot F^{-1}]$ ([F] Farad)
Acoustic resistance R		Ω	*Resistance* R	$R = \frac{E}{I}$	Ω
Acoustic characteristicim pedance of the ear canal Z_0	$Z_0 = \frac{\rho \cdot c}{A}$ (density of the air by speed of the sound over the canal cross-sectional area)	Ω $[\Omega = kg \cdot m^{-4} \cdot s^{-1}]$	*Characteristic Impedance (resonant impedance) of the transmission line* Z_0	$Z_0 = \frac{\omega \cdot L}{\omega^2 \cdot L \cdot C - 1}$	Ω
Resonant frequency f_0	$f_0 = \frac{1}{2\Pi} \sqrt{S / M}$ when $X_m - X_s = 0$	Hz (Hertz) $[Hz = s^{-1}]$	*Resonant ffrequency* f_0	$f_0 = \frac{1}{2\Pi \sqrt{LC}}$ when $\omega C - 1/\omega L = 0$	Hz (Hertz) $[Hz = s^{-1}]$
Reflectance (reflection coefficient) K	$K = \frac{p_r}{p_i}$ (reflected pressure over incident pressure)	Dimensionless	*Reflectance (reflection coefficient*) K	$K = \frac{E_r}{E_i}$ (reflected voltage over incident voltage)	Dimensionless
Angular frequency ω	$\omega = 2\Pi \cdot f$	$rad.s^{-1}$	*Angular ffrequency* ω	$\omega = 2\ \Pi \cdot f$	$rad \cdot s^{-1}$

Note, that the symbol for angular frequency, “ω”, is for easier manipulation with the equations omitted in this section. It should be understood that the quantities of reflectance, energy reflectance, impedance and some others are frequency dependent (NOT the characteristic impedance; characteristic impedance of the line is frequency independent).

B.2.2 Ear Canal as Electrical Uniform Lossless Transmission Line

Research show that the human ear canal could be modeled as a uniform lossless transmission line analogous to the electrical mode (see Figure A8)**.**

B.2.3 Reflectance-Impedance Equation

From the Figure A8 depicting ear-canal as electrical transmission line we can write equation for the tympanic membrane impedance:

$$Z_{TM} = \frac{\text{Total e}}{\text{Total i}} = \frac{e_{TMi} + e_{TMr}}{i_{TMi} + i_{TMr}} ,$$

Equation 2.3 /1

and, for the characteristic impedance:

$$Z_0 = \frac{e_{TMi}}{i_{TMi}} = -\frac{e_{TMr}}{i_{TMr}} ,$$

Equation 2.3 /2

Substituting from the Equation 2.3 /2in to the Equation 2.3 /1 we may further write:

$$Z_{TM} = \frac{e_{TMi} + e_{TMr}}{\frac{e_{TMi}}{Z_0} - \frac{e_{TMr}}{Z_0}} = Z_0 \frac{e_{TMi} + e_{TMr}}{e_{TMi} - e_{TMr}}$$

$$Z_{TM} (e_{TMi} - e_{TMr}) = Z_0 (e_{TMi} + e_{TMr})$$

$$Z_{TM} \cdot e_{TMi} - Z_{TM} \cdot e_{TMr} = Z_0 \cdot e_{TMi} + Z_0 \cdot e_{TMr}$$

$$Z_{TM} \cdot e_{TMi} - Z_0 \cdot e_{TMi} = Z_{TM} \cdot e_{TMr} + Z_0 \cdot e_{TMr}$$

$$e_{TMi} \cdot (Z_{TM} - Z_0) = e_{TMr} \cdot (Z_{TM} + Z_0)$$

$$\frac{Z_{TM} - Z_0}{Z_{TM} + Z_0} = \frac{e_{TMr}}{e_{TMi}} = K_{TM}$$

Equation 2.3 /3

K_{TM} is the reflectance (pressure reflection coefficient) at the termination of the line at the tympanic membrane (so called receiving end).

If $Z_{TM} = Z_0$, then $R_{TM} = 0$ and no reflection exists.

In analogy, with Equation .2.3/3, we may write for the ear canal measurement point reflectance following:

$$K_{EC} = \frac{e_{ECr}}{e_{ECi}} = \frac{Z_{EC} - Z_0}{Z_{EC} + Z_0}$$

Equation 2.3 /4 "Reflectance-Impedance Equation"

K_{EC} is the ear canal reflectance at the measurement point

Ear canal impedance Z_{EC} is in the design of the method of ear canal reflectance used to compute the ear canal reflectance K_{EC}

B.2.4 Reflectance-Reflectance Equation

The relationship between the tympanic membrane reflectance K_{TM} and the ear canal reflectance at the measurement point K_{EC}, is, as shown earlier in the section B.1.5, following:

$$K_{TM}(\omega,x) = K_{EC}(\omega,0) \cdot \in^{-2\Gamma LEC}$$

Equation 2.4/1 "Reflectance-Reflectance Equation"

The “reflectance-reflectance equation” utilizes the theory of rotating vector, Euler’s formula and it is formulated with respect to the changes along the line, in terms of the distance along the line.

B.2.4.1 *Rotating Vector*

The best method of handling sinusoidally varying quantities like electrical voltage or sound pressure is to express them in terms of rotating vectors. The concept of the rotating vector is depicted in Figure A.6.

Using trigonometry, the projection of the tip of the rotating vector of the voltage “E_m” on the horizontal axis may be expressed by following equation:

$$e = E_m \cdot \cos \omega t \ ,$$

Equation 2.4.1/1

where, e is instantaneous voltage
(projection of the tip of the rotating vector of the voltage on the horizontal axis)
E_m is voltage amplitude
ω is angular frequency defined by equation: $\omega = 2 \Pi f$

B.2.4.2 *Complex Number* $\in^{\omega t}$

Next we pay attention to the properties of the complex number $\in^{\omega t}$ (see Figure A7).

Based on Euler’s formula we may write:

$$\in^{j\omega t} = \cos \omega t + j \sin \omega t \ ,$$

Equation 2.4.2 /1

where, ωt is a real number, and
j equals square root of negative one ($j = \sqrt{-1}$)

Therefore, $\in^{j\omega t}$ is a complex number with the real part *cos* ω and the imaginary part *sin* ω.

If we imagine a unit vector of a sinusoidally-varying quantity in the complex plane (See Figure A6.) complex number $\in^{j\omega t}$ would be an algebraic representation of the unit vector. The projection of the rotating vector on the real axis may be then expressed:

$$e = \mathcal{Re}[\, E_m \in^{j\omega t} \,],$$

Equation 2.4.2 / 2

where, the symbol $\mathcal{Re}$ is read: *the real part of,*

$$\cos \omega t = \mathcal{Re}\,[\in^{j\omega t}]$$

Equation 2.4.2 / 3

The symbol $\mathcal{Re}$ is frequently omitted and following simplified equation is written:

$$e = E_m \in^{j\omega t} = E_m \cos \omega t$$

Equation 2.4.2 / 4

In a similar manner we would obtain equation for the projection of the current's rotating vector on the horizontal axis, or, in other words, real part of the current:

$$i = \mathcal{Re}\,[\, I_m \in^{j\omega t} \,],$$

Equation 2.4.2 / 5

or, simplified version:

$$i = I_m \in^{j\omega t} = I_m \cos \omega t$$

Equation 2.4.2 / 6

The amplitudes of voltage E_m and current I_m are related to the effective values of voltage E and current I by following equations:

$$E_m = \sqrt{2} \cdot E$$

Equation 2.4.2 /7

$$I_m = \sqrt{2} \cdot I$$

Equation 2.4.2 / 8

B.2.4.3. *A-C Steady-state solution for the Uniform Line*

E_m and I_m are the complex amplitudes of the voltage and current, respectively, and *E* and *I* are complex effective values of the same quantities. These quantities, generally speaking, will vary along the line. Therefore, they will have derivatives with respect to distance along the line, the only independent variable.

Let us imagine that the wave of the voltage and current travels from the sending end along the line in the positive direction (from the right to the left). The distance from the sending end to the chosen point on the line will be *x*. Certain equations in the following section will be written in pairs: first form, for a line in general, and second form, for a lossless line. The second form will be applied for the ear canal which, as mentioned earlier, may be conceptualized as essentially uniform lossless line.Some of the general equations (those which include losses along the transmission line) deduced in the following section will be utilized in the later section of this presentation dealing with the calibration. The change of the voltage across a section of length Δx, which is expressed as $(dE/dx) \cdot \Delta x$, is caused by current *I* flowing through the series impedance of the section $R\,\Delta x + j\omega L\,\Delta x$. (The minus sign in the following equation is used because a positive value of *I* causes *E* to decrease with increasing *x*):

$$\frac{dE}{dx} = -RI - j\omega LI ,$$

Equation 2.4.3 /1 General

and in case of a lossless line:

$$\frac{dE}{dx} = -j\omega LI$$

Equation 2.4.3 /1 Lossless

The change in current *I* between the two ends of the section Δx is caused by the voltage *E* acting on the shunt admittance $G\,\Delta x + j\omega C\,\Delta x$:

$$\frac{dI}{dx} = -GE - j\omega CE \ ,$$

Equation 2.4.3 /2 General

and in case of a lossless line:

$$\frac{dI}{dx} = -j\omega CE \ ,$$

Equation 2.4.3 /2 Lossless

where *R* is a resistance in ohms;

R = 0 on a lossless line

L is an inductance in henrys

G is a conductance in mhos;

G = 0 on a lossless line

C is capacitance in farads

The a-c series impedance per unit length of line is usually denoted *Z* and the shunt admittance is labeled *Y*. For series impedance *Z* we can write:

$$Z = R + j\omega L \ ,$$

Equation 2.4.3 / 3 General

for a lossless line:

$$Z = j\omega L$$

Equation 2.4.3 / 3 Lossless

Z is a-c series impedance per unit length

of line in ohms per unit length,

For shunt admittance *Y* we can write:

$$Y = G + j\omega C ,$$

Equation 2.4.3 / 4 General

for a lossless line:

$$Y = j\omega C$$

Equation 2.4.3 / 4 Lossless

Y is a-c series shunt admittance in mhos

per unit of the length

Differential equations 2.4.3 /1, 2.4.3 /2 may then be written as follows:

$$\frac{dE}{dx} = -ZI ,$$

Equation 2.4.3 / 5

$$\frac{dI}{dx} = -YE$$

Equation 2.4.3 / 6

These equations contain two unknowns, *E* and *I*. In order to eliminate *I*, we take the derivative of the first equation with respect to *x*, distance from the sending end, and receive:

$$\frac{d^2E}{dx^2} = -Z\frac{dI}{dx} ,$$

Equation 2.4.3 / 7

With substitution for *dI / dx* from Equation 2.4.3./6., we further obtain:

$$\frac{d^2E}{dx^2} = (YZ) \cdot E$$

Equation 2.4.3 / 8

The solution for A-C steady state uniform line is in exponential form:

$$E = A_1 \cdot \in^{-\sqrt{YZ}\cdot x} + A_2 \cdot \in^{+\sqrt{YZ}\cdot x}$$

Equation 2.4.3 / 9 Voltage equation in exponential form of the A-C steady-state uniform line

where A_1 and A_2 are constants with the dimensions of voltage.

The first term $A_1 \cdot \in^{-\sqrt{YZ}\,x}$ and the second term $A_2 \cdot \in^{\sqrt{YZ}\,x}$ represent the net sum of all the waves traveling from the sending end toward the termination at the receiving end, and all the waves traveling from the receiving end toward the sending end, respectively, at the chosen point on the line at the distance *x* from the sending end. The first term is called incident voltage, the second term is denoted reflected voltage.

$$E = E_i + E_r$$

Equation 2.4.3 /10

$$E_i = A_1 \cdot \in^{-\sqrt{YZ}\cdot x}$$

Equation 2.4.3 / 11

$$E_r = A_2 \cdot \in^{\sqrt{YZ}\cdot x}$$

Equation 2.4.3 / 12

The quantity $\sqrt{YZ}$ governs the manner, in which *E* and *I* vary with distance *x*, in other words, it controls the manner in which the waves are propagated. Therefore, it is called *propagation constant* or *propagation function* and is given the symbol Γ:

$$\Gamma = \sqrt{YZ} = \sqrt{(R + j\omega L)\cdot(G + j\omega C)}\ ,$$

Equation 2.4.3 /13 General

and in case of a lossless line:

$$\Gamma = \sqrt{YZ} = j\omega \cdot \sqrt{LC}$$

Equation.2.4.3 /13 Lossless

Γ is a function of frequency and, in general, will be a complex number. Γ consists of real part and imaginary part. The real part is denoted α and is referred to as the attenuation constant. It

describes the way in which the wave dies out or attenuates as it travels. The imaginary part is assigned the symbol β and is found to determine the variation in the phase position of *E* and *I* along the line.

$$\Gamma = \alpha + j\beta ,$$

Equation 2.4.3 / 14 General

and in case of a lossless line:

$$\Gamma = j\beta$$

Equation 2.4.3 / 14 Lossless

Substituting Γ back into Equation 2.4.3 / 9, we obtain:

$$E = A_1 \cdot \in^{-\Gamma x} + A_2 \cdot \in^{\Gamma x}$$

Equation 2.4.3 /15

To find the corresponding expression for *I*, we substitute the above equation (Equation 2.4.3 / 15) into Equation 2.4.3 /5 and obtain:

$$I = \frac{1}{\sqrt{Z / Y}} \cdot (A_1 \cdot \in^{-\Gamma x} - A_2 \cdot \in^{\Gamma x})$$

Equation 2.4.3 /16

The line itself is characterized by the, so called, characteristic impedance Z_0:

$$Z_0 = \sqrt{Z / Y} = \sqrt{(R + j\omega L) / (G + j\omega C)} ,$$

Equation 2.4.3 / 17 General

For a line with negligible loss, the characteristic impedance Z_0 reduces to pure resistance independent of frequency as defined by following equation:

$$Z_0 = \sqrt{Z /Y} = \sqrt{L/C}$$

Equation 2.4.3 / 17 Lossless

Note that the characteristic impedance does not depend on the length of the line or the character of the terminating load, but is determined only by the characteristics of the line per unit length.

Next, we will devote our attention to the constants A_1 and A_2 in the equations 2.4.3 / 15 and 2.4.3 / 16 In our case, because we are interested in the events at the receiving end, at the level of the tympanic membrane, it is going to be convenient to express the constants A_1 and A_2 in terms of the receiving end quantities I_{TM} and Z_{TM}. In order to achieve that, we will have to go through series of mathematical substitutions.

First, we substitute for distance x from $x = d$ into equations 2.4.3 / 15 and 2.4.3 / 16, and obtain following relations:

$$E = I_{TM} Z_{TM} = A_1 \cdot \in^{-\Gamma d} + A_2 \cdot \in^{\Gamma d}$$

Equation 2.4.3 / 18

$$I = I_{TM} = \frac{1}{Z_0} (A_1 \cdot \in^{-\Gamma d} - A_2 \cdot \in^{\Gamma d})$$

Equation 2.4.3 / 19

$$A_1 = (I_{TM} \cdot Z_{TM} - A_2 \cdot \in^{\Gamma d}) \cdot \in^{\Gamma d}$$

$$I_{TM} . Z_0 = (I_{TM} \cdot Z_{TM} - A_2 \cdot \in^{\Gamma d}) \cdot \in^{\Gamma d} \cdot \in^{-\Gamma d} - A_2 \cdot \in^{\Gamma d}$$

$$= I_{TM} \cdot Z_{TM} - A_2 \cdot \in^{\Gamma d} - A_2 \cdot \in^{\Gamma d}$$

$$I_{TM} \cdot Z_0 - I_{TM} . Z_{TM} = - 2 A_2 \in^{\Gamma d}$$

$$A_2 = \frac{I_{TM} \cdot (Z_{TM} - Z_0)}{2 \cdot \in^{\Gamma d}}$$

$$A_2 = \frac{I_{TM}}{2} (Z_{TM} - Z_0) \cdot \in^{-\Gamma d}$$

Equation 2.4.3 / 20

$$A_1 = [I_{TM} \cdot Z_{TM} - \frac{I_{TM}}{2} (Z_{TM} - Z_0) \cdot \in^{-\Gamma d} \cdot \in^{\Gamma d}] \cdot \in^{\Gamma d}$$

$$A_1 = \frac{2 \cdot I_{TM} \cdot Z_{TM} - I_{TM} \cdot Z_{TM} + I_{TM} \cdot Z_0}{2} \cdot \in^{\Gamma d}$$

$$A_1 = \frac{I_{TM}}{2} \cdot (Z_{TM} + Z_0) \cdot \in^{\Gamma d}$$

Equation 2.4.3 / 21

Substituting the above relations for the constants A_1 and A"(from the equations 2.4.3./20. and 2.4.3./21.) into equation 2.4.3./18. and using for distance from receiving end to measurement point:

$$\lambda = d - x$$

we obtain solution for voltage E in the following form:

$$E = \frac{I_{TM}}{2} \cdot (Z_{TM} + Z_0) \cdot \in^{\Gamma (x + \lambda)} \cdot \in^{-\Gamma x} + \frac{I_{TM}}{2} \cdot (Z_{TM} - Z_0) \cdot \in^{-\Gamma(x+\lambda)} \cdot \in^{\Gamma x}$$

$$E = \frac{I_{TM}}{2} \cdot [(Z_{TM} + Z_0) \cdot \in^{\Gamma \lambda} + (Z_{TM} - Z_0) \cdot \in^{-\Gamma \lambda}] ,$$

Equation 2.4.3 / 22

where, distance λ is measured

from the receiving end, in

direction to the left, toward

the measurement point or

sending en

In our design, however, the distance between the ear canal measurement point and the receiving end at the tympanic membrane is measured from the ear canal measurement point to the right, toward the receiving end, rather than from the receiving end to the left

toward the ear canal measurement point. Therefore, we substitute for λ from:

$$L_{EC} = -\lambda \ ,$$

and we obtain:

$$E = \frac{I_{TM}}{2} \left[(Z_{TM} + Z_0) \cdot \in^{-\Gamma LEC} + (Z_{TM} - Z_0) \cdot \in^{\Gamma LEC} \right]$$

Equation 2.4.3 / 23

And further we can write for the reflected and incident voltage:

$$E_i = \frac{I_{TM}}{2} \cdot [(Z_{TM} + Z_0) \cdot \in^{-\Gamma LEC}]$$

Equation 2.4.3 /24

$$E_r = \frac{I_{TM}}{2} \cdot [(Z_{TM} + Z_0) \cdot \in^{\Gamma LEC}]$$

Equation 2.4.3 / 25

The ratio of the reflected voltage to the incident voltage at the ear canal measurement point expressed in terms of the receiving end quantities was earlier introduced as ear canal reflection coefficient or ear canal reflectance:

$$K_{EC} = \frac{E_r}{E_i} = \frac{\frac{I_{TM}}{2} \cdot [(Z_{TM} - Z_0) \cdot \in^{\Gamma LEC}]}{\frac{I_{TM}}{2} \cdot [(Z_{TM} + Z_0) \cdot \in^{-\Gamma LEC}]}$$

$$K_{EC} = \frac{Z_{TM} - Z_0}{Z_{TM} + Z_0} \cdot \in^{2\Gamma LEC} = K_{TM} \cdot \in^{2\Gamma LEC} ,$$

Equation 2.4.3 / 26

or, substituting from *Reflectance-Impedance Equation* (Equation 2.3./4.), we may write:

$$K_{TM} = K_{EC} \cdot \in^{-2\Gamma L} = \frac{Z_{EC} - Z_0}{Z_{EC} + Z_0} \cdot \in^{-2\Gamma LEC}$$

Equation 2.4.3 /27

For variety of angular frequencies we may write identically with the already earlier introduced “reflectance-reflectance equation” (Section B.2.4. – Equation 3.6./1., Section B.4. – Equation 4.2./5.):

$$K_{TM}(\omega,L) = K_{EC}(\omega,0) \cdot \in^{-2\Gamma(\omega) LEC}$$

Equation 2.4.3 / 28

On summary, assuming that the canal is uniform and the losses are negligible, the ear canal is analog of electrical uniform lossless transmission line. The ear canal acoustical stimulation, defined by the acoustical pressure, is viewed as a correlate of a voltage on a-c steady state transmission line. Tympanic membrane is modeled by impedance at the termination of the line. The distance from the measurement point along uniform lossless transmission line, does not affect magnitude of the reflectance. Therefore, the magnitude of K_{EC} equals magnitude of K_{TM} and only difference in phase factor, as function of distance L_{EC} along the line, will be observed. From the slope of the phase of reflectance in the high frequencies the distance L_{EC} between the ear canal measurement point and tympanic membrane is estimated. Ear canal reflectance at the measurement point K_{EC} is, as shown in this section, computed from the ear canal impedance Z_{EC}.

B.2.5 Impedance Measurements

Unlike in the case of electrical transmission lines, no direct impedance measurements are possible on the acoustical transmission line and there are no convenient commercial devices for acoustical

impedance measurements. Ear canal reflectance method computes ear canal impedance Z_{EC} from ear canal pressure p_{EC} measurement. The reasons for the lack of acoustical impedance measurement instruments reportedly include the unavailability of low distortion acoustic sources (0.005 % distortion), unavailability of precisely calibrated acoustic impedances, and the complications introduced by the wave like nature of the sound and its relatively low speed of propagation (Allen, 1985).

The technique determining the ear canal impedance Z_{EC} is based on *Thevenin theorem* and precise estimation of the, so-called, *Thevenin parameters* of the sound delivery system as a function of the frequency.

The Thevenin parameters of the sound delivery system are the equivalent pressure p_{eq}, equal to open circuit pressure, and the equivalent impedance Z_{eq}. They are obtained during the calibration using uniform tubes as an acoustical transmission line. Once the Thevenin equivalent source parameters p_{eq} and Z_{eq} of the sound delivery system are known, the unknown ear canal impedance Z_{EC} may be computed from the ear canal pressure p_{EC} obtained at the measurement part of the method.

This technique of impedance measurement was used by number of researchers in the past [Beranek (1949), Mawardi (1949), Tonndorf and Khanna (1967), Lynch (1974)]. It underwent significant modifications by Allen (1985). Those modifications, improving both, instrumentation and technique, reportedly decrease sound delivery to acoustic transmission line impedance mismatch and lead to more accurate Thevenin parameters estimates and ear canal impedance measurements (Allen; 1985.)

The relation for ear canal impedance Z_{EC} is following:

$$Z_{EC}(\omega) = Z_{eq}(\omega) \cdot \frac{p_{EC}(\omega)}{p_{eq}(\omega) - p_{EC}(\omega)}$$

Equation 2.5 / 1

$p_{eq}(\omega)$ is Thevenin equivalent source pressure
of the transducer at radian frequency "ω"

$Z_{eq}(\omega)$ is Thevenin equivalent source impedance
of the transducer at radian frequency "ω"

Similarly, as in preceding sections, this relation (Equation 2.5 /1) is deduced from the electrical theory. It stems from electrical circuit analysis, in particular it is an application of, the so called, Ohm's law, Kirchhoff's laws and Thevenin's Theorem.

B.3 Calibration

B.3.1 Introduction

As clear from the a foregoing explanation, in order to be able to determine ear canal impedance Z_{EC},, magnitude of equivalent source pressure p_{eq} and equivalent source impedance Z_{eq}, so-called *Thevenin parameters*, must be known beside the measured ear canal pressure p_{EC} (see Equation 2.5 /I). These parameters are obtained as complex quantities for all the values of angular frequency ω.

Thevenin parameters, equivalent source pressure p_{eq} and equivalent source impedance Z_{eq}, are determined during the acoustic calibration procedure using the so called "four cavity method". The calibration in essence consists of matching the response data to a closed tube model.

B.3.2 Calibration Assembly

For calibration, there are used four cavities in a shape of cylindrical tubes closed at far end. All the tubes have the same diameter, equal to that of an average human ear canal (0.74 cm) and different physical lengths "l_{tn}" (l_1 = 1.13 cm; l_2 = 1.72 cm; l_3 = 2.06 cm; l_4 =3.02 cm;). These cavities present four different acoustic loads. Tubal model impedance Ztn at the measurement point may describe the acoustic load of each tube (see Figure A8.) The same probe as the one

used for the ear canal pressure p_{EC} measurement is inserted into each cavity and complex tubal pressure frequency response p_{ti} of each cavity is measured. The acoustic lengths L_{tn} of the calibration tubes are defined as the distance from the measurement point to the termination of the tube at the closed end. The acoustical lengths L_{tn} depend on the depth of the insertion of the foam tip into the calibration tube. The acoustical lengths L_{tn}, as apparent, differ from the physical lengths l_{tn} of the calibration tubes.

B.3.3 Calibration Tube Impedance

Tubal model impedance Z_{ti} is computed for each of the four calibration tubes. This impedance represents the load at the measurement point. Its analogy in the ear canal is the ear canal impedance Z_{EC}.

The tubal impedance Z_{tn} is a function of the angular frequency ω and is calculated from the characteristic tubal impedance Z_{0t}, acoustical lengths of the tubes L_{tn} and impedance propagation wave number. Since the cross-sectional area is the same in all the 4 calibration tubes, the two values of Z_{0t} and Γ_t are the same for all four tubes. Past research showed that thermoviscous wave propagation losses must be included in order to obtain accurate estimates of tubal impedances Z_{tn}.

B.3.3.1 *Tubal load impedance at the measurement point Z_{ti}*

Following equation is used to determine the values of "Z_{tn}".

$$Z_{tn}(\omega) = Z_{0t}(\omega) \coth [\Gamma_t(\omega) L_{tn}]$$

Equation .3.3.1 /1 (Keefe, 1984)

where, $Z_{tn(\omega)}$ is the complex load impedance of the n-th cylindrical tube at the measurement point

Z_{0t} is characteristic impedance

$\Gamma t(\omega)$ is the complex propagation wave

number of the of the calibration

tube

L_{tn} is the acoustic length of the n-th

calibration tube

B.3.3.2 *Characteristic Impedance of the Calibration Tube Z_0*

Characteristic impedance Z_0 of the calibration tubes may be defined to be the input impedance looking into an infinite length of the cylindrical tubing.

Should not the losses associated with the wave propagation – the thermoviscous losses, be included, simple equation may be used to calculate the characteristic impedance $Z_{0.}$:

$$Z_0 = \frac{\rho . c}{A}$$

Equation 3.3.2 /1

where, Z_0 is the characteristic impedance

ρ is the density of the air

c is the speed of the sound

A is the cross-sectional area of the entryway

This equation is used to calculate the characteristic impedance of the ear canal.

To minimize the error, the exact speed of the sound may be used. As known, the speed of the sound is a function of the ambient temperature:

$$c = 331.4 \sqrt{\frac{T}{273}}$$

Equation 3.3.2 / 2

where, *331.4* is the speed of the sound in m/s at the

freezing temperature (of pure distilled H_2O)

T is the ambient temperature in Kelvin

273 is H_2O freezing temperature in Kelvin

Equation 3.3.2 /1 is utilized in the wideband reflectance method to calculate characteristic impedance of the ear canal, essentially lossless transmission line (in which case nominal ear canal cross-sectional area is used for *A)*. However, in case of the characteristic impedance of the calibration tubes, the research shows that the estimates of thermoviscous losses must be included in order to avoid error of an unacceptable size. Several investigators formulated viscothermal loss approximation equations. As per personal communication with Jont B. Allen the best approximation is yielded by the equations formulated by Keefe (1984). These equations provide estimates of the following transmission line parameters: series resistance *R*; series inertance *L*, shunt compliance *C*, shunt conductance *G*.(Recall that these quantities are analogous to the electrical quantities of series resistance *R*, series inductance *L*, shunt capacitance *C* and shunt conductance *G*, respectively).Calibration tubes' series impedance *Z* and shunt admittance *Y* are then calculated according to the earlier presented equations: Equation 2.4.3 /3General for the series impedance, and Equation 2.4.3 /4 General for the shunt admittance. The characteristic impedance Z_0 is then obtained from the earlier deduced equation: Equation 2.4.3 /17 General.

$$Z_{0t}(\omega) = \sqrt{Z / Y} = \sqrt{(R + j\omega L) / (G + j\omega C)}$$

Equation 3.3.2 / 1 (Equation 2.4.3 /17 General)

B.3.3.3 *Propagation Wave Number* Γ_t

The propagation wave number Γ_t of the transmission line may be defined as the phase change per unit length at an arbitrary fixed time along the semi-infinite cylindrical tube. As in case of the characteristic impedance Z_{0t} the propagation wave number Γ_t is calculated from the calibration tube series impedance *Z* and shunt admittance *Y* (see Equation 2.4.3 /13 General), utilizing the transmission line parameter approximations formulated by Keefe (1984).

$$\Gamma_t(\omega) = \sqrt{Z \cdot Y} = \sqrt{(R + j\omega L) \cdot (G + j\omega C)}$$

Equation 3.3 /1 (Equation 2.4.3 /13 General)

B.3.3.4 *Acoustical Lengths* L_{tn}

The acoustical tubal lengths L_{tn} are different than the physical lengths l_{ti}. Precise estimate of the acoustical lengths L_{tn} is essential for precise estimate of the values of the tubal impedance Z_{tn}. The acceptable estimate of the acoustic lengths L_{tn} is obtained from the solution of the system of the overspecified equations formulated for the Thevenin equivalent circuit (see Section B.3.4.). Acoustic lengths L_{tn} are then applied to Equation 3.3.1 /1, yielding the values of tubal impedances Z_{tn}.

Physical lengths l_{tn} or antiresonant estimates of the acoustical lengths $L_{ni/antiresonant}$ may be used as the initial values for the first solution of the system of the overdetermined equations.

The antiresonant estimates of the acoustical lengths L_{tn} are approximations obtained from the first antiresonance of the impedance, that is, finding the frequency f_0 at which tubal impedance Z_{tn} equals zero. Frequency f_0 may be estimated from the pressure response: the pressure exhibits zeroes at the impedance zeroes. The approximation of the acoustic length L_{tn} is then determined from the following equation:

$$L_{tn/antiresonant} = c / 4 f_0$$

Equation 3.3.4 / 1

where, $L_{tn/antiresonant}$ is the antiresonant estimate of the acoustical length L_{tn} of the i-th tube

c is the speed of the sound

f_0 is the first antiresonant frequency

B.3.4 Thevenin Theorem and Thevenin Parameters

The analogy between the acoustic and electrical transmission lines is utilized to determine the values of the equivalent source pressure p_{eq} and equivalent source impedance Z_{eq}.

A linear electrical network, which is energized by one or more sources of emf, may be utilized by making a connection to two output terminals. According to the Thevenin theorem, such a network at those terminals, cannot be distinguished from a single source of emf in a series with single impedance or using the Norton equivalent circuit, the network at the terminals cannot be differentiated from the source of current that is shunted with impedance. The equivalent circuit for the calibration assembly is depicted in the Figure A9. In our case, it is the sound delivery system, which is as a network replaced by the Thevenin equivalent circuit. (Johnson, 1950)

Using the Ohm's and Kirchoff's laws we may write for the Thevenin equivalent circuit:

$$E_{tn} - E_{eq} + I_{tn} \cdot Z_{eq} = 0$$

Equation 3.4 / 2

$$E_{tn} - E_{eq} + \frac{E_{tn}}{Z_{tn}} \cdot Z_{eq} = 0$$

$$E_{tn} + \frac{E_{tn}}{Z_{tn}} \cdot Z_{eq} = E_{eq}$$

$$E_{tn} \cdot \left(1 + \frac{Z_{eq}}{Z_{tn}} \right) = E_{eq}$$

$$E_{tn} \cdot \left(\frac{Z_{tn} + Z_{eq}}{Z_{tn}} \right) = E_{eq}$$

$$\frac{E_{tn}}{E_{eq}} = \frac{Z_{tn}}{Z_{tn} + Z_{eq}}$$

Equation 3.4 /3

Substituting analogous acoustical values into the above-presented equation will produce:

$$\frac{p_{tn}}{p_{eq}} = \frac{Z_{tn}}{Z_{tn} + Z_{eq}}$$

Equation 3.4 /4

For the four calibration tubes, there are four equations with two unknown quantities, Thevenin parameters p_{eq} and Z_{eq}. There are also four pairs of the measured tubal pressure responses p_{tn} and derived tubal impedances Z_{tn}, specifically p_{t1}, Z_{t1}, p_{t2}, Z_{t2}, p_{t3}, Z_{t3}, p_{t4}, Z_{t4}. Initially, the values of the tubal impedances Z_{tn} are based on the initial estimates of the acoustic lengths L_{tn}.

The earlier deduced Equation 3.4 / 4 is applied for the four calibration tubes as a system of overspecified equations in a following fashion:

$$\begin{pmatrix} Z_{t1} & -p_{t1} \\ \cdot & \cdot \\ Z_{tn} & -p_{tn} \\ \cdot & \cdot \\ Z_{tq} & -p_{tq} \end{pmatrix} \begin{pmatrix} p_{eq} \\ \cdot \\ Z_{eq} \end{pmatrix} = \begin{pmatrix} p_{t1}Z_{t1} \\ \cdot \\ p_{tn}Z_{tn} \\ \cdot \\ p_{tq}Z_{tq} \end{pmatrix}$$

Equation (system of equations) 3.4 / 5, by Allen (1985)

This system of equations must be solved separately for each angular frequency ω.

The solution for the Thevenin parameters p_{eq} and Z_{eq} in each angular frequency ω is following:

$$\begin{pmatrix} p_{eq} \\ Z_{eq} \end{pmatrix} = \begin{pmatrix} 1 \\ \hline \Delta \end{pmatrix} \cdot \begin{pmatrix} \sum_{n=1}^{q} |p_{tn}|^2 & \sum_{n=1}^{q} Z_{tn}^{*} p_{tn} \\ \sum_{n=1}^{q} p_{tn}^{*} Z_{tn} & \sum_{n=1}^{q} |Z_{tn}|^2 \end{pmatrix} \times \begin{pmatrix} \sum_{n=1}^{q} |Z_{tn}|^2 p_{tn} \\ -\sum_{n=1}^{q} |p_{tn}|^2 Z_{tn} \end{pmatrix},$$

Where mean square error Δ is:

$$\Delta = \left[\sum_{n=1}^{q} |Z_{tn}|^2 \right] \cdot \left[\sum_{n=1}^{q} |p_{tn}|^2 \right] - \left[\sum_{n=1}^{q} Z_{tn}^{*} p_{tn} \right]$$

Equation 3.4 / 6

The optimal Thevenin parameters are then computed by minimizing the sum of the mean square error functions over the range of frequencies ω of the above system of equations (Equation 2.5 /5) with respect to the Thevenin parameters.

The mean square error function $C(\omega)$ is calculated at each angular frequency ” using the next equation:

$$C(\omega) = \sum_{n=1}^{q} | Z_{tn} p_{eq} - p_{tn} Z_{eq} - p_{tn} Z_{tn} |^2 ,$$

Equation 3.4 / 7

And sum of the mean square error functions C_T (computed over the range of values of the angular frequency ω) is following:

$$C_T(\omega) = \sum_{\omega\ \text{lowest}}^{\text{highest}} C(\omega)$$

Equation 3.4 / 8

The lengths L_{tn} are selected so, that the error C_T is minimized. The eventual four values of the optimized tubal acoustical lengths L_{tn} must be used for all the values of angular frequency ω.

APPENDIX C:

WIDEBAND REFLECTANCE METHOD (METHOD OF J.B. ALLEN)

C.1 Introduction

C.2 Calibration

C.2.1 Measurements of four complex pressure frequency responses $p_{ti}(\omega)$ to chirp signal in four sealed cavities

C.2.2 Initial estimation of four effective (acoustic) tubal lengths L_{t1}, L_{t2}, L_{t3}, L_{t4} of the four cavities

C.2.3 Initial estimate of tube model load impedances Z_{t1}, Z_{t2}, Z_{t3}, Z_{t4}

C.2.4 System of overspecified equations

C.2.5 Optimization of acoustical lengths L_{tn}

C.2.6 Thevenin parameters computation

C.3 Ear canal complex pressure response measurements and impedance and reflectance computation

C.3.1 Measurement of complex ear-canal pressure response $p_{EC}(\omega)$

C.3.2 Computation of complex ear canal impedance $Z_{EC}(\omega)$

C.3.3 Computation of ear-canal wideband (complex) reflectance $K_{EC}(\omega)$

C.3.4 Computation of ear-canal wideband (complex) energy reflectance $R_{EC}(\omega)$

C.1 Introduction

Preceding sections lent familiarity with acoustical and electrical concepts applied in the method of wideband reflectance. Following section lists the steps of the wideband reflectance method as employed by J. B. Allen, one of the leading researchers in this field. His approach served as the basis for the development of several prototypes of the

wideband reflectance equipment (e.g.: Mimosa RMS [Mimosa Reflectance Measurement System], Power Flow). The later versions reportedly incorporated certain improvements in design, for example, inclusion of thermoviscous losses in the calibration cavities, shorter probe tubing, etc. Several pieces of the Mimosa RMS equipment are currently used in major U.S. research centers, including Graduate School University Center, CUNY

C.2 Calibration

C.2.1 Measurements of four complex pressure frequency responses $p_{ti}(\omega)$ to chirp signal in four sealed cavities.

The cavities were developed by Mead Killion from Etymotic Research.The complex frequenct pressure response measurements are performed using SYSid (SYSid is a trademark of Ariel Corp., Highland Park, N.J., USA))system, which is a software package combined with digital signal-processing board (ArielDSP - 16+) with a 16-bit A/D and D/A analogue I/O ports. Complex frequency response measurements using a chirp signal are obtained. 12.8 ms may be selected as FFT length. Signal averaging could be performed 200 times and sampling frequency 40 kHz with a sampling period 25 x 10^{-6} s (allowing a maximum stimulus frequency 20 kHz). (Some earlier testings were conducted with stimulation up to 30 kHz (Allen, 1985). Other studies' high frequency cut-off was 8000 Hz with recordings starting at low 39 Hz.)

C.2.2 Initial estimation of four effective (acoustic) tubal lengths L_{t1}, L_{t2}, L_{t3}, L_{t4} of the four cavities.

Following values may serve as the initial estimates:

1. physical lengths l_{t1}, l_{t2}, l_{t3}, l_{t4} of the calibration cavities

2. acoustical length estimates calculated from the frequencies at which the first pressure antiresonances occur. Analysis of the measured complex cavity pressures p_{t1}, p_{t2}, p_{t3}, p_{t4} provides the estimates of the first antiresonant pressure of each cavity.

C.2.3 Initial estimate of tube model load impedances Z_{t1}, Z_{t2}, Z_{t3}, Z_{t4}

Initial estimate of tube model load impedances Z_{t1}, Z_{t2}, Z_{t3}, Z_{t4} are estimated at each frequency using the acoustic transmission line equation.The same estimated values of the acoustic lengths L_{t1}, L_{t2}, L_{t3}, L_{t4} must used in the acoustic transmission line equation for all the frequencies ω.

The acoustic transmission line equation includes effect of viscothermal losses and may be formulated to include effect of exact speed of he sound based on the room air temperature.

$$Z_{tn}(\omega) = Z_{0t}(\omega) .\coth [\, \Gamma_t(\omega) .L_{tn} \,]$$

C.2.4 System of overspecified equations

Values of measured cavity pressures p_{tn} and estimated tube load impedances Z_{tn} are entered into the system of equations for the equivalent circuit. It is an overspecified system with four equations and two unknown Thevenin parameters p_{eq}, Z_{eq} in each angular frequency ω:

$$\begin{pmatrix} Z_{t1} & p_{t1} \\ Z_{t2} & p_{t2} \\ Z_{t3} & p_{t3} \\ Z_{t4} & p_{t4} \end{pmatrix} \cdot \begin{pmatrix} p_{eq} \\ Z_{eq} \end{pmatrix} = \begin{pmatrix} p_{t1}. Z_{t1} \\ p_{t2} .Z_{t2} \\ p_{t3} . Z_{t3} \\ p_{t4} . Z_{t4} \end{pmatrix},$$

with a following solution for the Thevenin parameters p_{eq} and Z_{eq}:

$$\begin{pmatrix} p_{eq} \\ \\ Z_{eq} \end{pmatrix} = \frac{1}{\Delta} \begin{pmatrix} \sum_{n=1}^{q} |p_{tn}|^2 & \sum_{n=1}^{q} Z_{tn}^{*} p_{tn} \\ \\ \sum_{n=1}^{q} p_{tn}^{*} Z_{tn} & \sum_{n=1}^{q} |Z_{tn}|^2 \end{pmatrix} x \begin{pmatrix} \sum_{n=1}^{q} |Z_{tn}|^2 p_{tn} \\ \\ -\sum_{n=1}^{q} |p_{tn}|^2 Z_{tn} \end{pmatrix}$$

where Δ is mean square error:

$$\Delta = [\sum_{n=1}^{q} |Z_{tn}|^2] \cdot [\sum_{n=1}^{q} |p_{tn}|^2] - [\sum_{n=1}^{q} Z_{tn}^{*} p_{tn}]$$

C.2.5 Optimization of acoustical lengths L_{tn}

The earlier described overspecified system yields an error caused mainly by imprecise cavity impedance determination based on imprecise initial acoustical length L_{ti} estimation. Mean square error function $C(\omega)$ over the range of stimuli frequencies ω and sum (total) error function C_T as the sum of the mean square error functions $C(\omega)$ are computed.Original estimates of the acoustic lengths L_{tn} are adjusted. New adjusted tubal impedances $Z_{tn}(\omega)$ and Thevenin equivalent parameters $p_{eq}(\omega)$ and $Z_{eq}(\omega)$ are calculated. This process may be repeated several times, until optimized values of the acoustical lengths L_{tn} are obtained.

C.2.6 Thevenin parameters computation

Once the optimized acoustic lengths L_{tn} are obtained, the optimized Thevenin parameters, the source pressure $p_{eq}(\omega)$ and the source impedance $Z_{eq}(\omega)$ (for each stimulus frequency ω) are computed. The same four optimized acoustic lengths are used across all the stimulus frequencies.

C.3 Ear canal complex pressure response measurements and impedance and reflectance computation

C.3.1 Measurement of complex ear-canal pressure response $p_{EC}(\omega)$

Complex ear canal pressure response measurements $p_{EC}(\omega)$ are obtained in both subject's ear canals.

C.3.2 Computation of complex ear canal impedance $Z_{EC}(\omega)$

Complex Thevenin parameters $p_{eq}(\omega)$, $Z_{eq}(\omega)$ and complex ear canal pressure response $p_{EC}(\omega)$ are used to compute complex ear canal impedance $Z_{EC}(\omega)$.

$$Z_{EC}(\omega) = Z_{eq}(\omega) \cdot \frac{p_{EC}(\omega)}{p_{eq}(\omega) - p_{EC}(\omega)}$$

Complex ear canal impedance $Z_{EC}(\omega)$ is normalized by the ear canal characteristic impedance Z_0 (calculated as a ratio of multiplication of air density and speed of sound in the nominator, and nominal ear canal cross-sectional area in the denominator), yielding normalized complex ear canal impedance $\mathcal{Z}_{EC}(\omega)$.

$$\mathcal{Z}_{EC}(\omega) = \frac{Z_{EC}(\omega)}{Z_0} \qquad Z_0 = \frac{\rho c}{A}$$

C.3.3 Computation of ear-canal wideband (complex) reflectance $K_{EC}(\omega)$

Complex ear canal wideband reflectance $K_{EC}(\omega)$is computed from the values of the normalized complex ear canal impedance $\mathcal{Z}_{EC}(\omega)$. Ear canal reflectance is magnitude reflectance whose value remains constant in the ear canal regardless of the distance from the tympanic membrane.

$$K_{EC}(\omega) = \frac{Z_{EC}(\omega) - 1}{Z_{EC}(\omega) + 1}$$

C.3.4 Computation of ear-canal wideband (complex) energy reflectance $R_{EC}(\omega)$

Ear canal wideband energy reflectance $\mathcal{R}_{EC}(\omega)$ is computed from the ear canal wideband reflectance $K_{EC}(\omega)$. It provides information about the percentage of energy reflected at given angular frequency ω.

$$\mathcal{R}_{EC}(\omega) = [\, K_{EC}(\omega)]^2 \,.\, 100 \quad (\%)$$

APPENDIX D:

INFORMATION & DATA RECORD FORMS

List of the forms

PhD Program in Speech and Hearing
Graduate School University Center
The City University of New York
365 Fifth Avenue
New York, NY 10016-4309
TEL: 212-817-8800

PARTICIPATION CONSENT FORM

My name is Helen Salus. I am certified clinical audiologist as well as graduate doctoral student.in the PhD program at the Graduate School University Center, CUNY, New York. My study's title is Wideband Reflectance Acoustic Reflex Thresholds In Normal Ears Of Young And Older Adults. Results of the study may be used in my dissertation.

The purpose of this study is to obtain ear function measurements using a new device called Wideband Reflectance (or Power Flow Reflectance) Measurement System in response to ear stimulation with sounds. Wideband Reflectance measures what proportion of the sound presented into ear canal is reflected back by the middle ear and perhaps inner ear. Two different types of sounds will be presented into both of your ears at approximately same time and wideband reflectance response will be measured in one ear at the time. Because this is a new method, people with normal hearing and without a history of ear problems are tested. That would give us better understanding about how normal ears work. The results will also help to build a database and may be compared to measurements obtained using earlier technology.

If you decide to participate in this study I will ask you about your hearing, ear problems and overall health. I will look into your ear canal to check whether you do not have ear wax. You will undergo hearing test where you will be asked to respond to some sounds presented to you through headphones or earphones. If you do not show normal hearing appropriate for your age you will be referred to physician.

After the hearing test both of your ears will be evaluated using several tests which are in current clinical use. Soft tips will be placed into the opening of your ear, sounds will be introduced into your ear canals and ear responses will be measured. In one of the tests you may feel a short pressure change in your ear. It does not give pain or affect your hearing. In order to obtain valid results you will be required to remain still and quiet during the measurements. The total testing time will be approximately 1 to 2 hours. You may stop your participation at any time. You will be compensated at a rate of $ 10.00 an hour.

The tests performed pose no known risks. The experimental measurement is similar to several in current clinical use. Potential benefits include better understanding of human ear function and development of more sensitive methods for ear disorders diagnosis.

The data obtained from this study will be used and published for research purposes only. The names of the people and any identifying information will not be used in any of the publications. All information that you provide will be kept confidential and stored in locked cabinet that is directly under my control. If you would like to learn about the results of the study, please let me know and I will provide the information when the research will be completed..

If you have any questions about this study feel free to contact me at (212) 754-0885, or Hrsalus@AOL.com.

Thank you for your participation in this study. I will give you a copy of this form to take with you.

If you agree to participate, please sign below.

_____ _____ _____ ____

Participant's signature Date Investigator's signature Date

Figure D1. Consent form.

OTOLOGIC & AUDIOLOGIC HISTORY & OTOSCOPY RECORD

Participant's ID (Assigned if Inclusion Criteria Met)**: ____ ( ) Y ( ) O Age:___ Date: _____**

Participant's Name: _____ DOB:_____

History

Hearing loss	Right	Left
Severity		
Onset		
Progress		
Previous evaluations		

Communication problems

Ear problems	Right	Left
Pain		
Discharge		
Fullness		
Middle ear infection Hx		
Ear canal infection Hx		
Surgery		
Tinnitus (Onset, Intermittent / Constant, Contin./Pulsatile, Peripheral/Central, Progress, Maskability, Attitude)		

Balance problems (Onset, Episode duration & frequency, Situations)
Noise exposure / Noise trauma
Ototoxicity (Cochleo- / vestibulo-)
Head trauma
General health
Allergies
Neurological problems & Headaches
Visual disturbances
Facial pain / Numbness

Other

Otoscopy	Right	Left
External auditory canal		
Tympanic membrane		

Follow-up / Recommendations

Figure D2. Otologic and audiologic history and otoscopy record.

AUDIOGRAM.

Participant's ID (Assigned if Inclusion Criteria Met)**: ____ ( ) Y ( ) O Age:____ Date: _____**

Participant's Name: _____ DOB:_____

	Frequency							
	250	**500**	**1000**	**2000**	**3000**	**4000**	**6000**	**8000** **[Hz]**
Intensity								
0								
10								
20								
30								
40								
50								
60								
70								
80								
90								
100								
110								
[dBHL]								

LEGEND

Right AD	Left AS	
Air Unmasked	O	×
Air Masked	Δ	□
Bone Unmasked	<	>

Retest at 1000 Hz: Rt ____dBHL Lt _____dBHL

Reliability: [] Good []Fair []Poor

Recommendations:

Figure D3. Audiogram

SUBJ I.D.	AGE	ACTIV EAR	TIME	EXPORTED FILES (EXCEL FILE NAME)	ACTIVATOR LEVEL [dB HL]
					Baseline
					Baseline
					Baseline
					Baseline
					Baseline
					Baseline
					Baseline
					Baseline
					Baseline
					Baseline
					Baseline
					Baseline
					Baseline
					Baseline
					Baseline
					Baseline
					Baseline
					Baseline
					Baseline
					Baseline
					Baseline
					Baseline
					Baseline

					Baseline
					Baseline
					Baseline
					Baseline
					Baseline
					Baseline
					Baseline
					Baseline
					Baseline
					Baseline
					Baseline
					Baseline
					Baseline
					Baseline
					Baseline
					Baseline
					Baseline
					Baseline
					Baseline
					Baseline
					Baseline
					Baseline
					Baseline
					Baseline
					Baseline

					Baseline
					Baseline
					Baseline
					Baseline
					Baseline
					Baseline
					Baseline
					Baseline
					Baseline
					Baseline
					Baseline
					Baseline
					Baseline
					Baseline
					Baseline
					Baseline

Figure D4. Subject summary of exported wideband reflectance (WBR) files.

APPENDIX E: INDIVIDUAL PARTICIPANTS' RESULTS

Individual participants' results are presented in tables E1 through E10.

Table E1.

Individual Audiometric Results

Participant	Activator Side For WBR-	Pure-Tone Test Ear	Air-conduction thresholds (dB HL)						Bone-conduction thresholds (dB HL)					
			250 Hz	500 Hz	1000 Hz	2000 Hz	3000 Hz	4000 Hz	250 Hz	500 Hz	1000 Hz	2000 Hz	3000 Hz	4000 Hz
Younger Participants														
001	Left	Right	5	10	10	10	5	5	10	10	10	10	10	10
		Left	5	10	10	10	10	5						
002	Right	Right	10	5	10	5	0	0						
		Left	10	10	10	5	5	5	5	5	5	5	0	0
003	Left	Right	15	15	15	20	20	10						
		Left	15	20	15	20	15	15	10	15	10	10	15	10
004	Right	Right	0	5	0	5	0	5	0	5	0	0	0	0
		Left	5	0	-5	0	-5	0						
005	Left	Right	5	0	5	0	0	5	0	5	0	0	0	0
		Left	0	0	0	0	0	0						
006	Left	Right	-5	0	0	-5	0	5						
		Left	5	5	0	-5	5	5	-5	0	0	0	0	5
007	Left	Right	5	5	5	5	0	0	0	5	0	5	5	5
		Left	5	5	5	0	0	5						
008	Right	Right	5	5	0	5	0	5	10	10	0	0	0	5
		Left	5	5	0	0	0	0						
009	Right	Right	10	5	5	5	5	10	0	5	0	5	5	10
		Left	10	0	5	5	5	5						
010	Right	Right	5	5	5	5	0	0	0	0	5	5	0	0
		Left	10	10	5	0	0	5						
Older Participants														
101	Left	Right	15	15	20	10	20	25	15	10	15	10	15	20
		Left	10	10	15	15	20	25						
102	Right	Right	10	10	5	5	10	15						
		Left	15	10	5	10	15	25	5	5	5	0	10	15
103	Left	Right	15	10	10	15	10	5	5	10	10	15	10	10
		Left	15	10	10	10	10	15						
104	Left	Right	20	20	20	20	15	25	15	20	20	20	20	25
		Left	20	20	20	15	20	20						
105	Left	Right	10	15	15	10	5	15						
		Left	10	15	15	10	10	15	10	10	10	10	10	15
106	Right	Right	5	5	10	10	10	15						
		Left	15	10	10	10	10	10	5	5	5	5	5	10
107	Left	Right	15	15	5	5	15	10						
		Left	15	15	10	15	15	20	5	10	10	5	10	10
108	Right	Right	15	15	10	5	5	20	5	10	5	5	5	15
		Left	5	5	10	10	0	15						
109	Right	Right	15	10	10	10	15	10						
		Left	15	10	10	10	5	5	5	5	5	10	10	10
110	Right	Right	15	15	15	15	20	25	5	10	10	10	20	20
		Left	15	15	10	10	15	20						

Table E2.

Individual Participants' TPPs (daPa), SAAs (mmho), and 500-, 1000- and 2000-Hz Tonal and BBN- CARTs (dB HL) as Obtained via the Acoustic-Immittance Method (AI-CART)

Participants	Activator Side For	Right Ear						Left Ear					
		TPP	SAA	500-Hz AI-	1000-Hz AI-	2000-Hz AI-	BBN AI-	TPP	SAA	500-Hz AI-	1000-Hz AI-	2000-Hz AI-	BBN AI-
Younger Participants													
001	Left	5	0.6	105	90	85		10	0.6	90	86	85	74
002	Right	-5	0.6	85	85	85		-5	0.5	90	88	80	78
003	Left	0	0.4	95	95	100		0	1.2	95	92	100	76
004	Right	10	0.5	100	92	100	74	5	0,4	95	100	95	
005	Left	15	0.7	95	88	95	74	15	0.9	95	90	95	
006	Left	-10	1.1	85	80	85		5	1.2	95	90	90	72
007	Left	5	0.5	90	85	85		5	0.5	85	84	85	74
008	Right	20	0.6	100	94	90	80	5	0.5	95	90	90	
009	Right	15	0.5	100	92	90	78	5	0.4	90	90	90	
010	Right	5	0.5	100	92	90	76	5	0.4	85	85	80	
Older Participants													
101	Left	20	1.4	90	85	85		15	0.6	90	92	85	80
102	Right	10	0.8	95	94	85	72	5	0.8	85	85	80	
103	Left	10	0.8	75	76	75		5	0.6	80	80	75	72
104	Left	5	0.4	NR	95	95		20	0.3	110	96	95	88
105	Left	-5	0.3	100	95	90		15	0.3	95	90	90	80
106	Right	15	1.0	90	86	85	74	20	1.3	100	95	95	
107	Left	-40	0.9	95	90	90		-20	0.7	100	90	95	82
108	Right	5	1.3	100	86	80	78	20	1.2	95	95	85	
109	Right	0	0.4	90	80	80	74	15	0.6	95	85	85	
110	Right	-5	0.3	95	98	95	92	0	0.3	95	90	90	

Table E3

Individual AI-CARTs (dB HL and WBR-CARTS (dB HL)

Participant	Test	AI-CART[a] [dB HL]	Visually Estimated WBR-CART [dB HL]	Computed WBR-CART 1SD/10f [dB HL]	1SD/10f Criterion-based frequency range at the CART level [Hz]
			Younger group		
001	BBN Test	74	64	66	490-797
	BBN Retest	NT[b]	72	74	444-961
	1000-Hz Test	86	92	94[c]	492-868
	1000-Hz Retest	NT	92	94[c]	468 – 844
002	BBN Test	78	62	62	373-797
	BBN Retest	NT	66	66	514-797
	1000-Hz Test	88	94	94	420-727
	1000-Hz Retest	NT	NR[d]	NR	-
003	BBN Test	76	70	70	327-704
	BBN Retest	NT	70	70	404-891
	1000-Hz Test	92	92	NR	-
	1000-Hz Retest	NT	NR	NR	-
004	BBN Test	74	62	62	327-539
	BBN Retest	NT	60	60	538-821
	1000-Hz Test	92	96[c]	96[c]	232-797
	1000-Hz Retest	NT	96[c]	96[c]	396-844
005	BBN Test	74	60	60	444-680
	BBN Retest	NT	64	64	303-774
	1000-Hz Test	88	88	88	444-750
	1000-Hz Retest	NT	86	90	420-844
006	BBN Test	72	56	56	209-750
	BBN Retest	NT	60	66	420-727
	1000-Hz Test	90	92	NR	-
	1000-Hz Retest	NT	94[c]	NR	-
007	BBN Test	74	40	38[e]	397-704
	BBN Retest	NT	58	56	397-680
	1000-Hz Test	84	84	84	303-750
	1000-Hz Retest	NT	84	84	327-680
008	BBN Test	80	68	68	537-774
	BBN Retest	NT	70	66	537-797
	1000-Hz Test	94	98[c]	98[c]	4,285-5603
	1000-Hz Retest	NT	NR	NR	-
009	BBN Test	78	68	68	349-891
	BBN Retest	NT	66	66	467-844
	1000-Hz Test	92	92	92	443-844
	1000-Hz Retest	NT	98	98	373-914
010	BBN Test	76	66	66	537-797
	BBN Retest	NT	66	64	327-539
	1000-Hz Test	92	96	96	468-750
	1000-Hz Retest	NT	94	94	467-914

[a]2-dB step size.
[b]Not tested
[c]WBR-CART occurring at the maximum activator level.
[d]No reflectance response at the maximum activator level.
[e]WBR-CART occurring at the lowest activator level.

Table E3 (Continued)

Participant	Test	AI-CART[a] [dB HL]	Visually Estimated WBR-CART [dB HL]	Computed WBR-CART 1SD/10f [dB HL]	1SD/10f Criterion-based frequency range at the CART level [Hz]
			Older group		
101	BBN Test	80	80	76	514-844
	BBN Retest	NT	78	82	491-774
	1000-Hz Test	92	90	90	1,756-2,016
	1000-Hz Retest	NT	96[c]	96[c]	1,381-1,875
102	BBN Test	72	64	62	537-1079
	BBN Retest	NT	62	62	819-1102
	1000-Hz Test	94	86	86	3,162-3,727
	1000-Hz Retest	NT	94[c]	94[c]	538-750
103	BBN Test	72	62	62	421-704
	BBN Retest	NT	60	60	374-704
	1000-Hz Test	80	84	84	396-797
	1000-Hz Retest	NT	78	78	3,069-3,399
104	BBN Test	88	84	NR	-
	BBN Retest	NT	84[c]	84[c]	491-704
	1000-Hz Test	96	NR	NR	-
	1000-Hz Retest	NT	104[c]	102	2,175-3,680
105	BBN Test	80	56	56	490-844
	BBN Retest I	NT	60	62	514-820
	1000-Hz Test	90	94[c]	NR	-
	1000-Hz Retest	NT	92	94[c]	561-821
106	BBN Test	74	62	62	3,303-3,539
	BBN Retest	NT	62	58	3,089-4,383
	1000-Hz Test	86	88	88	256-633
	1000-Hz Retest	NT	88	88	3,138-3,586
107	BBN Test	82	78	78	444-821
	BBN Retest	NT	64	62	444-750
	1000-Hz Test	90	94	96	678-1,055
	1000-Hz Retest	NT	90	94	561-915
108	BBN Test	78	66	66	2,811-3,024
	BBN Retest	NT	66	66	2,693-3,188
	1000-Hz Test	86	88	90	397-680
	1000-Hz Retest	NT	84	84	2,623-3,200
109	BBN Test	74	34	34	3,233-3,446
	BBN Retest	NT	56	58	327-657
	1000-Hz Test	80	84	84	421-657
	1000-Hz Retest	NT	80	80	397-680
110	BBN Test	92	78	78	443-891
	BBN Retest	NT	78	78	561-844
	1000-Hz Test	98	98	100	420-868
	1000-Hz Retest	NT	102	100	561-797

[a]2-dB step size.
[b]Not tested
[c]WBR-CART occurring at the maximum activator level.
[d]No reflectance response at the maximum activator level.
[e]WBR-CART occurring at the lowest activator level.

Table E4

The Individula AI BBN CARTs, AI 1000-Hz CARTs, and Resultant AI NTDs for the Younger Group

Participant	AI BBN CART	AI 1000-Hz CART	AI NTD
001	74	86	12
002	78	88	10
003	76	92	16
004	74	92	18
005	74	88	14
006	72	90	18
007	74	84	10
008	80	94	14
009	78	92	14
010	76	92	16

Table E5

The Individula AI BBN CARTs, AI 1000-Hz CARTs, and Resultant AI NTDs for the Older Group

Participant	AI BBN Test CART	AI 1000-Hz Test CART	NTD
101	80	92	12
102	72	94	22
103	72	80	8
104	88	96	8
105	80	90	10
106	74	86	12
107	82	90	8
108	78	86	8
109	74	80	6
110	92	98	6

Table E6

Individula Test and Retest WBR BBN CARTs in the Younger and Older Adult Groups

Younger adult group			Older adult group		
Participant	WBR BBN CART Test	WBR BBN CART Retest	Participant	WBR BBN CART Test	WBR BBN CART Retest
001	66	74	101	80	82
002	62	66	102	62	62
003	70	70	103	62	60
004	62	60	104	NR	84
005	60	64	105	56	62
006	56	66	106	62	58
007	38	56	107	78	62
008	68	66	108	66	66
009	68	66	109	34	58
010	66	64	110	78	78

Table E7

Individual Test and Retest WBR 1000-Hz CARTs in the Younger and Older Adult Groups.

Younger adult group			Older adult group		
Participant	WBR 1000-Hz Test CART	WBR 1000-Hz Retest CART	Participant	WBR 1000-Hz Test CART	WBR1000-Hz Retest CART
001	94	94	101	90	96
002	94	92	102	86	94
003	NR	NR	103	84	78
004	96	96	104	NR	102
005	88	90	105	NR	94
006	NR	NR	106	88	88
007	84	84	107	96	94
008	98	NR	108	90	84
009	92	98	109	84	80
010	96	94	110	100	100

Table E8

Individual WBR NTD in the Younger and Older Adult Groups

Younger adult group		Older adult group	
Participant	WBR NTD	Participant	WBR NTD
001	28	101	10
002	32	102	24
003	-	103	22
004	34	104	-
005	28	105	-
006	-	106	26
007	46	107	18
008	30	108	24
009	24	109	50
010	30	110	22

Table E9

Individual AI-NTD and WBR NTD in Younger Participants

Participant	AI NTD	WBR NTD
001	12	28
002	10	32
003	16	-
004	18	34
005	14	28
006	18	-
007	10	46
008	14	30
009	14	24
010	16	30

Table E10

Individual AI-NTD and WBR NTD in Older Participants

Participant	AI NTD	WBR NTD
101	12	10
102	22	24
103	8	22
104	8	-
105	10	-
106	12	26
107	8	18
108	8	24
109	6	50
110	6	22

APPENDIX F:

INDIVIDUAL PARTICIPANTS'

ACTIVATOR BASELINE DIFFERENCES (ABDs)

Graphs showing the ABDs at the levels below the CART, at the CART levels and at the levels above the CART are displayed on the following pages.

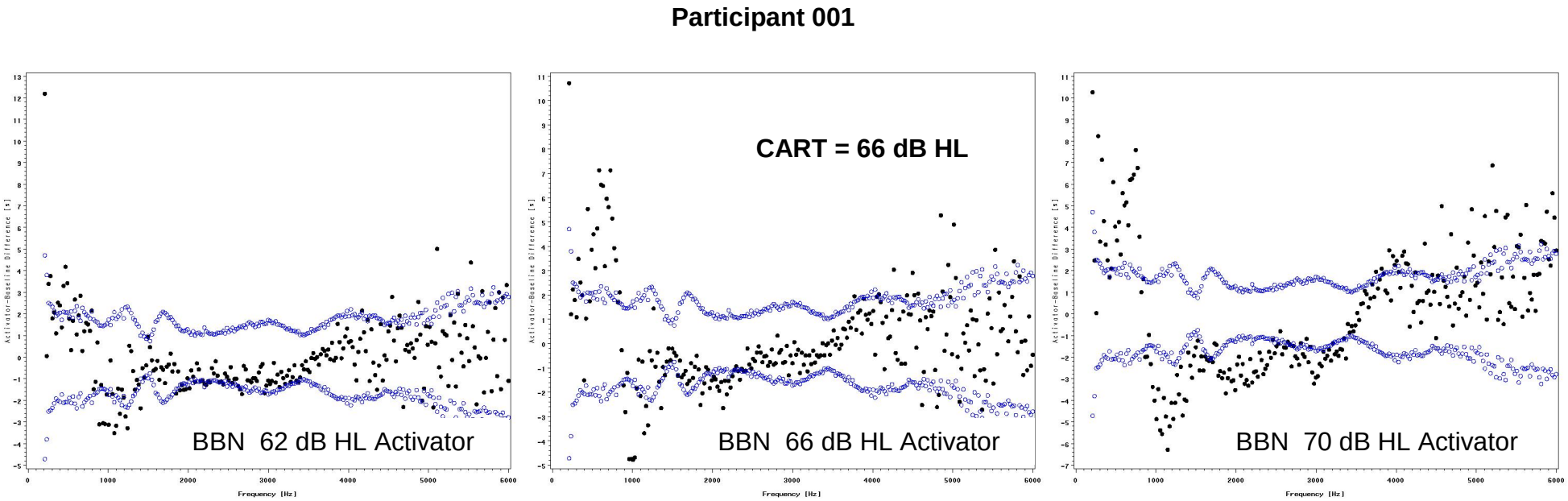

Figure F 1. ABDs for BBN activators: 62 dB HL, 66 dB HL, 70 dB HL in participant 001; CART identified at 66 dB HL Probe stimulus frequencies are shown on horizontal axis. The ABD (%) is shown on the vertical axis. The ± 1-SD limits (from the baseline variances) are shown in blue. Note the gradual formation and growth of the CART pattern as the activator intensity increases.

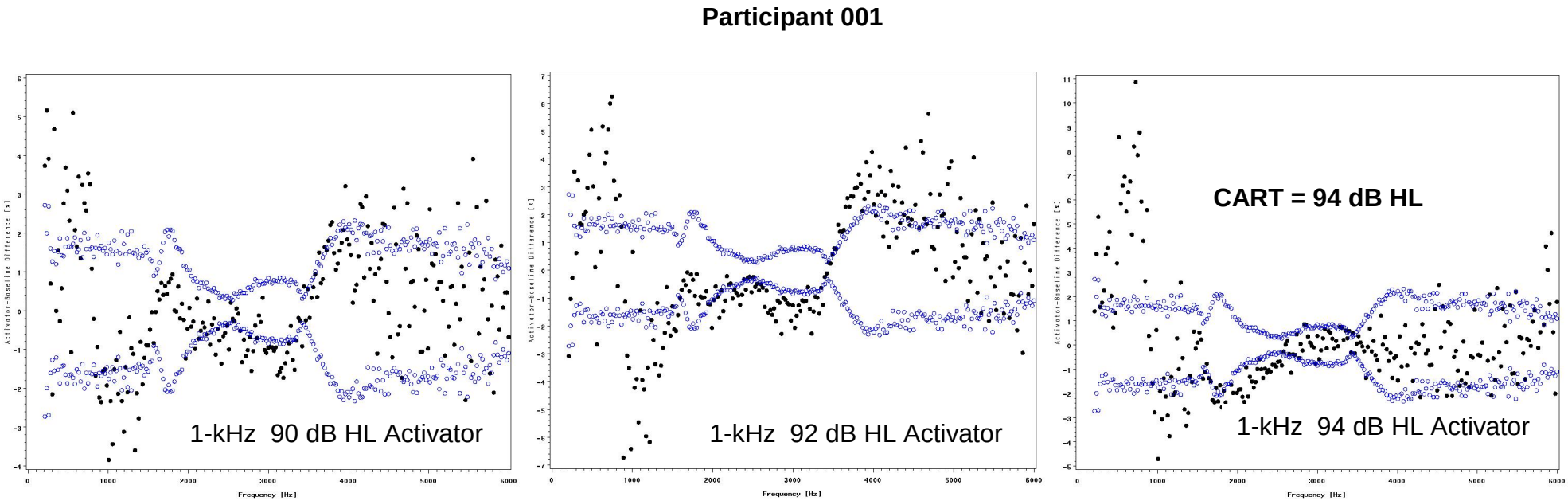

Figure F2. ABDs for 1-kHz activators: 90 dB HL, 92 dB HL, 94 dB HL in participant 001; CART identified at 94 dB HL, highest activator level. . Early formation of ART-like pattern was noticed for the 90- and 92-dB HL activators. Probe stimulus frequencies are shown on horizontal axis. The ABD (%) is shown on the vertical axis. The ± 1-SD limits (from the baseline variances) are shown in blue. Note the gradual formation and growth of the CART pattern as the activator intensity increases.

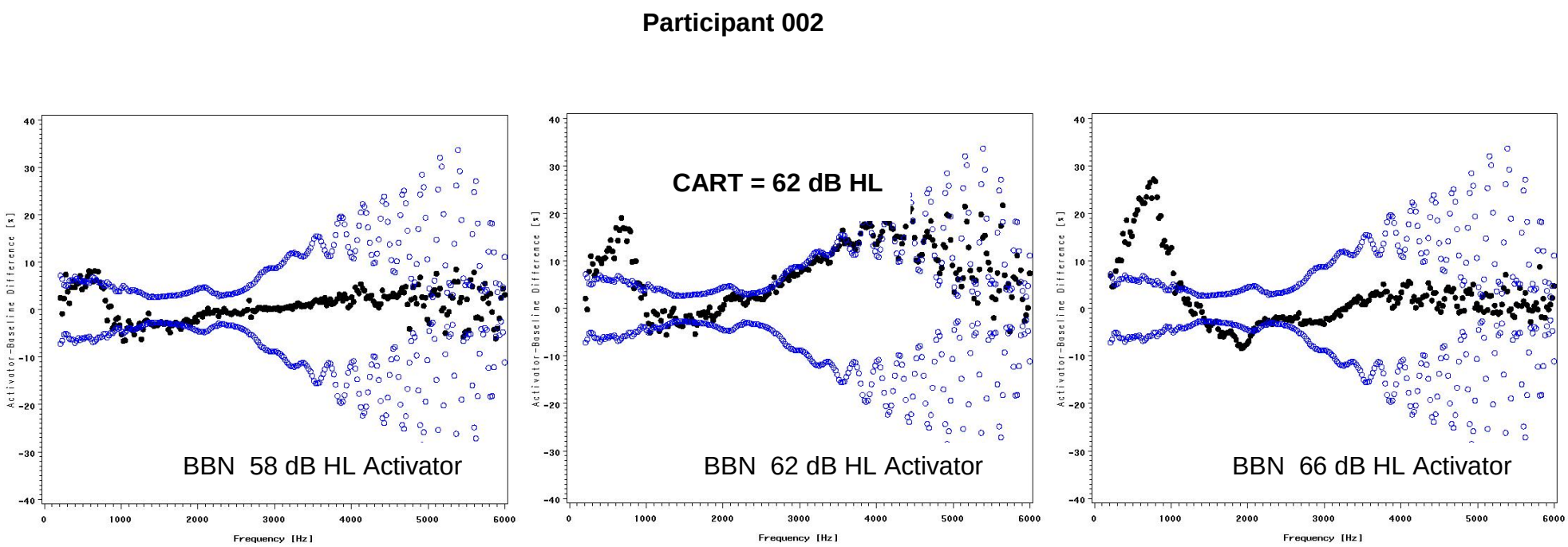

Figure F3. ABDs for BBN activators: 58 dB HL, 62 dB HL, 66 dB HL in participant 002; CART identified at 62 dB HL. Probe stimulus frequencies are shown on horizontal axis. The ABD (%) is shown on the vertical axis. The ± 1-SD limits (from the baseline variances) are shown in blue.

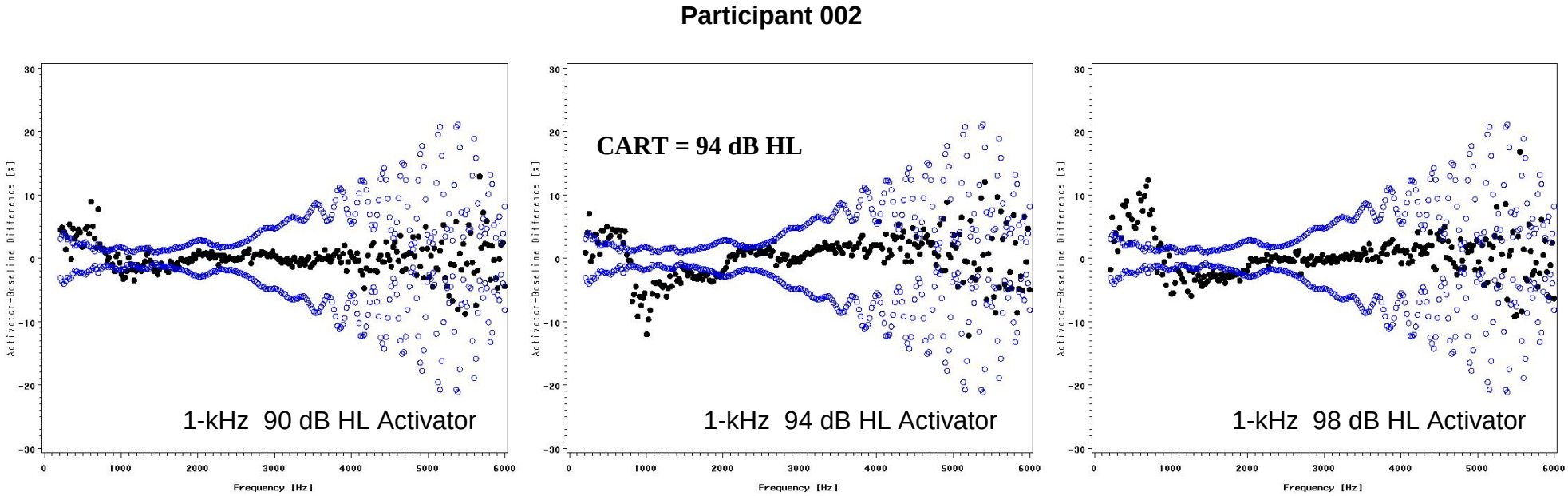

Figure F4. ABDs for 1-kHz activators: 90 dB HL, 92 dB HL, 94 dB HL in participant 002; CART identified at 94 dB HL. Probe stimulus frequencies are shown on horizontal axis. The ABD (%) is shown on the vertical axis. The ± 1-SD limits (from the baseline variances) are shown in blue. Note the gradual formation and growth of the CART pattern as the activator intensity increases.

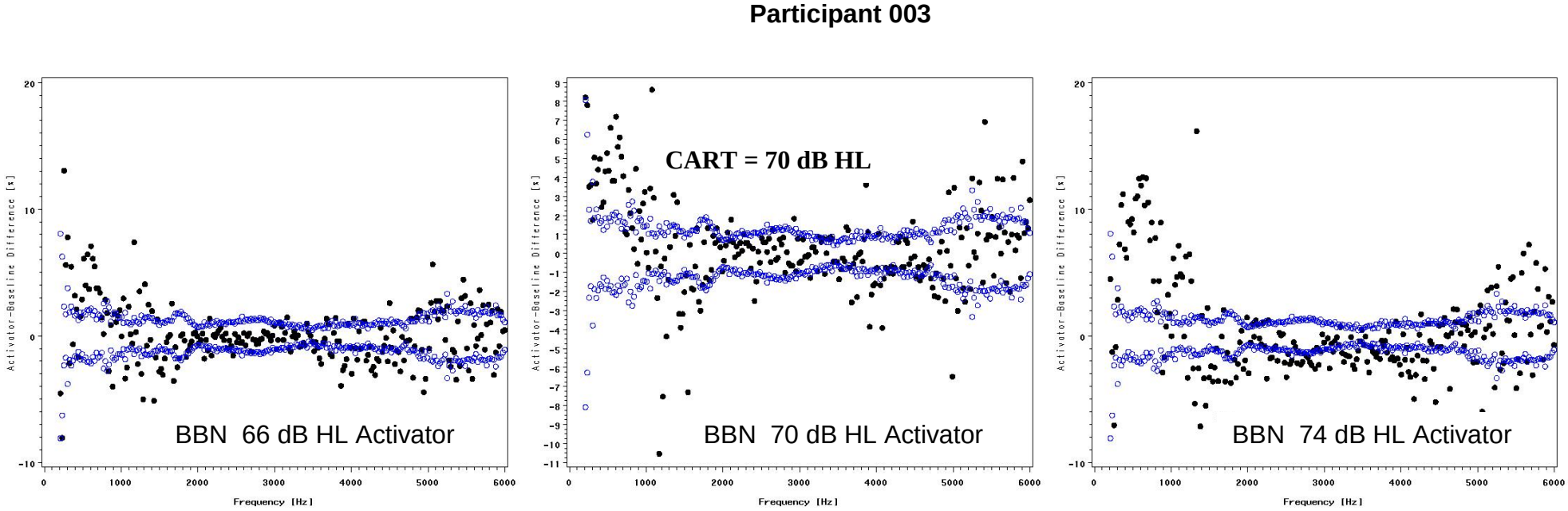

Figure F5. ABDs for BBN activators: 66 dB HL, 70 dB HL, 74 dB HL in participant 003; CART identified at 70 dB HL. Probe stimulus frequencies are shown on horizontal axis. The ABD (%) is shown on the vertical axis. The ± 1-SD limits (from the baseline variances) are shown in blue.

Participant 003

Absent CART

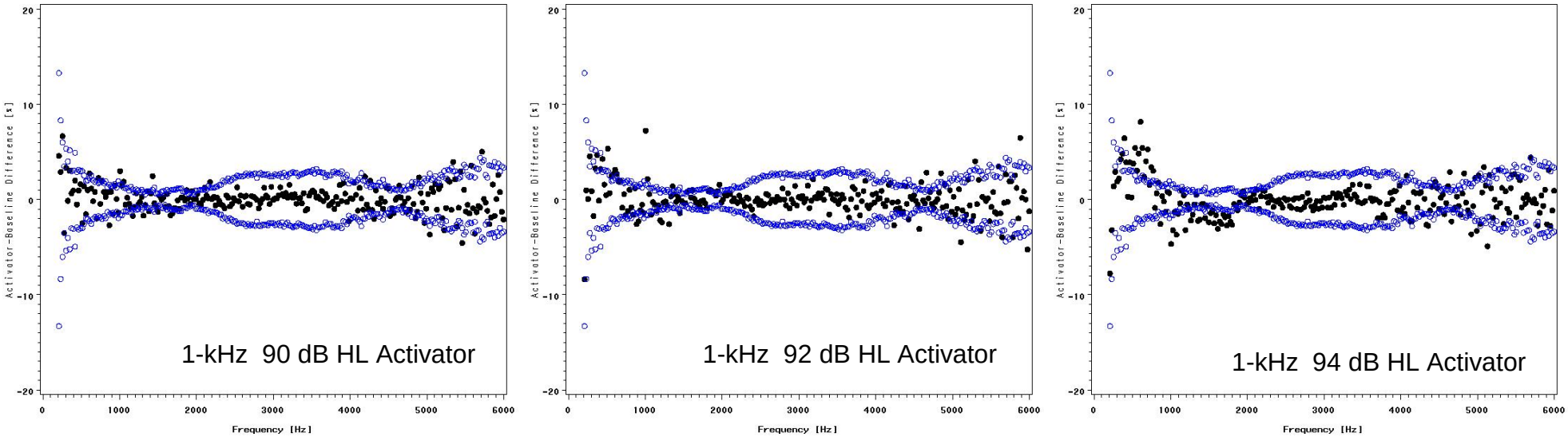

Figure F6. ABDs for 1-kHz activators: 90 dB HL, 92 dB HL, 94 dB HL in participant 003; no CART was identified. Early formation of ART-like pattern was noticed for the 92- and 94-dB HL activators. Probe stimulus frequencies are shown on horizontal axis. The ABD (%) is shown on the vertical axis. The ± 1-SD limits (from the baseline variances) are shown in blue.

Participant 004

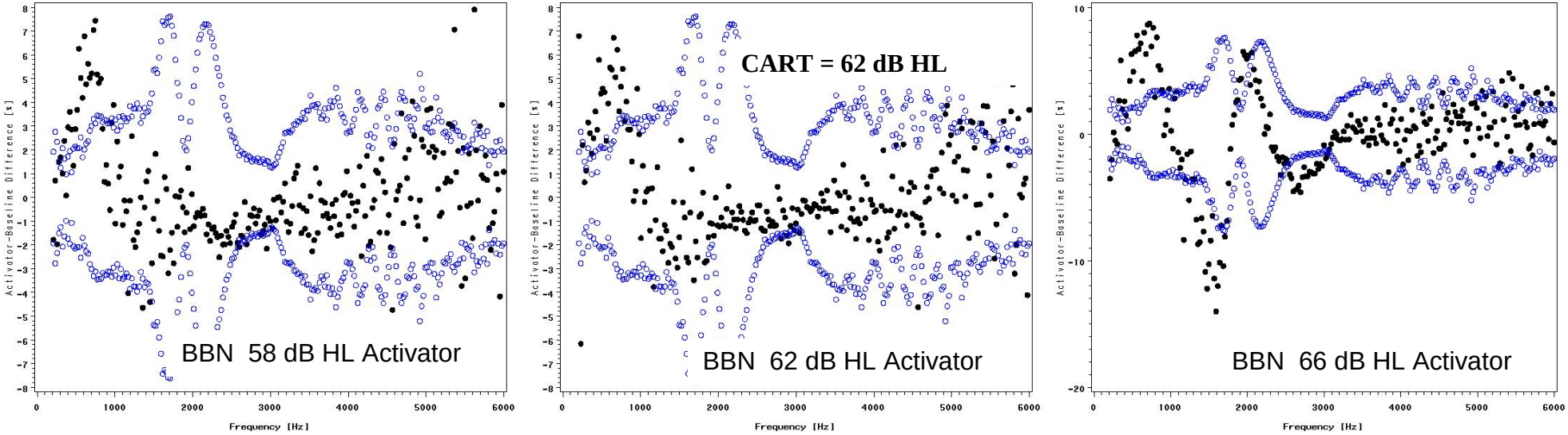

Figure F7. ABDs for BBN activators: 58 dB HL, 62 dB HL, 66 dB HL in participant 004; CART identified at 94 dB HL. Probe stimulus frequencies are shown on horizontal axis. The ABD (%) is shown on the vertical axis. The ± 1-SD limits (from the baseline variances) are shown in blue.

Participant 004

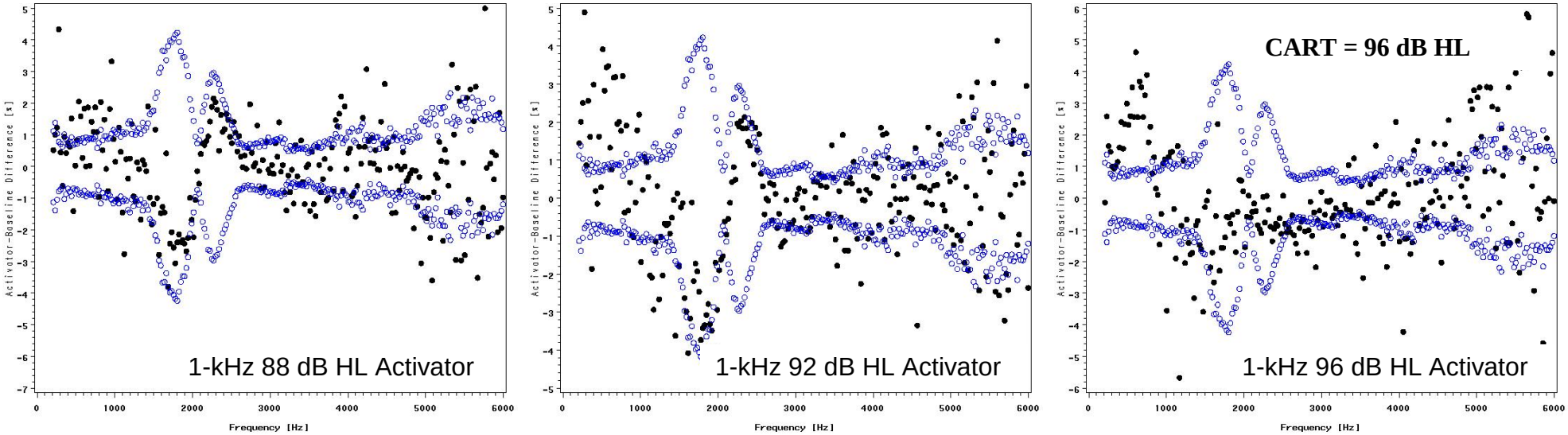

Figure F8. ABDs for 1-kHz activators: 88 dB HL, 92 dB HL, 96 dB HL in participant 004; CART was identified at 96 dB HL, highest activator level. Early formation of ART-like pattern was noticed for the 88- through 94-dB HL activators. Probe stimulus frequencies are shown on horizontal axis. The ABD (%) is shown on the vertical axis. The ± 1-SD limits (from the baseline variances) are shown in blue.

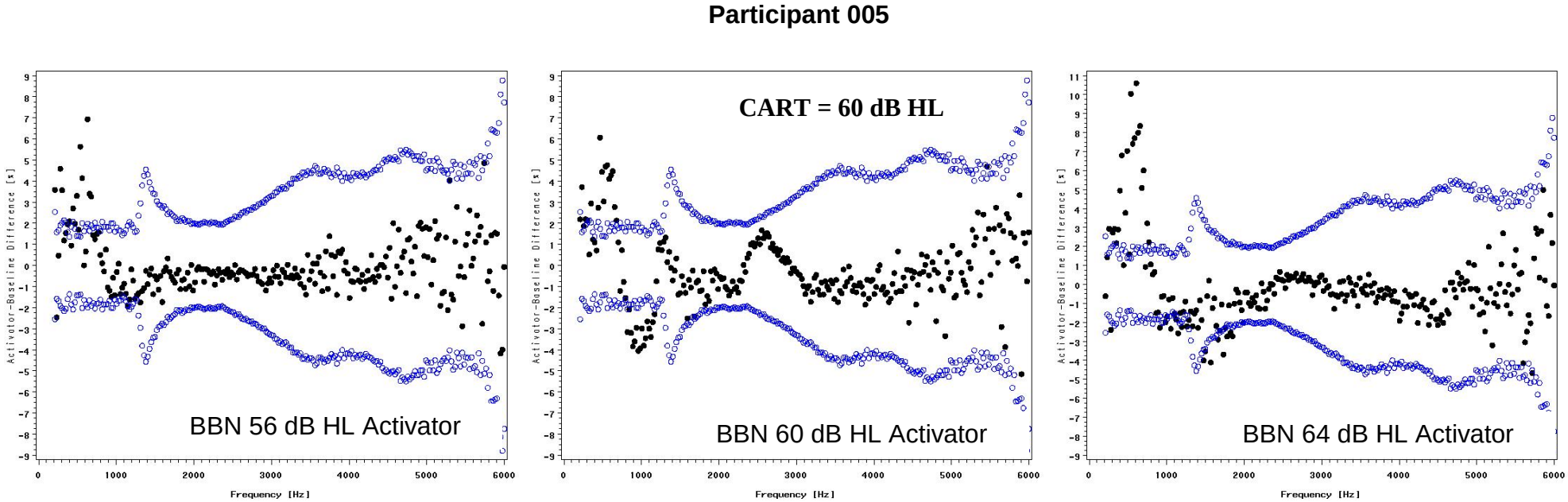

Figure F 9. ABDs for BBN activators: 56 dB HL, 60 dB HL, 64 dB HL in participant 005; CART identified at 60 dB HL. Probe stimulus frequencies are shown on horizontal axis. The ABD (%) is shown on the vertical axis. The ± 1-SD limits (from the baseline variances) are shown in blue.

Participant 005

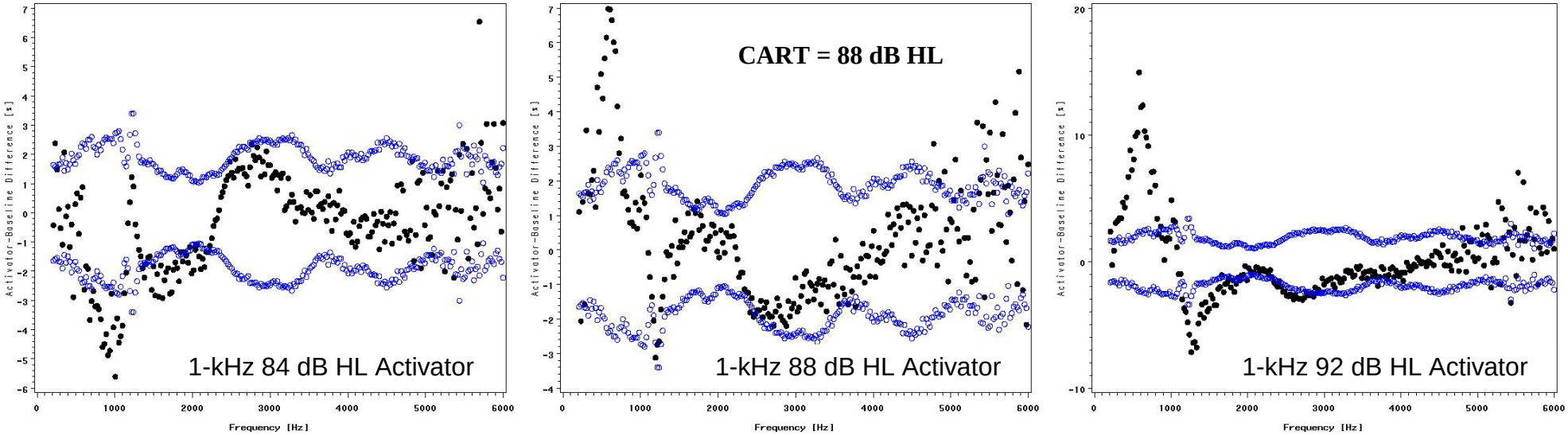

Figure F10. ABDs for 1-kHz activators: 84 dB HL, 88 dB HL, 92 dB HL in participant 005; CART was identified at 88 dB HL. Probe stimulus frequencies are shown on horizontal axis. The ABD (%) is shown on the vertical axis. The ± 1-SD limits (from the baseline variances) are shown in blue.

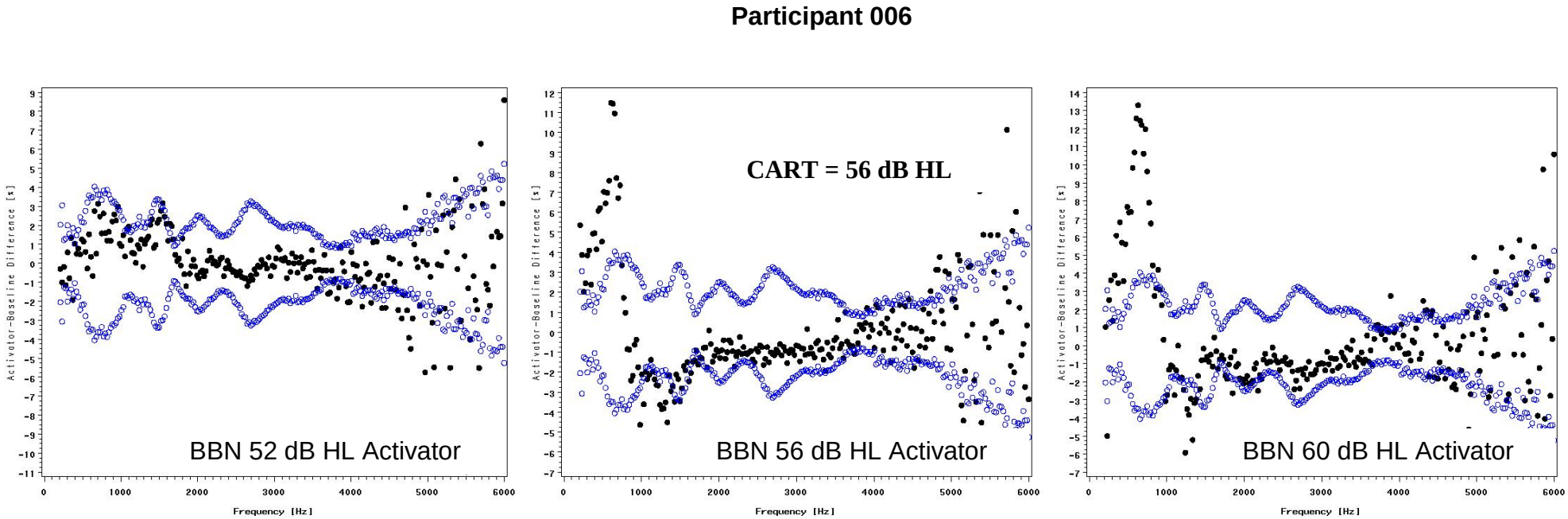

Figure F11. ABDs for BBN activators: 52 dB HL, 56 dB HL, 60 dB HL in participant 006; CART identified at 60 dB HL. Probe stimulus frequencies are shown on horizontal axis. The ABD (%) is shown on the vertical axis. The ± 1-SD limits (from the baseline variances) are shown in blue.

Participant 006

Absent CART

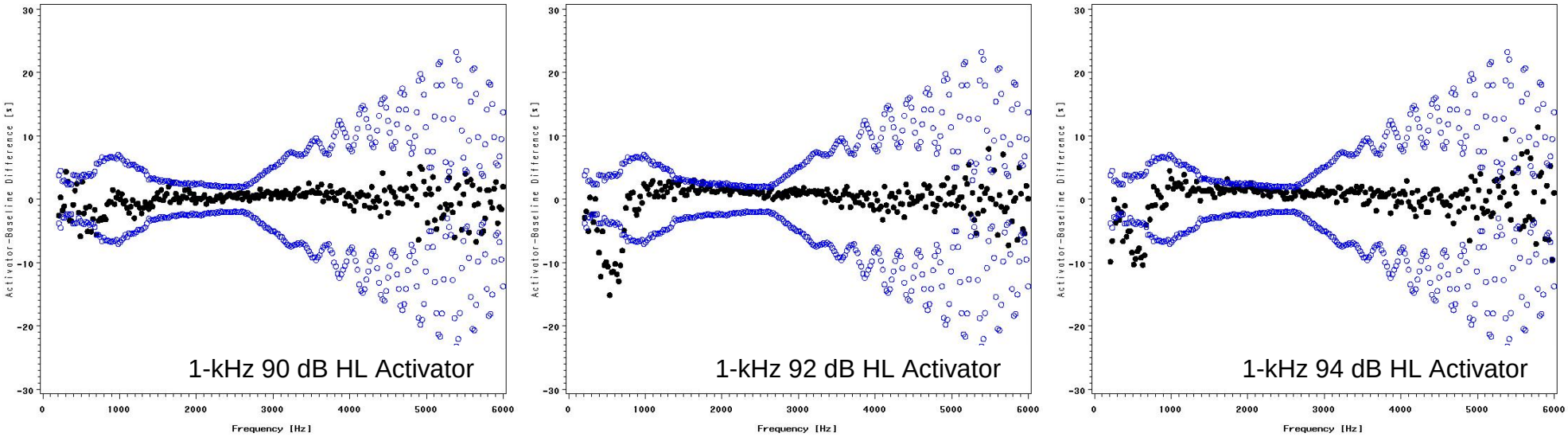

Figure F12. ABDs for 1-kHz activators: 90 dB HL, 92 dB HL, 94 dB HL in participant 006; CART was absent. Early formation of ART-like pattern was noticed for the 90- through 94-dB HL activators. Probe stimulus frequencies are shown on horizontal axis. The ABD (%) is shown on the vertical axis. The ± 1-SD limits (from the baseline variances) are shown in blue.

Participant 007

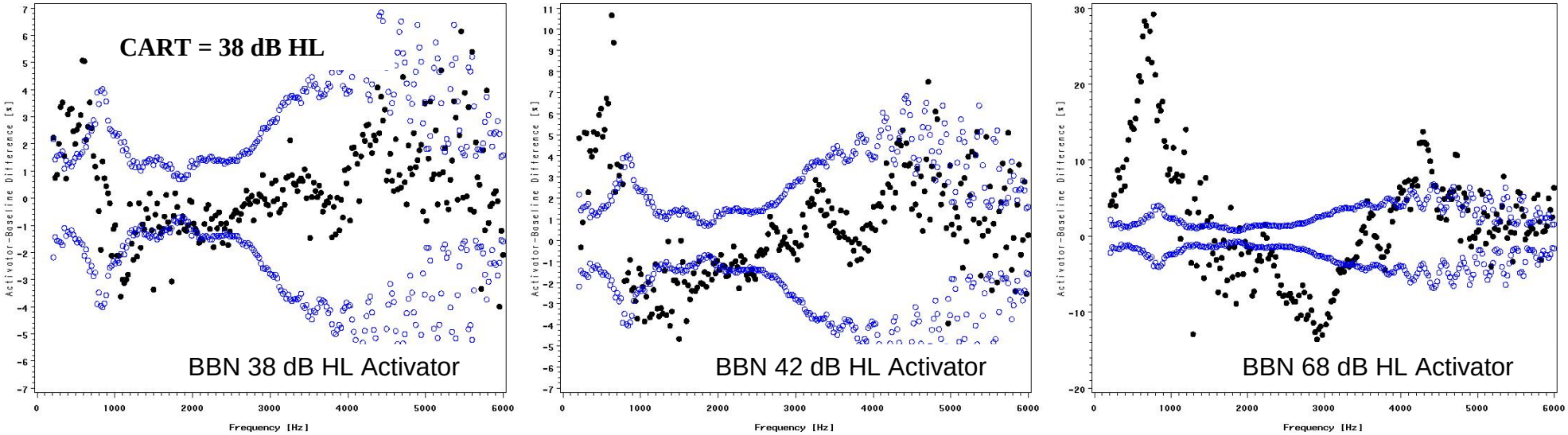

Figure F13. ABDs for BBN activators: 38 dB HL, 42 dB HL, 68 dB HL in participant 007; CART identified at 38 dB HL, the lowest activator level. Probe stimulus frequencies are shown on horizontal axis. The ABD (%) is shown on the vertical axis. The ± 1-SD limits (from the baseline variances) are shown in blue. Note the gradual growth of the CART pattern as the activator intensity increases.

Participant 007

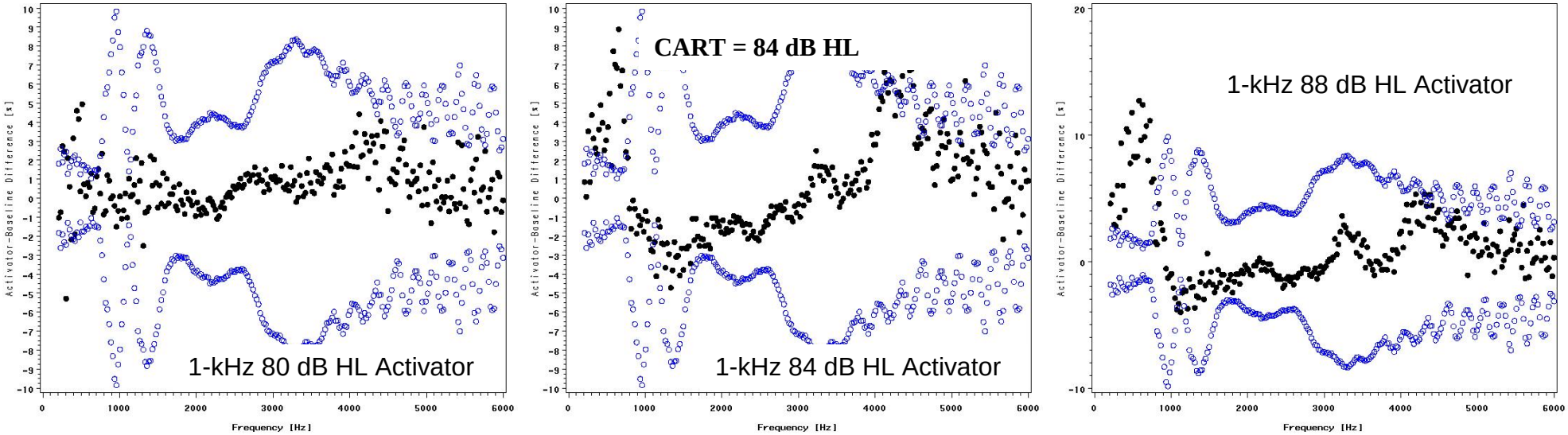

Figure F14. ABDs for 1-kHz activators: 80 dB HL, 84 dB HL, 88 dB HL in participant 007; CART was identified at 84 dB HL. Probe stimulus frequencies are shown on horizontal axis. The ABD (%) is shown on the vertical axis. The ± 1-SD limits (from the baseline variances) are shown in blue.

Participant 008

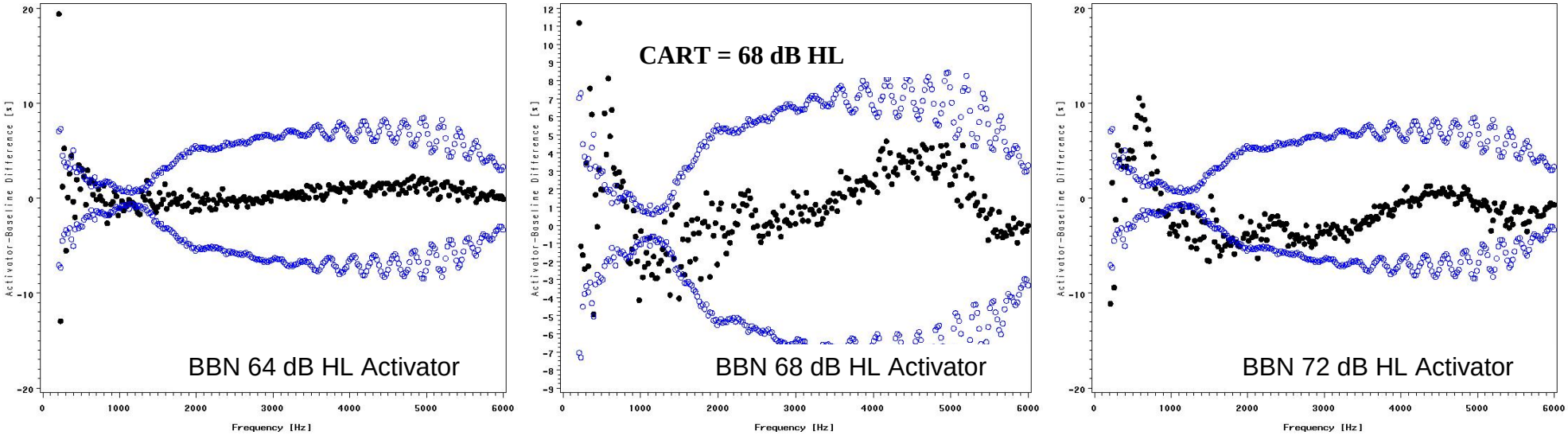

Figure F15. ABDs for BBN activators: 64 dB HL, 68 dB HL, 72 dB HL in participant 008; CART identified at 68 dB HL. Probe stimulus frequencies are shown on horizontal axis. The ABD (%) is shown on the vertical axis. The ± 1-SD limits (from the baseline variances) are shown in blue.

Participant 008

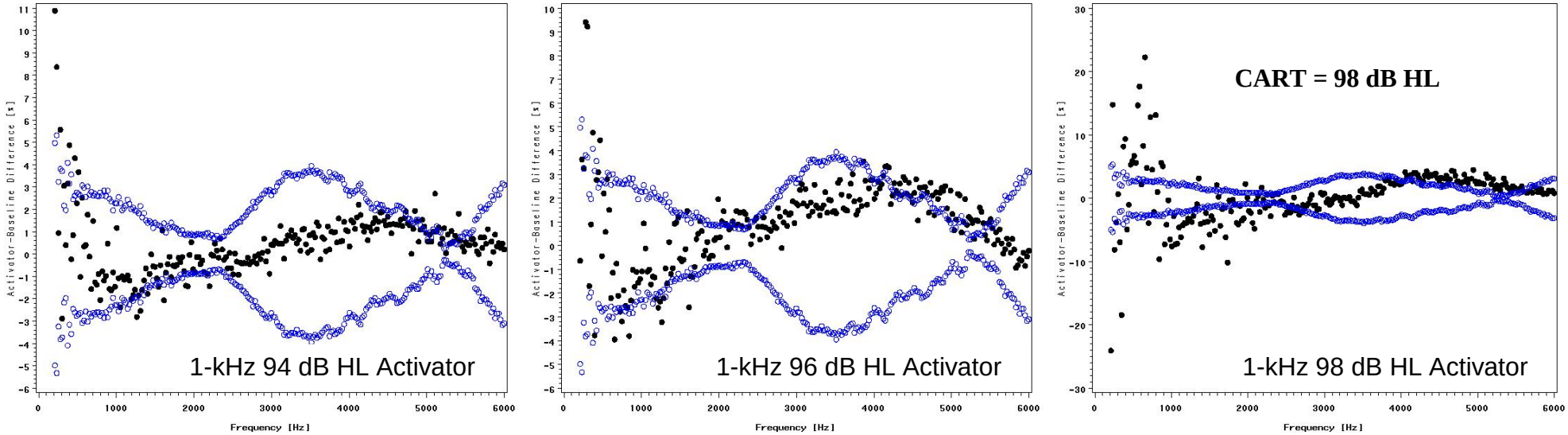

Figure F16. ABDs for 1-kHz activators: 94 dB HL, 96 dB HL, 98 dB HL in participant 008; CART identified at 98 dB HL, the highest activator level. Probe stimulus frequencies are shown on horizontal axis. The ABD (%) is shown on the vertical axis. The ± 1-SD limits (from the baseline variances) are shown in blue. Note the gradual growth of the CART pattern as the activator intensity increases.

Participant 009

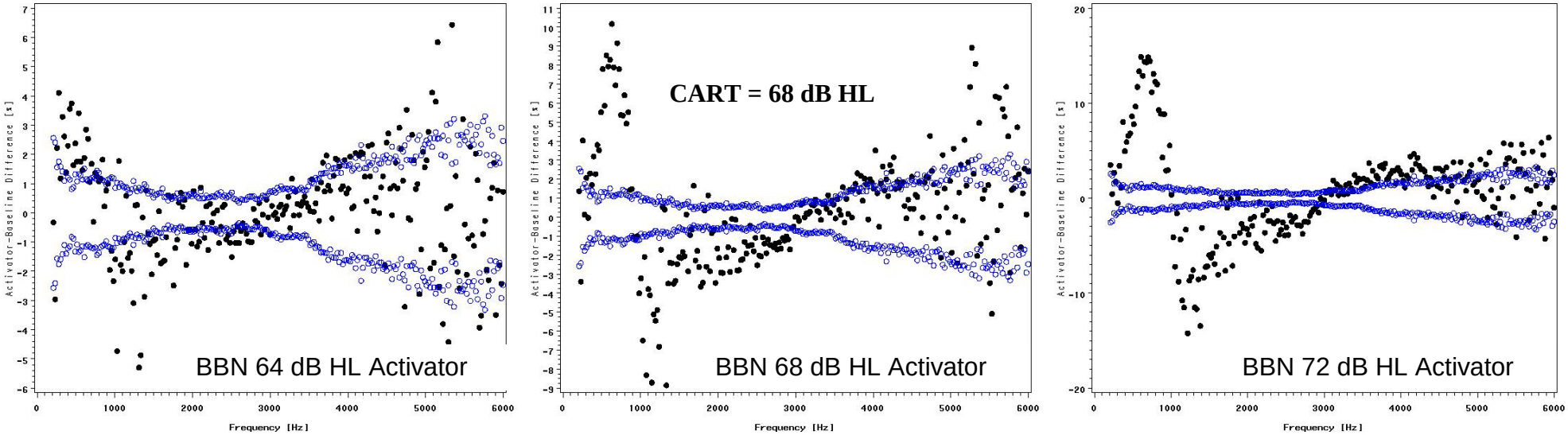

Figure F17. ABDs for BBN activators: 64 dB HL, 68 dB HL, 72 dB HL in participant 008; CART identified at 68 dB HL. Probe stimulus frequencies are shown on horizontal axis. The ABD (%) is shown on the vertical axis. The ± 1-SD limits (from the baseline variances) are shown in blue.

Participant 009

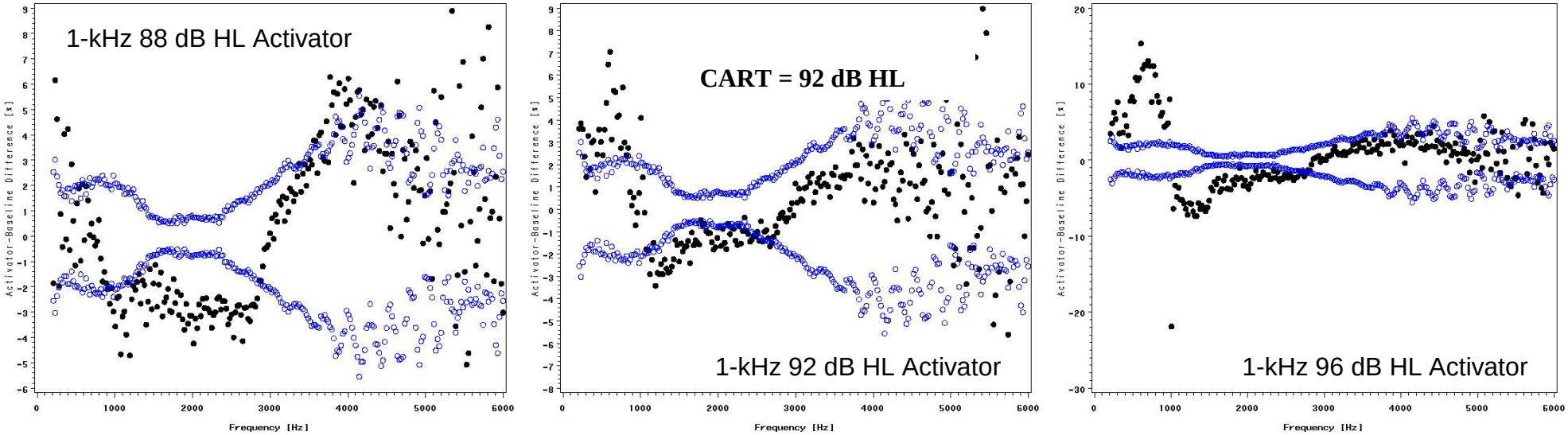

Figure F18. ABDs for 1-kHz activators: 88 dB HL, 92 dB HL, 96 dB HL in participant 009; CART identified at 92 dB HL, the highest activator level. Probe stimulus frequencies are shown on horizontal axis. The ABD (%) is shown on the vertical axis. The ± 1-SD limits (from the baseline variances) are shown in blue.

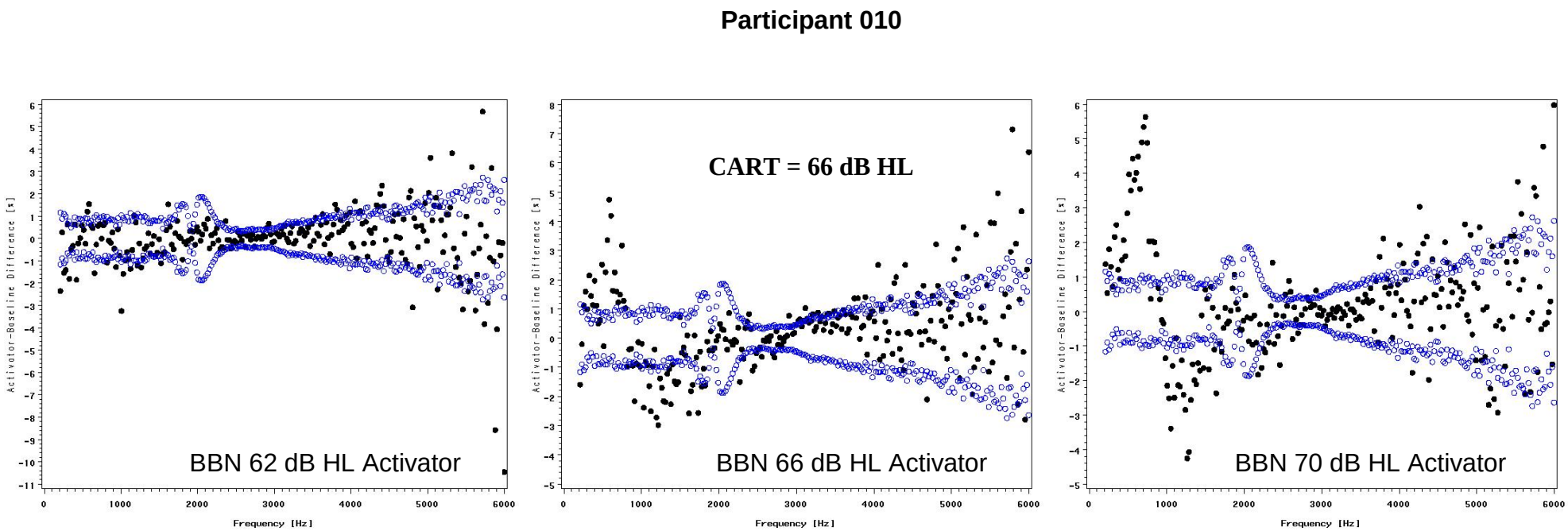

Figure F19. ABDs for BBN activators: 62 dB HL, 66 dB HL, 70 dB HL in participant 010; CART identified at 66 dB HL. Probe stimulus frequencies are shown on horizontal axis. The ABD (%) is shown on the vertical axis. The ± 1-SD limits (from the baseline variances) are shown in blue.

Participant 010

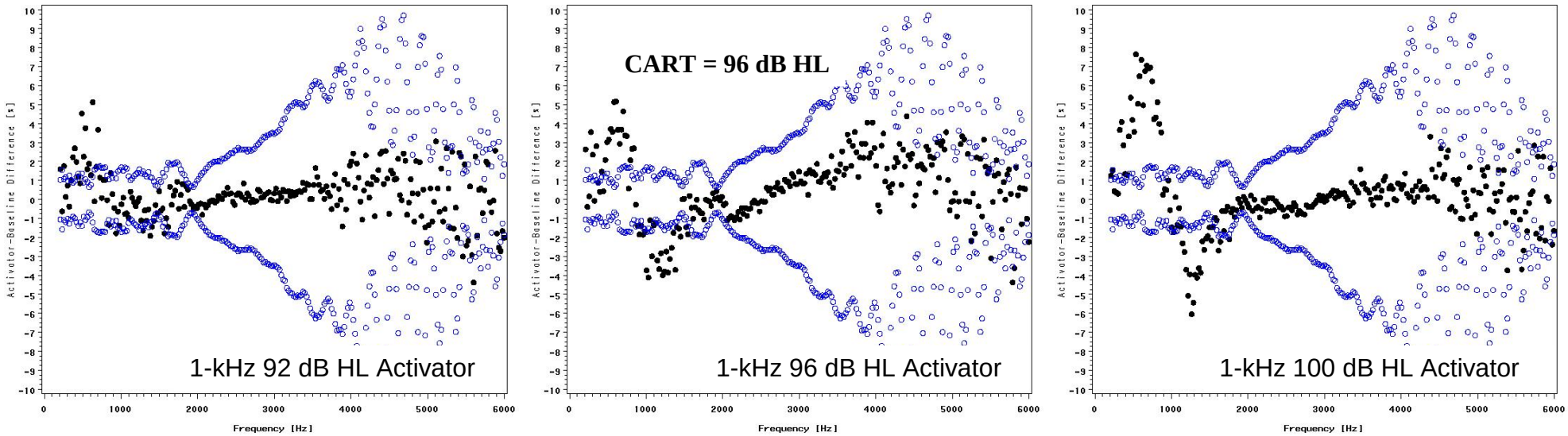

Figure F20. ABDs for 1-kHz activators: 92 dB HL, 96 dB HL, 100 dB HL in participant 010; CART identified at 96 dB HL. Probe stimulus frequencies are shown on horizontal axis. The ABD (%) is shown on the vertical axis. The ± 1-SD limits (from the baseline variances) are shown in blue.

Participant 101

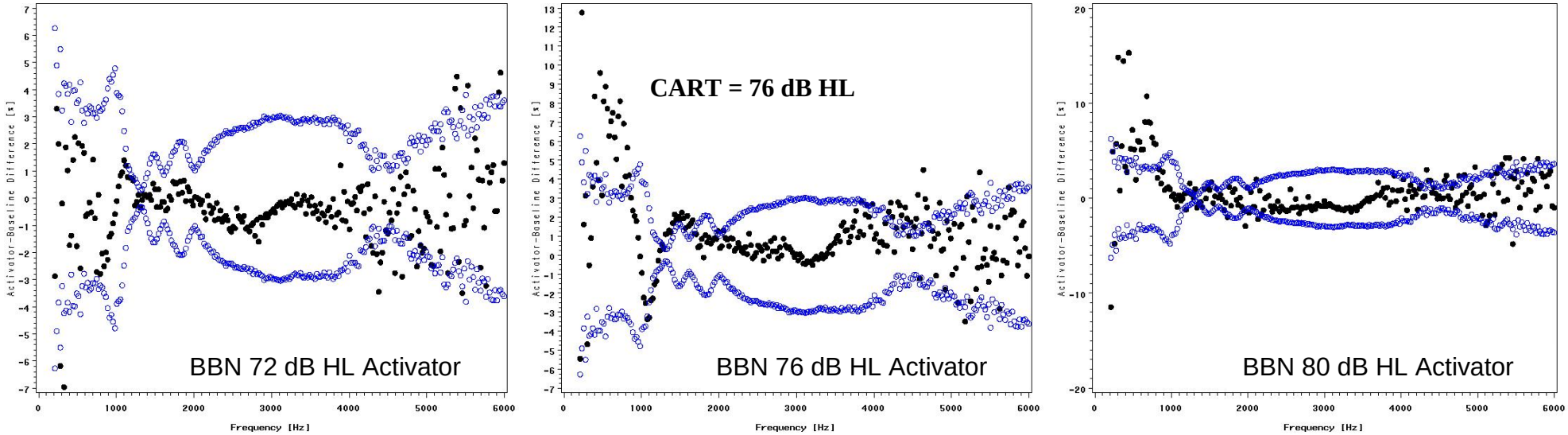

Figure F21. ABDs for BBN activators: 72 dB HL, 76 dB HL, 80 dB HL in participant 101; CART identified at 76 dB HL. Probe stimulus frequencies are shown on horizontal axis. The ABD (%) is shown on the vertical axis. The ± 1-SD limits (from the baseline variances) are shown in blue.

Participant 101

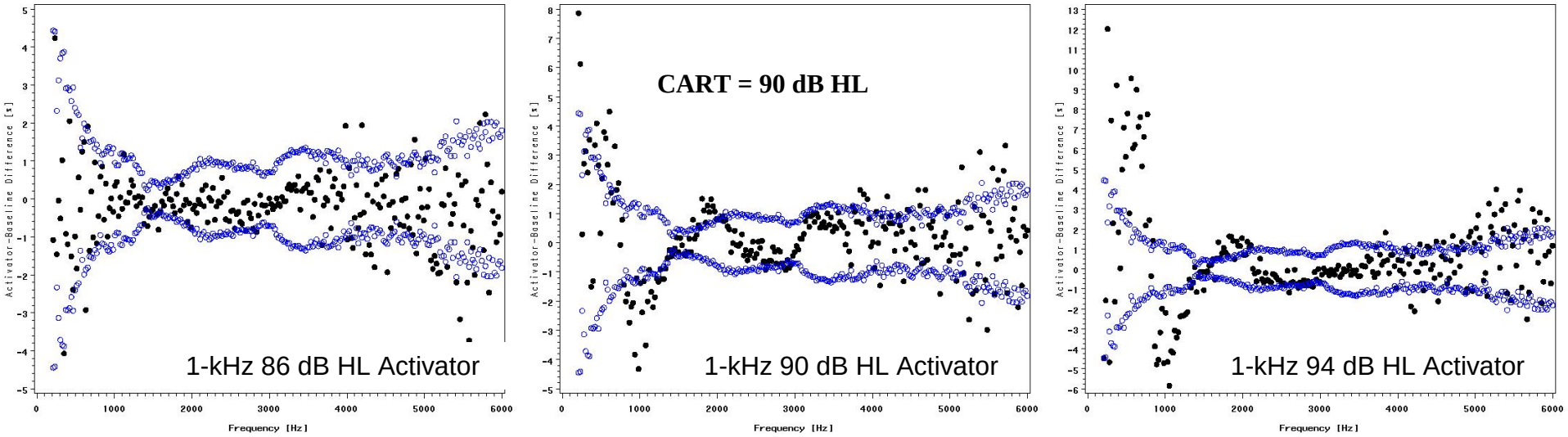

Figure F22. ABDs for 1-kHz activators: 86 dB HL, 90 dB HL, 94 dB HL in participant 101; CART identified at 90 dB HL. Probe stimulus frequencies are shown on horizontal axis. The ABD (%) is shown on the vertical axis. The ± 1-SD limits (from the baseline variances) are shown in blue.

Participant 102

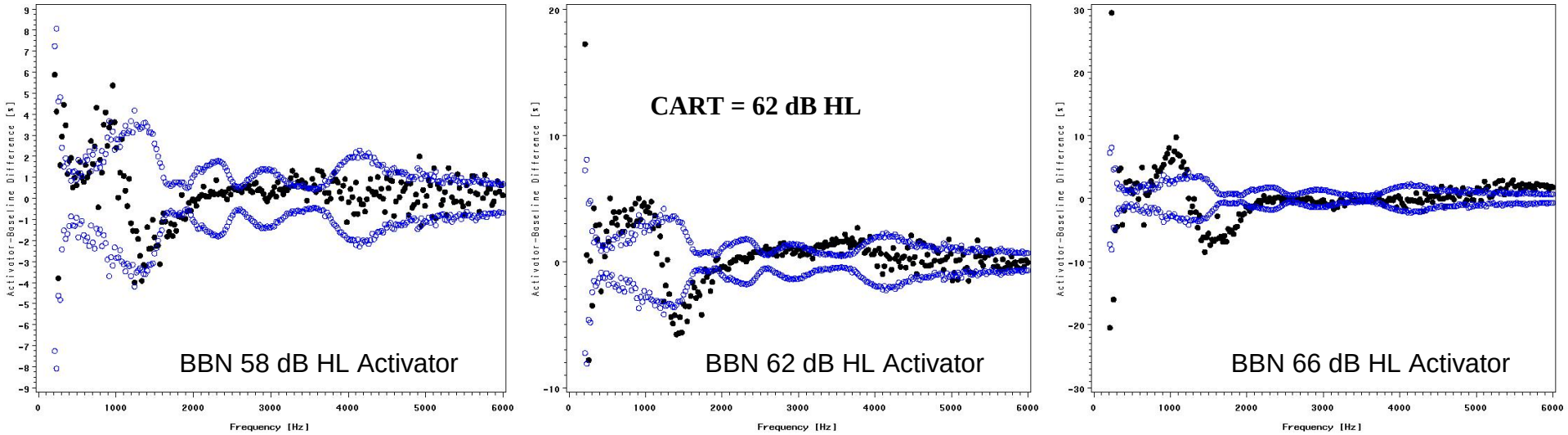

Figure F23. ABDs for BBN activators: 58 dB HL, 62 dB HL, 66 dB HL in participant 102; CART identified at 62 dB HL. Probe stimulus frequencies are shown on horizontal axis. The ABD (%) is shown on the vertical axis. The ± 1-SD limits (from the baseline variances) are shown in blue.

Participant 102

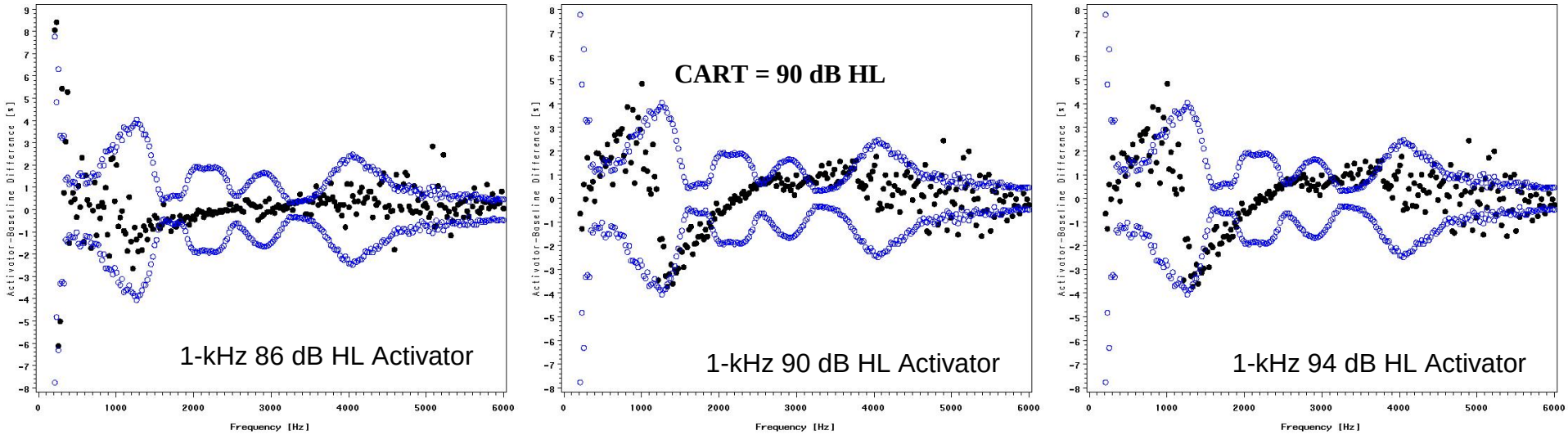

Figure F24. ABDs for 1-kHz activators: 86 dB HL, 90 dB HL, 94 dB HL in participant 102; CART identified at 90 dB HL. Probe stimulus frequencies are shown on horizontal axis. The ABD (%) is shown on the vertical axis. The ± 1-SD limits (from the baseline variances) are shown in blue.

Participant 103

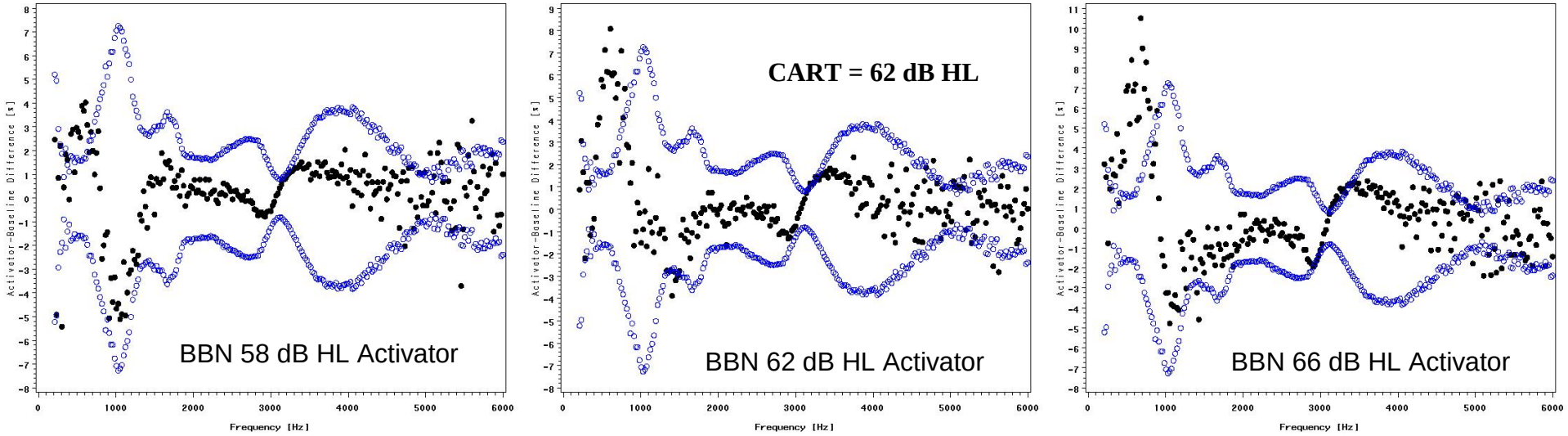

Figure F25. ABDs for BBN activators: 58 dB HL, 62 dB HL, 66 dB HL in participant 103; CART identified at 90 dB HL. Probe stimulus frequencies are shown on horizontal axis. The ABD (%) is shown on the vertical axis. The ± 1-SD limits (from the baseline variances) are shown in blue.

Participant 103

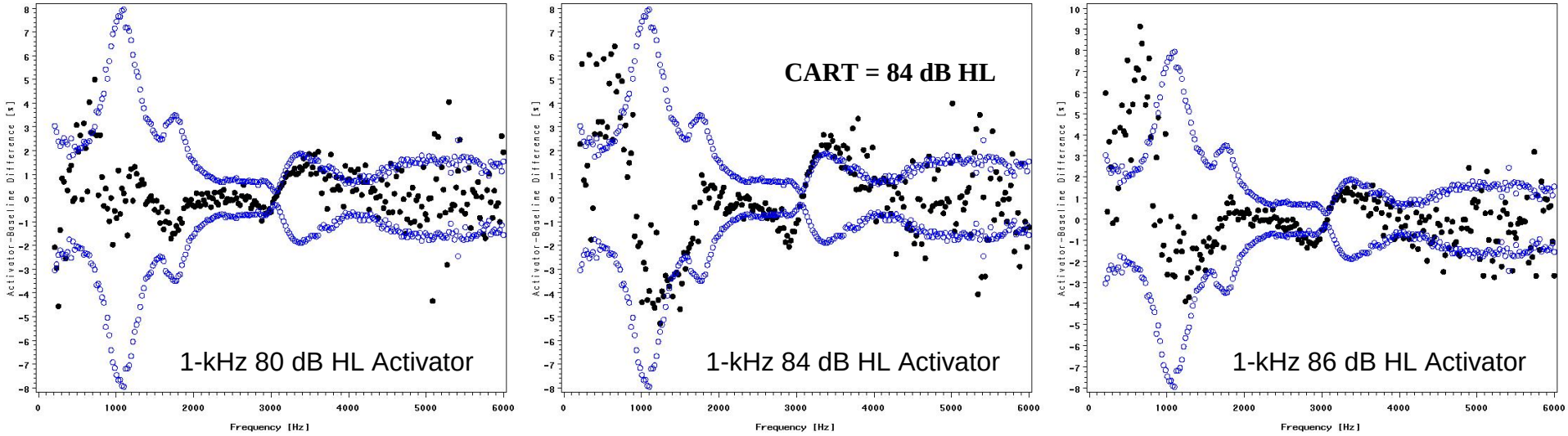

Figure F26. ABDs for 1-kHz activators: 80 dB HL, 84 dB HL, 86 dB HL in participant 103; CART identified at 84 dB HL. Probe stimulus frequencies are shown on horizontal axis. The ABD (%) is shown on the vertical axis. The ± 1-SD limits (from the baseline variances) are shown in blue.

Participant 104

CART Absent

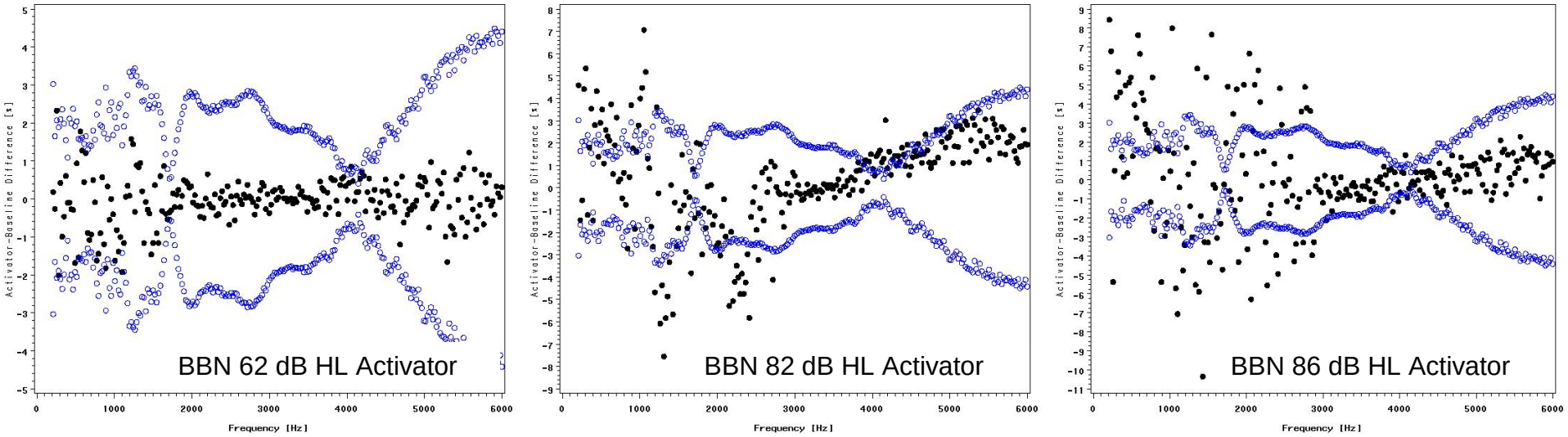

Figure F27. ABDs for BBN activators: 62 dB HL, 82 dB HL, 86 dB HL in participant 104; no CART identified. Probe stimulus frequencies are shown on horizontal axis. The ABD (%) is shown on the vertical axis. The ± 1-SD limits (from the baseline variances) are shown in blue.

Participant 104

CART Absent

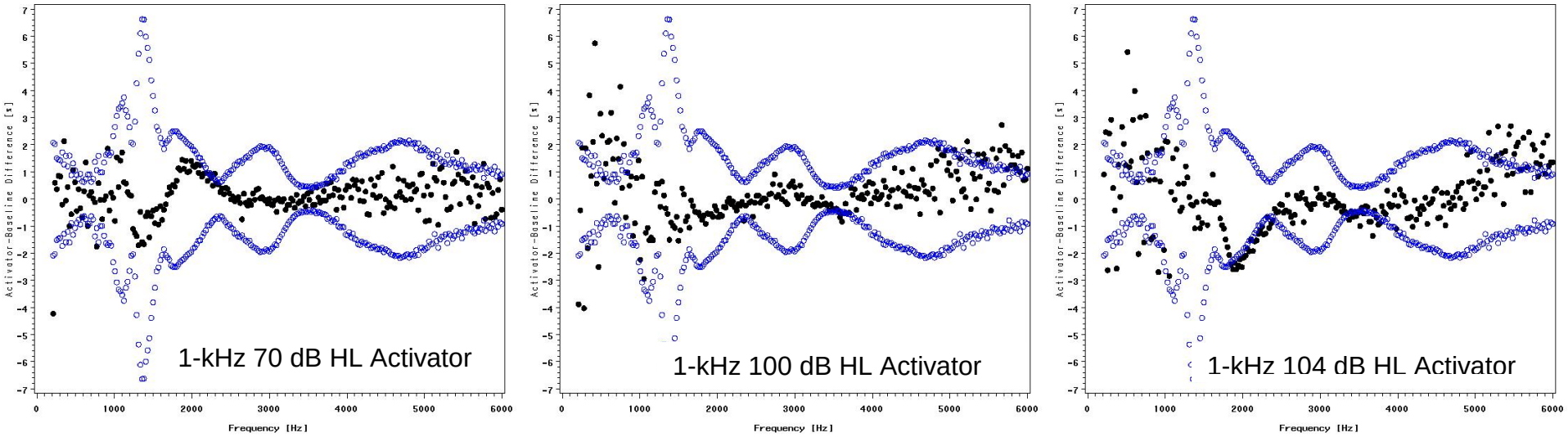

Figure F28. ABDs for 1-kHz activators: 70 dB HL, 100 dB HL, 104 dB HL in participant 104; no CART identified. Probe stimulus frequencies are shown on horizontal axis. The ABD (%) is shown on the vertical axis. The ± 1-SD limits (from the baseline variances) are shown in blue.

Participant 105

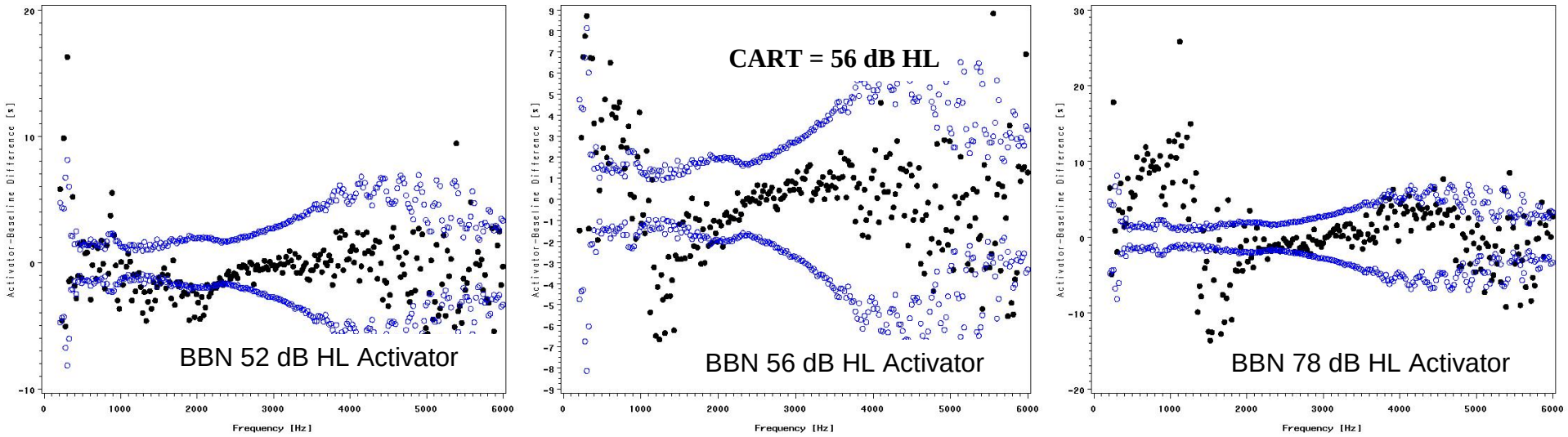

Figure F29. ABDs for BBN activators: 52 dB HL, 56 dB HL, 78 dB HL in participant 105; CART identified at 56 dB HL. Probe stimulus frequencies are shown on horizontal axis. The ABD (%) is shown on the vertical axis. The ± 1-SD limits (from the baseline variances) are shown in blue.

Participant 105

CART Absent

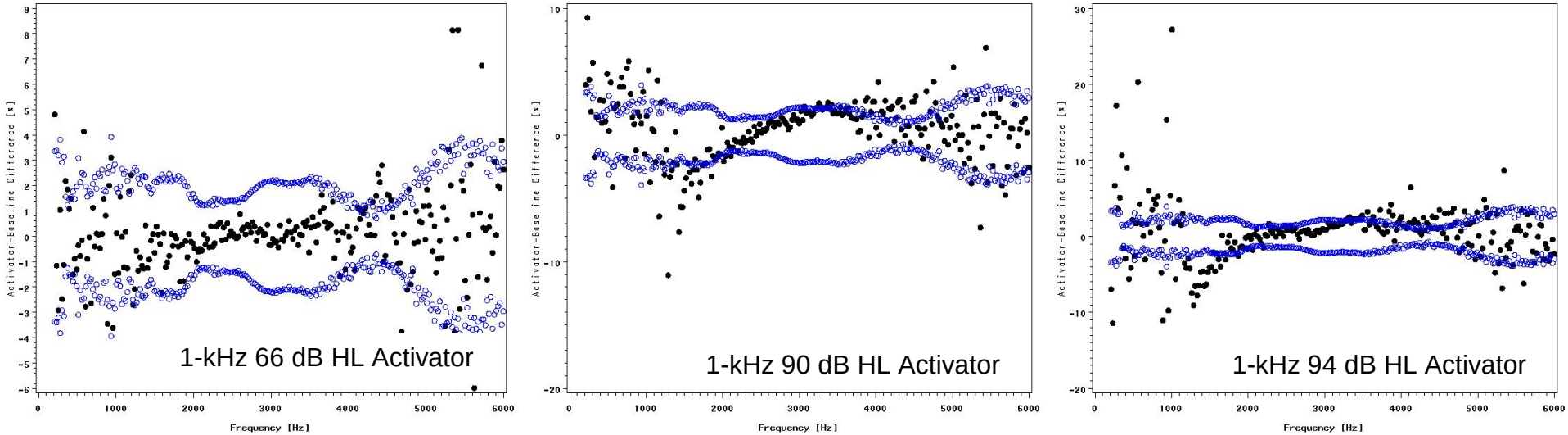

Figure F30. ABDs for 1-kHz activators: 66 dB HL, 90 dB HL, 94 dB HL in participant 105; no CART identified. Probe stimulus frequencies are shown on horizontal axis. The ABD (%) is shown on the vertical axis. The ± 1-SD limits (from the baseline variances) are shown in blue.

Participant 106

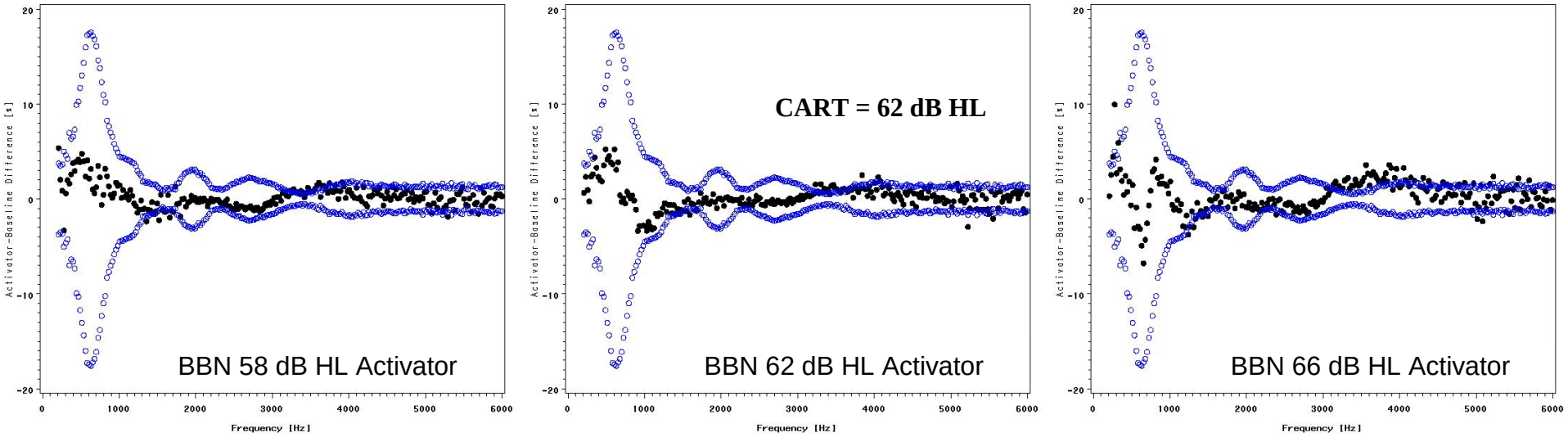

Figure F31. ABDs for BBN activators: 58 dB HL, 62 dB HL, 66 dB HL in participant 106; CART identified at 62 dB HL. Probe stimulus frequencies are shown on horizontal axis. The ABD (%) is shown on the vertical axis. The ± 1-SD limits (from the baseline variances) are shown in blue.

Participant 106

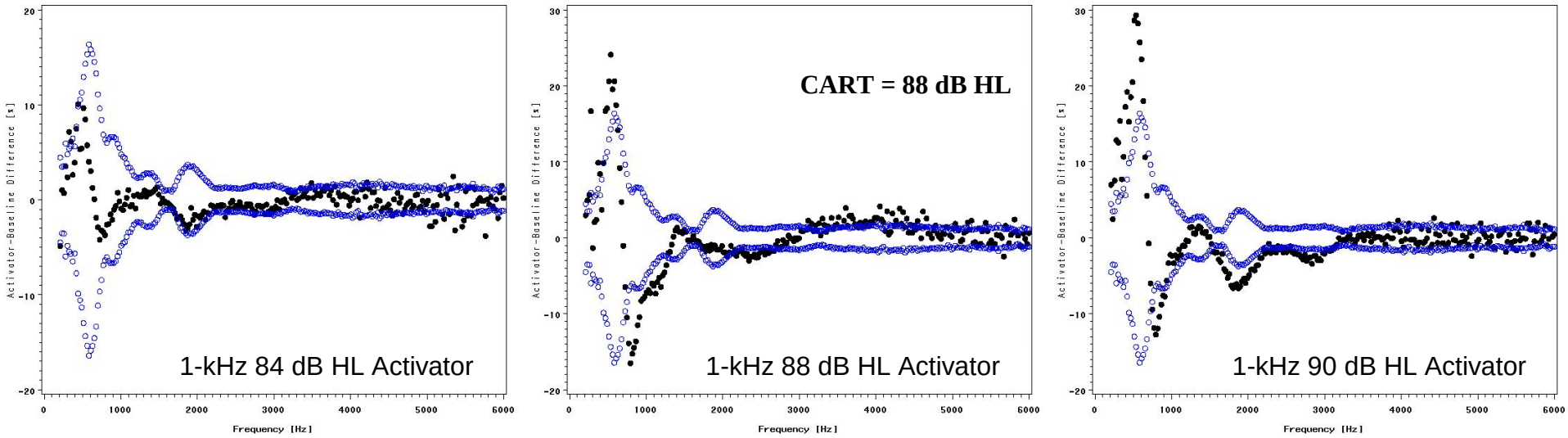

Figure F32. ABDs for 1-kHz activators: 84 dB HL, 88 dB HL, 90 dB HL in participant 106; CART identified at 88 dB HL. Probe stimulus frequencies are shown on horizontal axis. The ABD (%) is shown on the vertical axis. The ± 1-SD limits (from the baseline variances) are shown in blue.

Participant 107

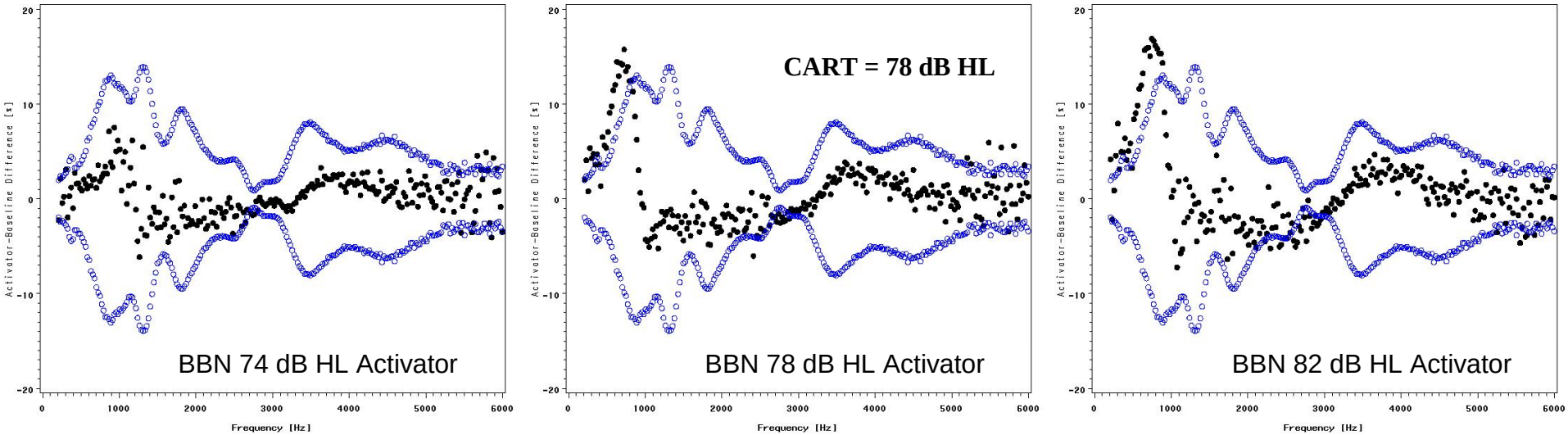

Figure F33. ABDs for BBN activators: 74 dB HL, 78 dB HL, 82 dB HL in participant 107; CART identified at 78 dB HL. Probe stimulus frequencies are shown on horizontal axis. The ABD (%) is shown on the vertical axis. The ± 1-SD limits (from the baseline variances) are shown in blue.

Participant 107

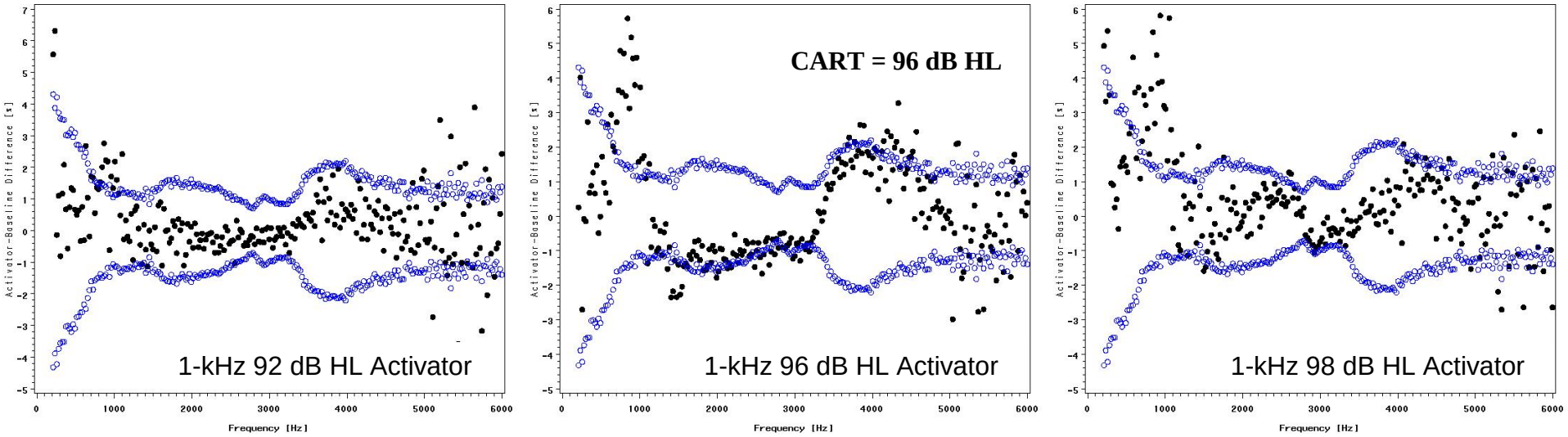

Figure F34. ABDs for 1-kHz activators: 92 dB HL, 96 dB HL, 98 dB HL in participant 107; CART identified at 96 dB HL. Probe stimulus frequencies are shown on horizontal axis. The ABD (%) is shown on the vertical axis. The ± 1-SD limits (from the baseline variances) are shown in blue.

Participant 108

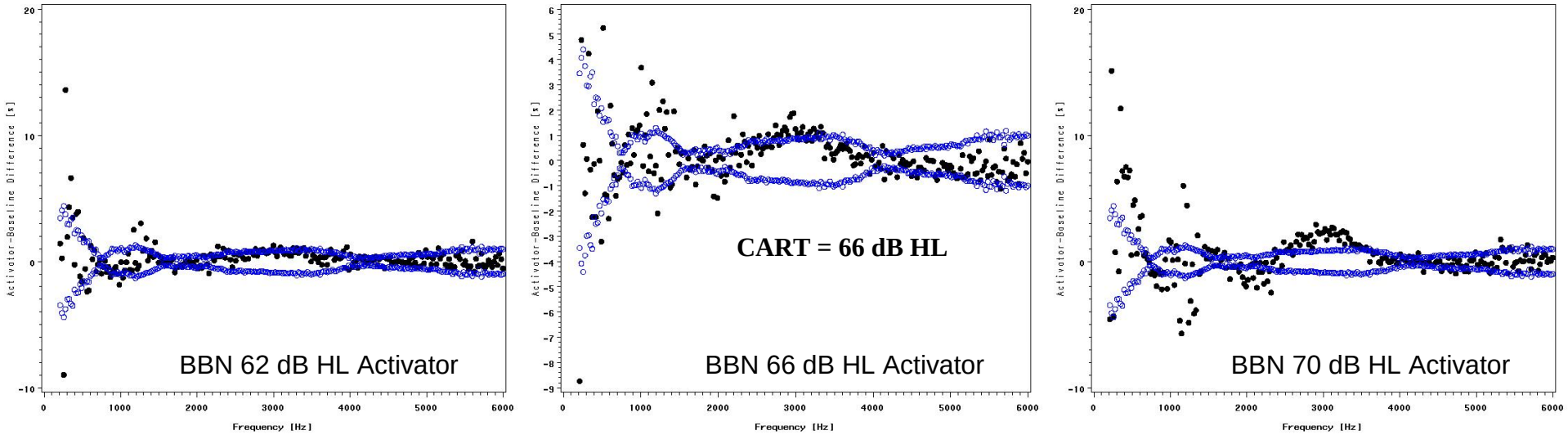

Figure F35. ABDs for BBN activators: 62 dB HL, 66 dB HL, 70 dB HL in participant 108; CART identified at 66 dB HL. Probe stimulus frequencies are shown on horizontal axis. The ABD (%) is shown on the vertical axis. The ± 1-SD limits (from the baseline variances) are shown in blue.

Participant 108

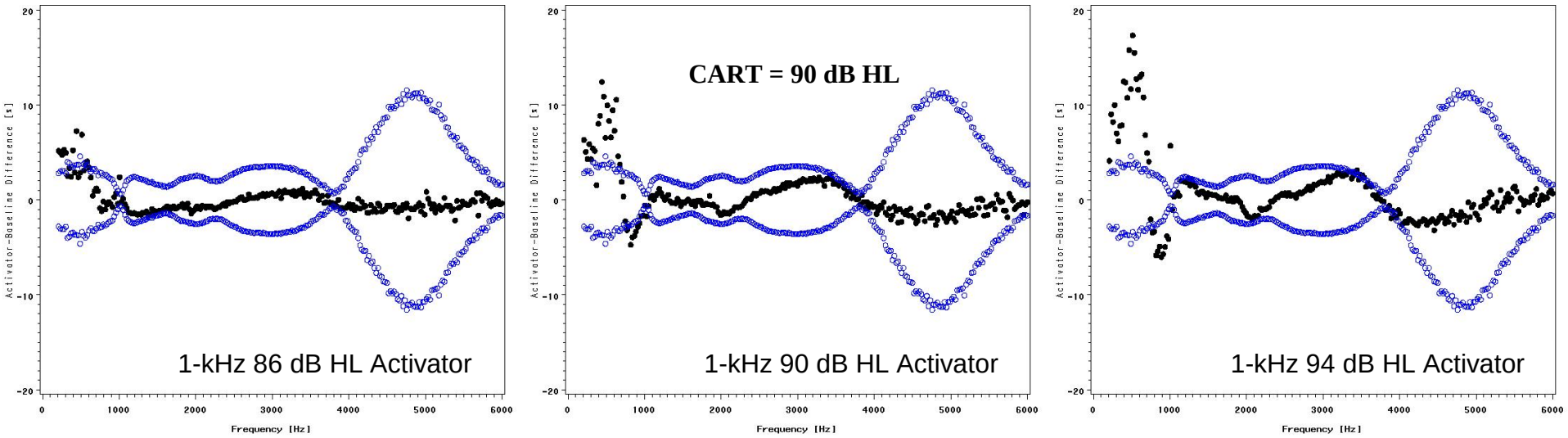

Figure F36. ABDs for 1-kHz activators: 86 dB HL, 90 dB HL, 94 dB HL in participant 108; CART identified at 90 dB HL. Probe stimulus frequencies are shown on horizontal axis. The ABD (%) is shown on the vertical axis. The ± 1-SD limits (from the baseline variances) are shown in blue.

Participant 109

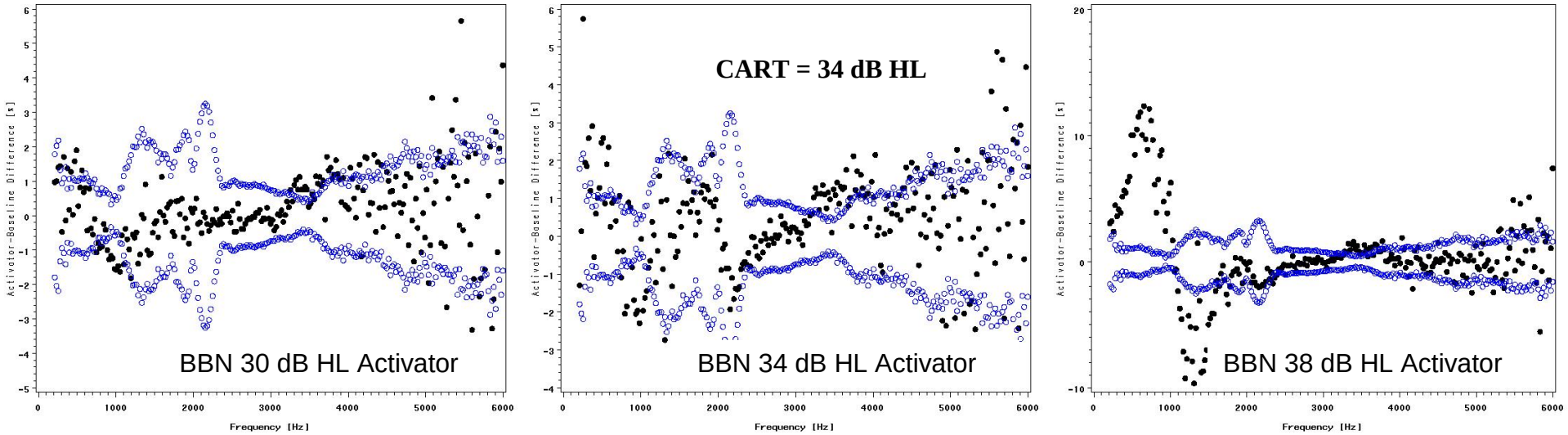

Figure F37. ABDs for BBN activators: 30 dB HL, 34 dB HL, 38 dB HL in participant 109; CART identified at 34 dB HL. Probe stimulus frequencies are shown on horizontal axis. The ABD (%) is shown on the vertical axis. The ± 1-SD limits (from the baseline variances) are shown in blue.

Participant 109

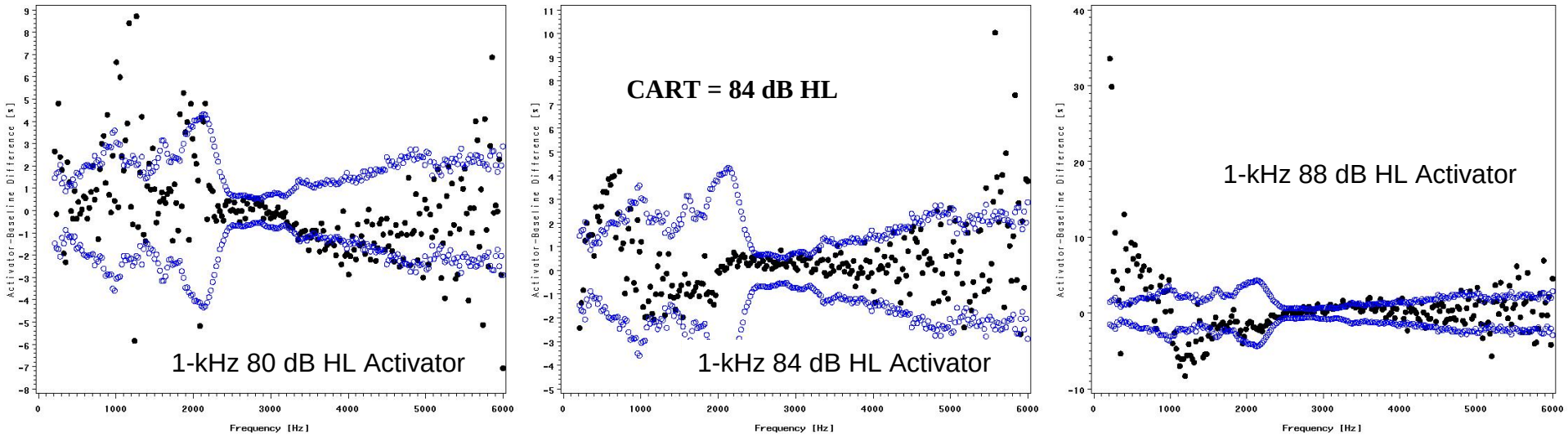

Figure F38. ABDs for 1-kHz activators: 80 dB HL, 84 dB HL, 88 dB HL in participant 109; CART identified at 84 dB HL. Probe stimulus frequencies are shown on horizontal axis. The ABD (%) is shown on the vertical axis. The ± 1-SD limits (from the baseline variances) are shown in blue.

Participant 110

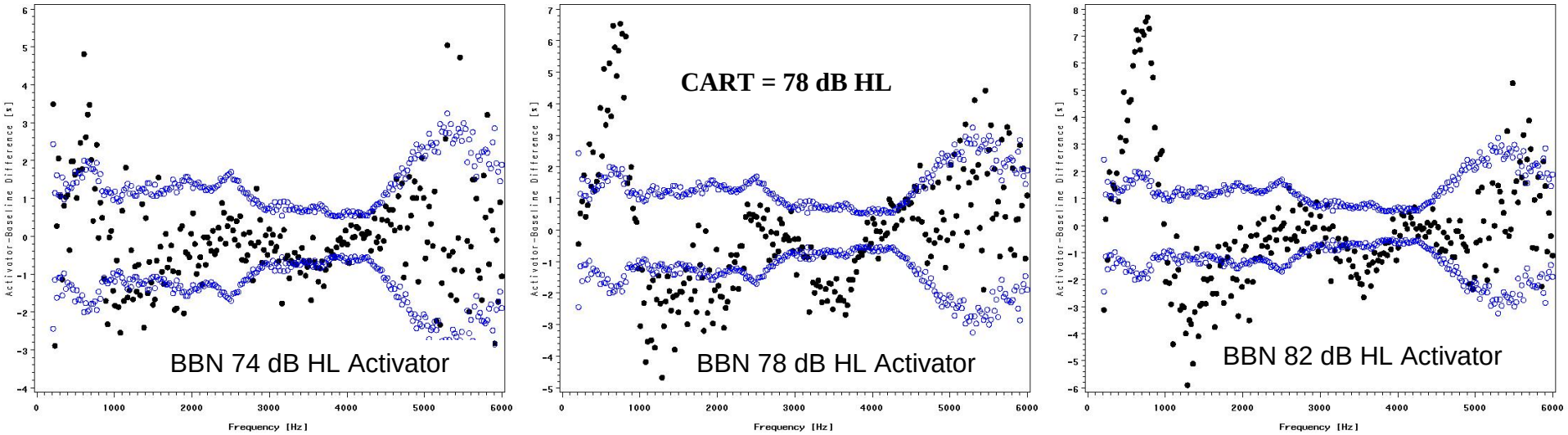

Figure F39. ABDs for BBN activators: 74 dB HL, 78 dB HL, 82 dB HL in participant 110; CART identified at 78 dB HL. Probe stimulus frequencies are shown on horizontal axis. The ABD (%) is shown on the vertical axis. The ± 1-SD limits (from the baseline variances) are shown in blue.

Participant 110

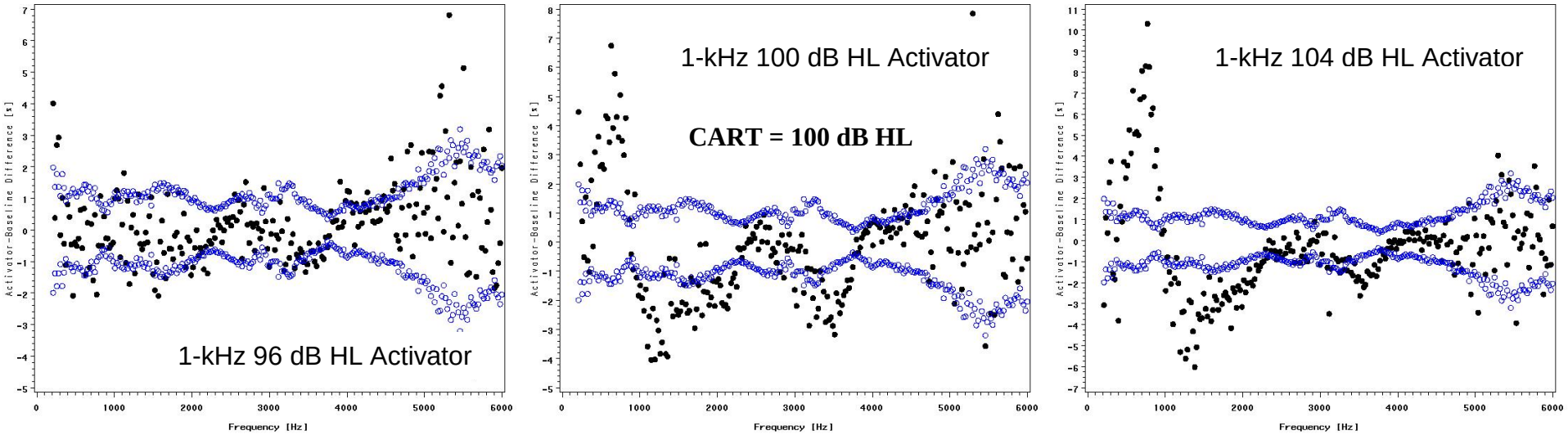

Figure F40. ABDs for 1-kHz activators: 84 dB HL, 88 dB HL, 90 dB HL in participant 110; CART identified at 100 dB HL. Probe stimulus frequencies are shown on horizontal axis. The ABD (%) is shown on the vertical axis. The ± 1-SD limits (from the baseline variances) are shown in blue.

CHAPTER VI: REFERENCES

Allen, J.B. (1985). Measurement of eardrum acoustic impedance. In J. B. Allen, J. L. Hall, A. Hubbard, S. T. Neely, A. Tubis (Eds.), *Peripheral Auditory Mechanisms* (44-51). New York: Springer-Verlag.

Arriaga, M.A., & Luxford, W.M. (1993). Impedance audiometry and iatrogenic hearing loss. *Otolaryngology and Head and Neck Surgery, 108,* 70-72.

Beattie, R.C., & Leamy, D.P. (1975). Otoadmittance: Normative values, procedural variables, and reliability. *Journal of the American Auditory Society, 1,* 21-27.

Beranek, L.L. (1954). *Acoustics.* New York: McGraw-Hill Book Company.

Block, S.L., Pichichero, M.E., McLinn, S., Aronovitz G., & Kimball S. (1999). Spectral gradient acoustic reflectometry: detection of middle ear effusion in suppurative otitis media. *Pediatric Infectious Disease Journal, 18,* 741-744.

Burke, K.S., & Herer, G.R. (1973). Impedance and admittance differences in middle ear study. *Journal of Auditory Research, 13,* 252-256.

Burns, E.M., Harrison, W.A., Bulen, J.C., & Keefe, D.H. (1993). Voluntary contraction of middle ear muscles: Effects on input impedance, energy reflectance and spontaneous otoacoustic emissions. *Hearing Research, 67,* 117-127.

Burns, E.M., Keefe, D.H., & Ling, R. (1998) Energy reflectance in the ear canal can exceed unity near spontaneous otoacoustic emission frequencies. *Journal of the Acoustic Society of America, 103,* 452-474.

Deutsch, L.J. (1972). The threshold of the stapedius reflex for pure tone and noise stimuli. *Acta Oto-Laryngologica, 74,* 248-251.

Djupesland, G., Flottorp, C., & Winther, F. (1966). Size and duration of acoustically elicited impedance changes in man. *Acta Oto-Laryngologica, 27*(Suppl. 224), 220-228.

Emmer, M.B. (2000). Temporal integration of the acoustic-reflex threshold and its age related changes (Doctoral dissertation, Graduate Center, CUNY, 2000). *Dissertation Abstracts International, 61, 02.*

Feeney, M.P., & Keefe, D.H. (1999). Acoustic reflex detection using wide-band acoustic reflectance, admittance and power measurements. *Journal of Speech, Language, and Hearing Research, 42,* 1029-1041.

Feeney, M. P., & Keefe, D.H. (2001). Estimating the acoustic reflex threshold from wideband measures of reflectance, admittance and power. *Ear and Hearing, 22,* 316-332.

Feeney, M.P., Keefe, D.H., & Marryott, L.P. (2003). Contralateral acoustic reflex thresholds for tonal activators using wideband energy reflectance and admittance. *Journal of Speech, Language, and Hearing Research, 46,* 128-136.

Feeney, M.P., Keefe, D.H., & Sanford, C.A. (2004). Wideband reflectance measures of the ipsilateral acoustic stapedius reflex threshold. *Ear and Hearing, 25,* 421-430.

Feeney, M.P., & Sanford, C.A. (2004). Age effects in the human middle ear: wideband acoustic measures. *Journal of the Acoustical Society of America, 116,* 3546-3558.

Galambos, R., & Rupert, A. (1959). Action of middle ear muscles in normal cats. *Journal of the Acoustical Society of America, 31,* 349-355.

Gelfand, S.A. (1984). The contralateral acoustic reflex threshold. In S. Silman (Ed.), *The acoustic reflex: Basic principles and clinical Applications*. New York: Academic Press.

Gelfand, S.A. (1998). *Hearing*. New York: Marcel Dekker.

Gelfand, S.A., & Piper, N. (1984). Acoustic reflex thresholds: Variability and distribution effects. *Ear and Hearing, 5,* 228-234.

Gelfand, S.A., Piper, N., & Silman, S. (1983). Effects of hearing levels at the activator and other frequencies upon the expected levels of the acoustic reflex threshold. *Journal of Speech and Hearing Disorders, 48,* 11-17.

Gelfand, S.A., Schwander, T., & Silman, S. (1990). Acoustic reflex thresholds in normal and cochlear-impaired ears: effects of no response rates on 90th percentiles in a large sample. *Journal of Speech and Hearing Disorders, 55,* 198-205.

Hall, J.W. (1982). Acoustic reflex amplitude: I. Effect of age and sex. *Audiology, 21,* 294-309.

Hall, J.W., & Koval, C.B. (1982). Accuracy of hearing prediction by acoustic reflex. *Laryngoscope, 92,* 140-149.

Hayes, D., & Jerger J. (1983). Signal-averaging of the acoustic reflex: Diagnostic applications of amplitude characteristics. *Scandinavian Audiology, 17(*Suppl.*),* 31-36.

Heaviside, O. (1886, July23). Electromagnetic induction and its propagation. Oscillatory impressed force at one end of a line. Its effect. Its application to long distance telephony and telegraphy. *The electrician, XXIV,* 149

Industrial Acoustics Company. (1990). *Rooms for the medical and life sciences* [Bulletin 5.0101.6 400-A Series]. Bronx, NY: Author.

Jakimetz, J.J., Silman, S., Miller, M.H., & Silverman, C.A. (1989). Some effects of signal bandwidth and spectral density on the acoustic-reflex threshold in the elderly. *Journal of the Acoustical Society of America, 86,* 1783-1789.

Jeng, P.S., Levitt, H., Lee, W.W., & Gravel, J.S. (1999). *Reflectance measures for detecting otitis media with effusion in children: Preliminary findings.* Poster session presented at

the Seventh International Symposium on Otitis Media with Effusion, Fort Lauderdale, FL.

Jerger, J. (1975). Diagnostic use of impedance measures. In J. Jerger (Ed.), *Handbook of clinical impedance audiometry* (pp. 149-174). Dobbs Ferry, NY: American Electromedics.

Jerger, J., Burney, P., Mauldin, L., & Crump, B. (1974). Predicting hearing loss from the acoustic reflex. *Journal of Speech and Hearing Disorders, 39,* 11-22.

Jerger, J., Hayes, D., Anthony, L., & Mauldin, L. (1978). Factors influencing prediction of hearing level from the acoustic reflex. *Monographs in Contemporary Audiology, 1,* 1-20.

Jerger, J., Mauldin, L., & Lewis, N. (1977). Temporal summation of the acoustic reflex. *Audiology, 16,* 177-200.

Jerger, J., & Oliver, T. (1987). Interaction of age and intersignal interval on acoustic reflex amplitude. *Ear and Hearing, 8,* 322-325.

Johnson, W.C. (1950). *Transmission lines and networks*. New York: McGraw-Hill.

Katz, J. (1994). *Handbook of clinical audiology* (4th ed.) Baltimore, MD: Williams and Wilkins.

Keefe, D.H. (1984). Acoustical wave propagation in cylindrical ducts. Transmission line parameter approximations for isothermal and nonisothermal boundary condition. *Journal of the Acoustical Society of America, 75,* 58-62.

Keefe, D.H. (1997) Otoreflectance of the cochlea and middle ear. *Journal of the Acoustical Society of America, 102,* 2849-2859.

Keefe, D.H., Bulen, J.C., Arehart, K., & Burns, M.E. (1993) Ear canal impedance and reflection coefficient in human infants and adults. *Journal of the Acoustical Society of America, 94,* 2617-2638.

Keefe, D.H, Folsom, R.C., Gorga, M.P., Vohr, B.R., Bulen, J.C., & Norton, S.J. (2000). Identification of neonatal hearing impairment: Ear canal measurements of acoustic admittance and reflectance in neonates. *Ear and Hearing, 21,* 443-461.

Keefe, D.H., Gorga, M.P., Neely, S.T., Zhao, F., & Vohr, B.R.(2003). Ear-canal acoustic admittance and reflectance effects in human neonates. II. Predictions of middle-ear dysfunction and sensori-neural hearing loss. *Journal of the Acoustical Society of America, 113,* 407-422.

Keefe, D.H., & Levi, E. (1996) Maturation of the middle and external ears: Acoustic power-based responses and reflectance tympanometry. *Ear and Hearing, 17,* 362-373.

Keefe, D.H., Ling, R., & Bulen, J.C. (1992). Method to measure acoustic impedance and reflection coefficient. *Journal of the Acoustical Society of America, 91,* 470-485.

Keefe, D.H., & Simmons, J.L. (2003). Energy transmittance predicts conductive hearing loss in older children and adults. *Journal of the Acoustical Society of America, 114,* 3217-3238.

Keefe, D.H., Zhao, F., Neely, S.T., Gorga, M.P., & Vohr, B.R.(2003). Ear-canal acoustic admittance and reflectance effects in human neonates. I. Predictions of otoacoustic emission and auditory brainstem responses. *Journal of the Acoustical Society of America, 113,* 389-406.

Khanna, S.M., & Stinson, M.R. (1985). Specification of the acoustical input to the ear at high frequencies. *Journal of the Acoustical Society of America, 77,* 577-589.

Lawton, B.W., & Stinson, M.R. (1986). Standing wave patterns in the human ear canal used for estimation of acoustic energy reflectance at the ear drum. *Journal of the Acoustical Society of America, 79,* 1003-1009.

Margolis, R.H., & Popelka, R.G. (1975). Loudness and acoustic reflex. *Journal of the Acoustical Society of America, 58,* 1330-1332.

Margolis, R.H., Saly, G.L., & Keefe, D.H. (1999). Wideband reflectance tympanometry in normal adults. *Journal of the Acoustical Society of America, 106,* 265-280.

Marston, L.E., & Goetzinger, C.P. (1972). A comparison of sensitized words and sentences for distinguishing non-peripheral auditory changes as a function of aging. *Cortex, 8,* 213-223.

Mawardi, O.K. (1949). Measurement of acoustic impedance. *Journal of the Acoustical Society of America, 21,* 84-91.

Metz, O. (1946). The acoustic impedance measured on normal and pathologic ears. *Acta Oto-Laryngologica, 63*(Suppl.), 1-254.

Miller, M.H., Hoffman, R.A., & Smallberg, G.J. (1984). Stapedius reflex testing and partially reversible acoustic trauma. *Hearing Instruments, 35,* 15-49.

Niemeyer, W., & Sesterhenn, C. (1974). Calculating the hearing threshold from the stapedius reflex threshold for different sound stimuli. *Audiology, 13,* 421-427.

Olsen, W.O., Bauch, C.A., & Harner, S.G. (1983). Application of the Silman and Gelfand (1981). 90th percentile levels for acoustic reflex thresholds. *Journal of Speech and Hearing Disorders, 48,* 330-332.

Osterhammel, D., & Osterhammel, P. (1979). Age and sex variation for the normal stapedial reflex thresholds and tympanometric compliance values. *Scandinavian Audiology, 8,* 153-158.

Piskorski, P., Keefe, D.H., Simmons, J.L., & Gorga, M.P. (1999). Prediction of conductive hearing loss based on ear-canal response using a multivariate clinical decision theory. *Journal of the Acoustical Society of America, 105,* 1749-1764.

Popelka, G.R. (1981). *Hearing assessment with the acoustic reflex.* New York: Grune & Stratton.

Popelka, G.R., Margolis, R.H., & Wiley T.L. (1976). Effect of activating signal bandwidth on acoustic reflex thresholds. *Journal of the Acoustical Society of America, 59,* 153-159.

Porter, T.A. (1972). Normative otoadmittance values for three populations. *Journal of Auditory Research, 12,* 53-58.

Silman, S. (1979). The effects of aging on the stapedius reflex thresholds. *Journal of the Acoustical Society of America, 66,* 735-738.

Silman, S., & Gelfand, S.A. (1981). The relationship between magnitude of hearing loss and acoustic reflex threshold levels. *Journal of Speech and Hearing Disorders, 46,* 312-316.

Silman, S., Popelka, G.R., & Gelfand, S.A. (1978). The effect of sensorineural hearing loss on acoustic stapedius reflex growth function. *Journal of the Acoustical Society of America, 64,* 1407-1411.

Silman, S., Silverman, C.A. (1991). *Auditory diagnosis: Principles and applications.* San Diego, CA: Singular Publishing.

Silman, S., Silverman, C.A., Showers, T., & Gelfand, S.A. (1984). Effect of age on prediction of hearing loss with the bivariate-plotting procedure. *Journal of Speech and Hearing Research, 27,* 12-19.

Silverman, C.A., Silman, S., & Miller, M.H. (1983). The acoustic reflex threshold in aging ears. *Journal of the Acoustical Society of America, 73,* 248-255.

Simmons, F.B. (1959). Middle ear muscle activity at moderate sound levels. *Annals of Otology, Rhinology and Laryngology, 68,* 1126-1143.

Stach, B.A., & Jerger, J.F. (1984). Acoustic reflex averaging. *Ear and Hearing, 5,* 289-296.

Sticht, T.G., & Gray, B.B. (1969). The intelligibility of time-compressed words as a function of age and hearing loss. *Journal of Speech and Hearing Research, 12,* 443-448.

Stinson, M.R. (1985). The spatial distribution of sound pressure within scaled replicas of the human ear canal. *Journal of the Acoustical Society of America, 78,* 1596-1602.

Stinson, M.R. (1990). Revision of estimates of acoustic energy reflectance at the human eardrum. *Journal of the Acoustical Society of America, 88,* 1773-1778.

Stinson, M.R., & Khanna, S.M. (1989). Sound propagation in the ear canal and coupling to the eardrum with measurements on model systems. *Journal of the Acoustical Society of America, 85,* 2481-2491.

Stinson, M.R., & Khanna, S.M. (1994). Spatial distribution of sound pressure and energy flow in the ear canals of cats. *Journal of the Acoustical Society of America 96,* 170-180.

Stinson, M.R., & Lawton, B.W. (1989). Specification of the geometry of the human ear canal for the prediction of sound-pressure level distribution. *Journal of the Acoustical Society of America, 85,* 2492-2503.

Stinson, M.R., Shaw, E.A., & Lawton, B.W. (1982). Estimation of acoustic energy reflectance at the eardrum from measurement of pressure distribution in the human ear canal. *Journal of the Acoustical Society of America, 72,* 766-773.

Terkildsen, K., Nielsen, S.S. (1960). An electroacoustic impedance measuring bridge for clinical use. *Archives of Otolaryngology-Head & Neck Surgery, 72,* 339-346.

Terkildsen, K., Osterhammel, P., & Bretlau, P. (1973). Acoustic middle ear reflexes in patients with otosclerosis. *Archives of Otolaryngology – Head & Neck Surgery 98,* 152-155.

Terkildsen, K., & Thomsen, K.A. (1959). The influence of pressure variations on the impedance of the human ear drum. *The Journal of Laryngology & Otology, 73,* 409-418.

Tipler, P.A. (1976). *Physics.* New York: Worth Publishers.

Thompson, D.J., Sills, J.A., Recke, K.S., & Bui, D.M. (1980). Acoustic reflex growth in aging adult. *Journal of Speech and Hearing Research, 5,* 215-227.

Voss, S.E., & Allen, J.B. (1994). Measurement of acoustic impedance and reflectance in the human ear canal. *Journal of the Acoustical Society of America, 95,* 372-384.

Wallin, A., Mendez-Kurtz, L., & Silman, S. (1986). Prediction of hearing loss from acoustic-reflex thresholds in the older adult population. *Ear and Hearing, 7,* 400-404.

Webster, A.G. (1919). Acoustical impedance and theory of horns at the design of the phonograph. *Proceedings of the National Academy of Sciences, USA, 5,* 275-282.

West, W. (1928). Measurements of the acoustical impedance of human ears. *Post Office Electrical Engineers' Journal, 21,* 293.

Wiener, F.M., & Ross, D.A. (1946). The pressure distribution in the auditory canal in a progressive sound field. *Journal of the Acoustical Society of America, 18,* 401-408.

Wilson, R.H. (1981). The effects of aging on the magnitude of the acoustic reflex. *Journal of Speech and Hearing Research, 24,* 406-413.

Wilson, R.H., & McBride, L.M. (1978). Threshold and growth of the acoustic reflex. *Journal of the Acoustical Society of America, 63,* 147-154.

Zito, F., & Roberto, M. (1980). The acoustic reflex pattern studied by the averaging technique. *Audiology, 19,* 395-403.

Zwislocki, J. (1957). Some impedance measurements on normal and pathological ears. *Journal of the Acoustical Society of America, 29,* 1312-1317.